NASA TECHNICAL NOTE

NASA TN D-3283

c. 1

LOAN COPY: R
AFWL (W
KIRTLAND AF
0079788
TECH LIBRARY KAFB, NM

NASA TN D-3283

# AN EMPIRICAL METHOD FOR DETERMINING STATIC DISTRIBUTED AERODYNAMIC LOADS ON AXISYMMETRIC MULTISTAGE LAUNCH VEHICLES

*by Ralph J. Muraca*

*Langley Research Center*
*Langley Station, Hampton, Va.*

RECEIVED
29 MAR 1966
Technical Library
AF Weapons
Laboratory

NATIONAL AERONAUTICS AND SPACE ADMINISTRATION • WASHINGTON, D. C. • MARCH 1966

TECH LIBRARY KAFB, NM
0079788
NASA TN D-3283

# AN EMPIRICAL METHOD FOR DETERMINING STATIC DISTRIBUTED AERODYNAMIC LOADS ON AXISYMMETRIC MULTISTAGE LAUNCH VEHICLES

By Ralph J. Muraca

Langley Research Center
Langley Station, Hampton, Va.

NATIONAL AERONAUTICS AND SPACE ADMINISTRATION

For sale by the Clearinghouse for Federal Scientific and Technical Information
Springfield, Virginia 22151 – Price $1.30

# AN EMPIRICAL METHOD FOR DETERMINING STATIC DISTRIBUTED AERODYNAMIC LOADS ON AXISYMMETRIC MULTISTAGE LAUNCH VEHICLES

By Ralph J. Muraca
Langley Research Center

## SUMMARY

This paper presents an empirical method for determining the distributed aerodynamic loads of arbitrary configurations in the linear angle-of-attack range. The method is based upon a compilation of wind-tunnel force and pressure data. Existing test results for geometric components such as cones, tangent ogives, spherical segments, cylinders, frustums, and boattails have been correlated and reduced to the form of generalized loading functions. These generalized loading functions cover a wide range of Mach numbers and geometric parameters and can be quickly applied to arbitrary configurations. Distributed aerodynamic coefficients for several configurations have been calculated by using the data presented herein, and these results are compared with the results obtained from wind-tunnel pressure tests of the specific configurations.

## INTRODUCTION

The effects of body flexibility have been increasingly recognized as important factors in the dynamic loads and stability studies performed on spacecraft launch vehicles. The inclusion of body flexibility has introduced the need for an adequate description of the distributed aerodynamic loads acting on the deformed body.

The efforts required to obtain distributed data are considerably greater than those for obtaining total aerodynamic coefficients. However, the distributed aerodynamic data are essential to the adequate analysis of aeroelastic divergence, aeroelastic feedback coupling of closed-loop autopilot systems, and dynamic loads of flexible structures experiencing atmospheric disturbances. The severity of such instabilities and the load magnifications due to flexibility justify the extensive efforts required in generating appropriate distributed aerodynamics. Unfortunately, the ability to determine distributed aerodynamic loadings has not increased at the same rate as the need for such data.

Three methods are currently available to the aeroelastician for the acquisition of distributed aerodynamic coefficients. These methods can be classified as analytical, empirical, and experimental.

The analytical methods are based upon the assumptions that the partial differential equations governing the flow around a body and the associated boundary conditions can be simplified to an extent whereby they would be amenable to solution. Detailed derivations of the various analytical methods along with their limitations and ranges of applicability are given in references 1 to 7.

A second source of aerodynamic data is empirical methods. These methods can be derived from both analytical and experimental considerations. Detailed explanations of these methods and their limitations are given in references 8 to 13.

The most accurate sources of distributed loads are wind-tunnel tests of the specific configuration under consideration. These tests constitute the third method available to the engineer for determining distributed aerodynamic loads. Either pressure-test or force-test models may be used; however, distributed data can only be obtained by using pressure models unless the effect of body length on the total coefficients can be determined from the force-test results. For a detailed description of the distributed normal-force-coefficient slope on a body, pressure tests are the preferred method. However, the time and expense required to run pressure tests are considerable and this method cannot usually be justified in the preliminary stages of vehicle design.

This report presents an empirical method of determining the distributed normal-force-coefficient slope on arbitrary bodies in the linear angle-of-attack range. The method is based upon wind-tunnel results presented in references 14 to 46. These results have been utilized to obtain generalized loading functions which have been categorized by geometric components. These components and the ranges of geometric parameters for which the loading functions are available are shown in table I.

The empirical method presented herein is not submitted as a replacement for any of the other previously mentioned methods which would be applicable for a given design or for wind-tunnel testing but is intended to supplement such methods. The correlations presented in this paper provide a rapid means of determining distributed normal-force-coefficient slopes for a wide range of configurations and Mach numbers.

Included as appendixes A and B to this report are the equations which were used to reduce the various wind-tunnel results and a numerical example showing the application of this method to a typical launch-vehicle configuration composed of a blunted cone, a cylinder, a cone frustum, and a second cylinder. Further comparisons are also made over a range of Mach numbers for a few specific configurations for which wind-tunnel data were available.

## SYMBOLS

| | |
|---|---|
| A,B | coefficients (see eq. (A12)) |
| $b_n$ | bluntness ratio of nose, $D_s/D_1$ |

| | |
|---|---|
| $C_N$ | normal-force coefficient, $\frac{F_N}{qS}$ |
| $C_{N_\alpha}$ | normal-force-coefficient slope, $\frac{\partial C_N}{\partial \alpha}$, 1/radian |
| $D$ | local diameter, meters |
| $D_o$ | reference diameter, meters |
| $D_T$ | diameter of the nose cone at the tangency point to the nose sphere, meters |
| $D_1$ | diameter of cylinder following cone, meters |
| $D_2$ | diameter of cylinder following frustum, meters |
| $F_N$ | normal force, newtons |
| $f$ | fineness ratio of component, $\frac{l}{D_o}$, calibers |
| $l$ | length of component, meters |
| $M$ | free-stream Mach number |
| $p$ | static pressure, newtons/meter$^2$ |
| $q$ | dynamic pressure, $\frac{1}{2}\rho V^2$, newtons/meter$^2$ |
| $R$ | radius of sphere or radius of ogive, meters |
| $r$ | local radius of cross section at $x$ normal to vehicle axis of revolution, $D/2$ |
| $S$ | reference area, meters$^2$ |
| $V$ | velocity, meters/sec |
| $x$ | body coordinate of component, $x = \mu - \mu_o$, meters |
| $\left\{S \frac{dC_{N_\alpha}}{dx}\right\}$ | product of the reference area and the distributed normal-force-coefficient slope, meters/radian |
| $\frac{1}{D}\left\{S \frac{dC_{N_\alpha}}{dx}\right\}$ | generalized loading function, 1/radian |
| $\alpha$ | angle of attack, radians |

| | |
|---|---|
| $\theta_b$ | boattail angle, deg |
| $\theta_f$ | frustum angle, deg |
| $\theta_n$ | nose semivertex angle, deg |
| $\rho$ | free-stream density, kilogram/meter$^3$ |
| $\alpha_t$ | angle of attack compatible with $C_p$, radians |
| $\lambda$ | generalized loading function, $\frac{1}{D}\left\{S \frac{dC_{N_\alpha}}{dx}\right\}$, 1/radian |
| $\mu$ | coordinate along the axis of revolution of the assembled components, meters |
| $\mu_o$ | reference value of $\mu$ at the origin of the component under consideration, such that, $x = \mu - \mu_o$, meters |

Subscripts:

| | |
|---|---|
| a | afterbody |
| f | frustum |
| n | nose |
| 1 | component preceding the component under consideration |
| 2 | component following the component under consideration |
| $\infty$ | free stream |
| T | tangency point of sphere and cone |
| s | sphere |

## METHOD OF DATA REDUCTION

The generalized data which have been obtained are graphically displayed in this report as the variation of the generalized loading function $\frac{1}{D}\left\{S \frac{dC_{N_\alpha}}{dx}\right\}$ with the component length. In this expression for the loading function, $\left\{S \frac{dC_{N_\alpha}}{dx}\right\}$ represents the product of the reference area and the distributed normal-force-coefficient slope and $D$ is the local body diameter. To convert

the loading function to distributed normal force all that is required is multiplication by the local diameter, the local angle of attack, and the dynamic pressure of the stream. Geometric scale effects are accounted for and the need for defining a specific reference area is eliminated by including the reference area term as an integral part of the coefficient. This form for the generalized loading function $\frac{1}{D}\left\{S \frac{dC_{N_\alpha}}{dx}\right\}$ is most convenient to the aeroelastician since it can be readily incorporated into the various analyses mentioned previously.

The reference material used in compiling the loading functions presented in this report were presented in many diverse forms which necessitated specific processing to yield the desired results. The data-reduction operations necessary for reducing force-test and pressure-test results are recorded in appendix A. Test results obtained for angles of attack up to $5^{\circ}$ were included; therefore, the generalized loading functions are applicable in this range. It should be noted that a wide range of Reynolds numbers is covered in the referenced data; however, very little information was available from which Reynolds number effects on distributed loads could be obtained. In general, flight Reynolds numbers will be an order of magnitude higher than wind-tunnel test conditions. At present, neither analytical nor experimental methods are available for accurate determination of model to full-scale Reynolds number effects on distributed loads. It should be noted that a variety of systems of units were used in presenting the referenced data. The units used throughout this report are the meter, newton, and radian. Geometric angles are given in degrees.

## PRESENTATION AND DISCUSSION OF DATA

Space vehicles may be comprised of various geometrical components such as spheres, cones, cylinders, cone frustums, and other bodies of revolution generated by given arcs. Based upon these considerations, the loading functions applicable to components such as those mentioned previously have been determined and are presented for use with multicomponent vehicle configurations. The use of generalized data for individual components to determine distributed aerodynamic curves for complete configurations is not theoretically proper in the subsonic and transonic ranges as a result of the propagation of downstream disturbances upstream. Downstream component parameters will therefore affect the loading function on upstream components. However, the extent of this effect will depend upon the configuration and will be considered subsequently. The loading functions are presented in terms of geometrical parameters associated with the component under consideration and the other adjacent components. Figure 1 shows the relationship between the component geometry and the various parameters used in presenting the data.

### Spherical Nose Segments

Loading functions for spherical noses are presented in figure 2. These data are based upon results of references 44 and 15. An analytical expression

involving two Mach dependent coefficients was fitted to the pressure distributions of reference 44. The resulting empirical expression was used for computing generalized loading functions by the process of equation (A11) in appendix A. Generalized loading functions obtained from the analytically described pressure distributions were then matched with the maxima of comparative data from reference 15 in order to ascertain the previously undefined Mach dependent coefficients.

A comparison of the total normal-force coefficient for a spherical segment calculated by using Newtonion impact theory with that obtained by integration of the loading function of figure 2(b) at Mach 4.63 indicates that the results obtained by using the loading functions are about 15 percent lower than those obtained by using impact theory.

## Cones

The loading functions for cones are shown in figure 3 for various semivertex angles $\theta_n$ and Mach numbers. These data were obtained from reference 16, which presents analytical results, and from reference 17, which presents experimental results. The method of reference 16 does not provide data for those Mach numbers where the shock wave is detached. However, reference 17 presents wind-tunnel data on cones over the Mach number range from 0.50 to 4.06. It was found that, in the region where the analytical solution was applicable, the two sets of data agreed very well. The effect of blunting is also presented in reference 17. In the transonic range, blunting has little effect on $C_{N_\alpha}$ for all values of $\theta_n$. As Mach number increases, $C_{N_\alpha}$ decreases as a result of blunting. The amount of reduction in $C_{N_\alpha}$ is also a function of $\theta_n$. For small $\theta_n$ the reduction in $C_{N_\alpha}$ is considerable, but as $\theta_n$ increases $C_{N_\alpha}$ for a blunted cone approaches $C_{N_\alpha}$ for a sharp cone.

The loading functions of figures 2 and 3 were used to obtain total normal-force coefficients for blunted cones at various Mach numbers and nose angles. These calculated values of $C_{N_\alpha}$ were then compared with the wind-tunnel data of reference 17 and good agreement was observed. In general, this method will provide a good description of the distributed normal force on a blunted cone; however, the loading function on the cone portion of the sphere-cone combination is still considered to be constant with cone length as shown in the derivation in appendix A.

## Tangent Ogives

A tangent ogive is a body of revolution which is generated by revolving the area enclosed by the intersection of two equal circles having radius R about the common chord of the two circles. This configuration may be seen in the following sketch which also gives the relationship between $f_n$, R, and $D_o$.

$$\frac{R}{D_o} = \frac{1}{4} + f_n^2$$

$$f_n = \frac{l}{D_o}$$

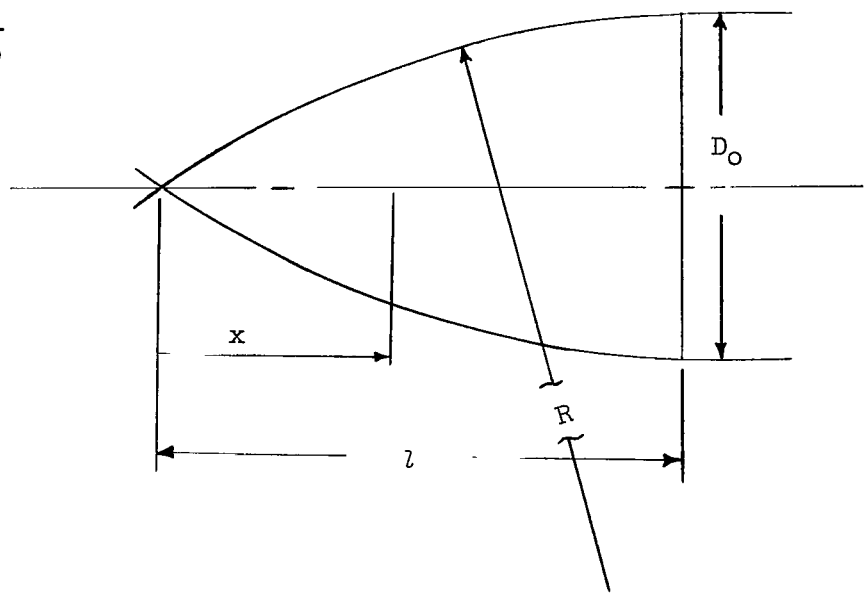


A tangent-ogive nose shape consists of the portion of the generated body of revolution from the sharp point to the maximum diameter $D_o$ and is of length $l$.

Very few wind-tunnel test results are available from which to determine loading functions for tangent ogives. The curves presented in figure 4 were obtained from references 18 to 20. These loading functions are based upon pressure test results.

Although the available information is limited, a method utilizing the cone data of figure 3 can be used to approximate ogive loading functions. This method is based upon the assumption that the loading function at a given ogive station is well approximated by that of a cone tangent to the ogive at the station. In this manner, a loading function for any ogive can be determined. This method tends to predict higher loading on the forward part of the ogive and lower loading on the aft portion of the ogive. It should be noted that the data obtained in this manner will have a value of zero at the cylinder tangency point. To overcome this inadequacy, the value at the tangency point should be obtained from the cylinder-following-ogives data of figure 5. The ogive curve in the vicinity of the cylinder should be faired to make the two curves tangent at the common intercept.

A comparison of the loading functions for a tangent ogive obtained by using the tangent-cone method and those obtained from the ogive data presented in figure 4 is shown in the following plot. This method is intended for use where loading functions for a specific ogive cannot be obtained from the data of figure 4.

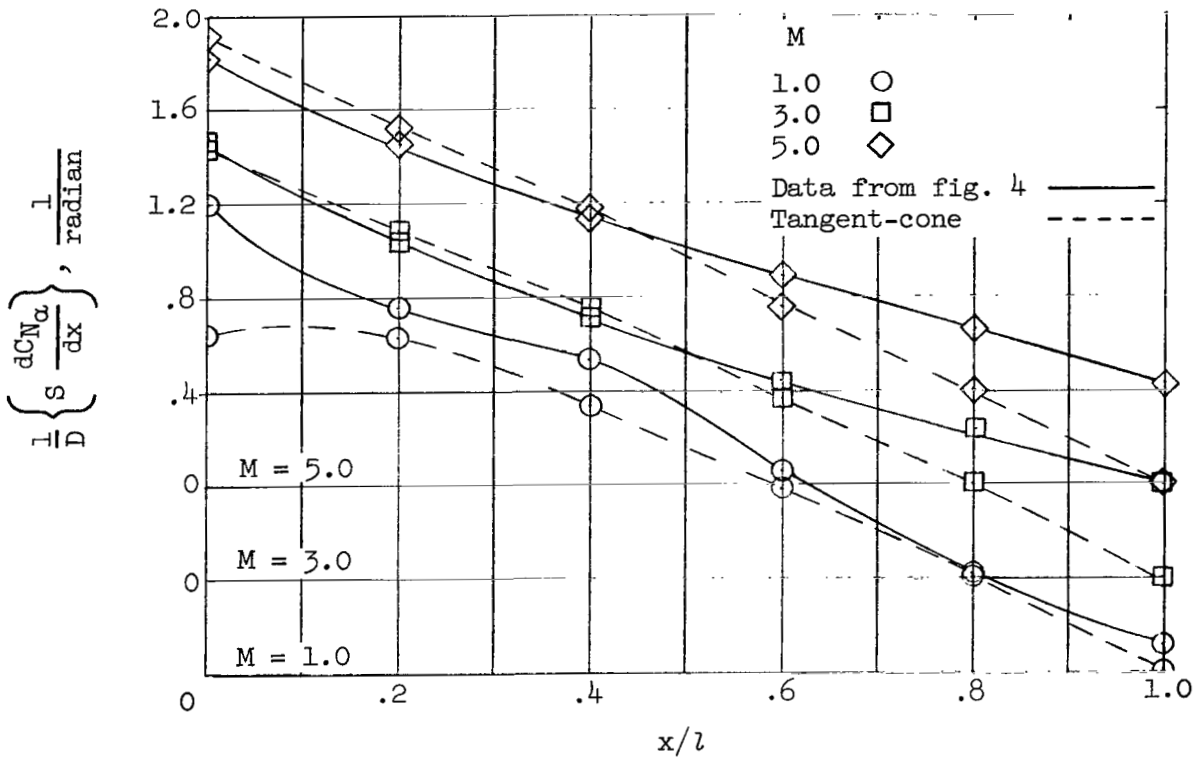


Cylinder Following Cones and Tangent Ogives

Figure 5 presents curves applicable to cylinders following cones and tangent ogives. Both pressure-test and force-test results were used in generating the curves of figure 5. In the transonic range the only data presented are from reference 21. This reference presents the results of a series of tests in which various geometric parameters were varied and the effects on pressure distributions were noted. Reference 21 represents the first means by which the engineer might predict the variation of local pressure with component parameter in the transonic range.

Some of the references which present force-test data using stacked models fail to provide a data point at $x/D_o = 0$ (i.e., forebody alone). Whenever this omission occurs for cone-cylinder configurations, the value of $C_{N_\alpha}$ for the appropriate cone was obtained from reference 16 or 17.

In general for $M > 1.5$ the value of the loading function at $x/D_o = 0$ increases as cone semivertex angle increases or Mach number decreases. It is apparent from figure 5 that the loading functions show less variation with body length as Mach number increases and approach an almost constant value at hypersonic velocities. In terms of total normal force, the data of figure 5 show that the contribution of a cylindrical afterbody increases with increasing $\theta_n$

at all Mach numbers above Mach 1.0. As Mach number increases the cylinder normal force increases for a given $\theta_n$ until it reaches a maximum between $M = 2$ and 3, and then decreases gradually as $M$ increases above $M = 3$. The center of pressure of cylinder afterbodies shows a shift rearward as Mach number increases. For example, the center-of-pressure location for a 6-caliber afterbody is between $1.2 < x/D_o < 1.6$ at $M = 1.5$ and moves aft to $2.0 < x/D_o < 2.4$ at $M = 6.86$.

It has been assumed that the effects of downstream components on the loading of the bodies preceding them are negligible; consequently, frustum parameters for the case of a frustum following a cylinder do not appear on the cylinder loading curves. It should be understood, however, that, even in the supersonic range, significant subsonic regions can exist in the boundary such that disturbances will be propagated upstream. This is particularly true in the case of cylinders preceding frustums. Large effects on cylinder loading functions due to Mach number and frustum-angle variation have been shown to exist by other investigations. These investigations show that the frustum angle can radically affect the cylinder loadings through the mechanism of flow separation. The point at which the flow separation takes place is a function of $\theta_f$ and $M$. The resultant cylinder loading can be drastically increased in the region of flow separation. When these phenomena occur, the loading functions on the frustum will also be affected. A list of references dealing with flow separation on cone-cylinder frustums and further discussion of this behavior are given in the next section. Insufficient data showing these interactions precluded an adequate treatment of these phenomena in terms of both cylinder and frustum parameters.

## Frustums Following Cone-Cylinders

Figure 6 presents the loading functions for frustums following cone-cylinders. The distributed normal force on frustums following cone-cylinders is a function of four parameters: Mach number ($M$), frustum angle ($\theta_f$), cylinder fineness ratio $\left(f_{a,l}\right)$, and nose semivertex angle ($\theta_n$). As presented in figure 6 each set of curves gives the variation of $\frac{1}{D}\left\{S\,\frac{dC_{N_\alpha}}{dx}\right\}$ with $x/D_o$ for various arrangements of the four parameters. For configurations in which the cylinder length was greater than 4 calibers, $\theta_n$ no longer significantly affects the frustum data and therefore is not included as a parameter. It is difficult to generalize with regard to the behavior of the loading function for the frustum. Besides the number of variables involved, the possibility of flow separation occurring on the cylinder cannot be ignored. Flow separation at supersonic speeds is related to the boundary-layer shock-wave interaction in the vicinity of the cylinder-frustum junction. Reference 22 indicates that flow separation increased with increasing Mach number and decreasing Reynolds number.

Reference 23 also indicates that, as frustum length or frustum angle increases, $C_{N_\alpha}$ increases rapidly with Mach number in the transonic range. As

mentioned previously, this effect is due primarily to flow separation and would be reflected in the distributed data as a sudden increase in loading function on the frustum. Unfortunately, prediction of these highly nonlinear effects is difficult and no attempt has been made to include them in the loading functions presented herein. In general, whenever a configuration is encountered where the nose and frustum are within 2 calibers of each other and where the frustum angle is greater than about $10^{\circ}$ it is quite possible that flow separation will be encountered. Reference 19 also shows that, as the ratio of frustum base area to cylinder base area increases, the point of flow separation moves forward on the cylinder. Other factors also affect separation; see, for example, references 47 and 48.

The parameters having the greatest effect on the load functions on a frustum are $\theta_f$ and M. The next most important parameter is $f_{a,1}$. If $f_{a,1}$ is great enough so that pressure following the expansion around the cone-cylinder shoulder has recovered, a load buildup will occur on the forward portion of the frustum.

The general trend of the frustum loading function is to approach the cone value asymptotically as frustum length increases. The loading-function variations from those of the cone value usually occur on the forward portion of the frustum within 2 calibers of the forebody-frustum junction.

Included in figure 7 are cross plots of the data of figure 6. These curves show the variation of frustum loading functions as $f_{a,1}$ is varied and all other parameters are held fixed. The curve for $f_{a,1} = 0$ was obtained from cone data. In addition to references 22 and 23, the data of figure 6 were obtained from references 12, 21, 24 to 29, and 40. Additional information concerning the effects of cone angle, cylinder length, and frustum angle on flow separation and the resultant nonlinear behavior of $C_{N_\alpha}$ can also be obtained from these references.

## Cylinders Following Frustums

The loading functions for cylinders following frustums are presented in figure 8. The available data on cylinders following frustums are very limited. References 21, 26, 27, and 30 were used to obtain these curves. The data of references 21, 26, and 27 were obtained from pressure models. The data of reference 30 were obtained from force-test models with stacked sections.

The parameters which affect the loading on a cylinder following a frustum are M, $\theta_f$, $f_{a,1}$, $\theta_n$, $D_1/D_o$, and $x/D_o$. However, it has been pointed out in reference 28 that, if $f_{a,1}$ is greater than about 4.5 calibers, the nose semivertex angle $\theta_n$ no longer significantly affects the loading on the cylinder following the frustum. Consequently, for data obtained from models with $f_{a,1} > 4.5$, $\theta_n$ and $f_{a,1}$ do not appear as parameters. The general trends of the loading function of a cylinder following a frustum are similar to those of

a cylinder following a cone. The parameters having the greatest effect on the functions are frustum angle $\theta_f$ and the cylinder-diameter ratio $D_1/D_o$. In the supersonic Mach number range as $D_1/D_o$ increases, the influence of $\theta_f$ decreases and, at $D_1/D_o > 0.75$, $\theta_f$ has no effect on the cylinder loading functions. In the event that data for a configuration with a diameter ratio less than 0.25 are required, the data for cylinders following cones can be used, giving a curve for $D_1/D_o = 0$. These data presented in figure 9 represent the loading function for cylinders following frustums and are cross plots of the data of figure 8, with the diameter ratios $D_1/D_o$ varied for specific values of $\theta_f$ and Mach number.

## Boattails and Rearward-Facing Step

In the determination of the loading functions for boattail and rearward-facing-step configurations, the problems of flow separation, Reynolds number effects, and component interactions once again present themselves. The data presented in figures 10 and 11 can be considered representative of the load distribution on these components. Although interpolation of these data is permissible, extrapolations beyond the limits of the parameters given on the individual curves should be avoided. Potentially large errors can be introduced when these data are extrapolated.

The boattail loading functions are presented in figures 10 and 11. The boattail data can be broken up into two parts: boattails following short cone-cylinders and boattails following long cylinders. Figure 10 presents data of the first type; the parameters of interest are $\theta_b$, M, $\theta_n$, $\theta_{f,2}$, and $f_{a,1}$. In general the boattail loading functions tend to approach positive values as boattail length increases. This trend might be due to the presence of the component following the boattail. This same trend is also seen in the curves of figure 11 which presents data for boattails following long cylinders with the end of the boattail representing the base of the models. These models were sting mounted. Consequently, the sting might have had the same effect on the boattail loads as a cylinder. In figure 11 the only body parameter is $\theta_b$ since the cylinders used in these tests were long enough that $\theta_n$ had no effect on the boattail loading. The data of figures 10 and 11 were obtained from references 21 and 32 to 34.

Figure 12 presents the effect of a rearward-facing step on the loading function of a cylinder following a cone. These data were obtained with a model in which the step was located 2.4 calibers downstream from the cone-cylinder shoulder. The parameters which affect the loading function are $D_1/D_o$, M, $f_{a,1}$, and $\theta_n$. However, if the shoulder is located far enough downstream of the cone, the effect of a variation in $\theta_n$ will be secondary. Reference 46 presents the only data which could be used to show the effect of a rearward-facing step on cylinder loading functions, consequently, it was not possible to determine the effect of a variation of $D_1/D_o$, $\theta_n$, or $f_{a,1}$ on the loading function.

## Comparison of Wind-Tunnel and Empirical Results

In an effort to provide some indication of the accuracy of the empirical method outlined herein, some comparisons with data obtained from wind-tunnel tests of specific configurations have been made. Configurations for which wind-tunnel results were classified, or which were used to generate the empirical loading functions of this report were avoided.

Figure 13 shows a comparison of the distributed normal-force-coefficient slope $\left\{ S \frac{dC_{N_\alpha}}{dx} \right\}$ obtained from wind-tunnel pressure-distribution tests of the specific models indicated with similar data obtained through the use of the method outlined herein. The configuration shown in figure 13(a) has an upper-stage cylinder length of over 4 calibers, and a frustum angle of $5^{\circ}$. For this model, flow separation does not occur to a degree where it would drastically affect the load distributions. The calculated distributions are in good agreement with the experimental data except at a Mach number of 1.6. No explanation can be given at this time for the poor agreement at Mach 1.6. Some differences are also seen for the cylinders just behind the cone and frustum at Mach 2.0 and 2.36.

The models in figures 13(b) and 13(c) have the frustum and nose in close proximity to one another, and their respective angles are such that flow separation does occur on the intermediate cylinders just forward of the frustum and on the forward portion of the frustum. Along these segments of the model, the estimated data tend to predict considerably lower load distributions. For those configurations where significant regions of separated flow are likely to occur, the predicted loads in general will tend to show fluctuations with less extreme peak values. It should be noted that the geometries and Mach numbers of figures 13(b) and 13(c) represent a severe test for the empirical data of this report.

## CONCLUDING REMARKS

The empirical method for determining distributed loads presented herein will yield acceptable results for most configurations and Mach numbers. Care must be exercised in applying this method to configurations where flow separation is anticipated. The assumption of linearity limits the use of this method to angles of attack less than about $5^{\circ}$. The equations used to reduce the basic experimental data are included and will allow the user to incorporate additional data which might become available.

Langley Research Center,
National Aeronautics and Space Administration,
Langley Station, Hampton, Va., September 20, 1965.

## APPENDIX A

## DETERMINATION OF DISTRIBUTED AERODYNAMIC COEFFICIENTS FROM FORCE- AND PRESSURE-TEST DATA

### Force-Test Data

Loading functions can be derived from force-test data in which the variation of the normal-force coefficient with model length has been determined. The following sketch illustrates a typical curve of $C_{N_\alpha}$ plotted against $x/D_o$ from such a test.

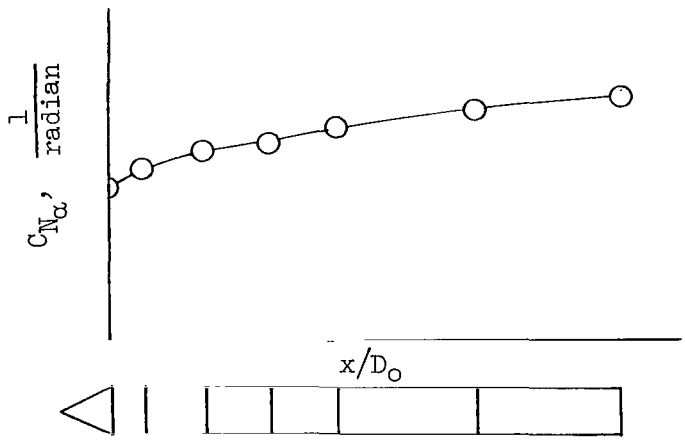


The change in model length is usually achieved by changing the length of one of the geometric components used in the configuration through the use of stacked segments. The change in $C_{N_\alpha}$ due to the addition of a segment provides a means of determining the contribution of the segment.

Unfortunately, the curves of $C_{N_\alpha}$ plotted against component length were not always smooth and determining the slopes of the curves by differentiation allowed for potentially large errors. Both graphical and numerical means were employed to determine the slopes and the results were weighted in light of continuity of data. Where possible, the method of least squares was used to fit a curve to the data points and the derivative of this curve was calculated and used. The slopes were also calculated by differentiation of the Lagrangian interpolation formula. The coefficients developed in reference 14 were used in this procedure. The slopes calculated by these various techniques were compared wherever questionable results were obtained. For those cases where the data scatter was especially bad, intuitive estimates were made based upon similar results. The exact procedures used for the various component parts of a vehicle configuration are subsequently developed.

## APPENDIX A

The total normal force is usually given by

$$F_N = q\alpha C_{N_\alpha} S \tag{A1}$$

Taking the partial derivative of equation (A1) with respect to $x$ (where $\alpha$ is assumed to be constant) along the body yields,

$$\frac{\partial F_N}{\partial x} = q\alpha\left(\frac{\partial C_{N_\alpha}}{\partial x} S + C_{N_\alpha} \frac{\partial S}{\partial x}\right) \tag{A2}$$

The reference area $S$ is allowed to be a possible function of $x$ at this point.

By definition, the dimensionless loading function, $\lambda$, is related to $F_N$ by:

$$\frac{\partial F_N}{\partial x} = q\alpha\left\{S \frac{dC_{N_\alpha}}{dx}\right\} = q\alpha\lambda D \tag{A3}$$

Substituting equation (A3) into equation (A2) yields

$$\lambda = \frac{1}{D}\left(C_{N_\alpha} \frac{\partial S}{\partial x} + S \frac{\partial C_{N_\alpha}}{\partial x}\right) \tag{A4}$$

Using the form in which the referenced force-test data for the various components was usually presented, the following specific data-reduction equations have been derived.

Cones.- The total normal-force coefficient $C_{N_\alpha}$ for cones is usually presented as a function of cone semivertex angle and Mach number only. By allowing the reference area to be the cone base area, $C_{N_\alpha}$ becomes a constant with cone length. In this case $\frac{\partial C_{N_\alpha}}{\partial x} = 0$ and equation (A4) becomes

$$\lambda = \frac{1}{D} C_{N_\alpha} \frac{\partial S}{\partial x} \tag{A5}$$

but

$$\frac{\partial S}{\partial x} = \frac{\pi}{2} \frac{x}{f_n^2} \tag{A6}$$

Substituting equation (A6) into equation (A5) yields

$$\lambda = \frac{\pi}{2} \frac{C_{N_\alpha}}{f_n} \quad \text{where} \quad f_n = \frac{x}{D} = \frac{l}{D_o} \tag{A7}$$

Cylinders.- For cylindrical elements, the reference area S is taken as a constant equal to the cylinder cross-sectional area. Equation (A4) then becomes

$$\lambda = \frac{\pi}{4} \frac{\partial C_{N_\alpha}}{\partial \frac{x}{D_o}} \tag{A8}$$

Frustums and boattails.- For both frustums and boattails, the reference area is usually taken to be a constant value; therefore, equation (A4) becomes, for frustums,

$$\lambda = \frac{\pi}{4}\left(\frac{1}{1 + 2\frac{x}{D_o}\tan\theta_f}\right)\frac{\partial C_{N_\alpha}}{\partial \frac{x}{D_o}} \tag{A9}$$

where $D = D_o + 2x \tan \theta_f$, and for boattails,

$$\lambda = \frac{\pi}{4}\left(\frac{1}{1 - 2\frac{x}{D_o}\tan\theta_b}\right)\frac{\partial C_{N_\alpha}}{\partial \frac{x}{D_o}} \tag{A10}$$

where $D = D_o - 2x \tan \theta_b$.

Equations (A7) to (A10) were used extensively in reducing the referenced force-test data to the loading functions presented in this paper.

## Pressure-Test Data

The conversion from pressure-test data to the previously defined loading function is presented in reference 15. The final form of the equation relating load functions to pressure coefficients as presented in reference 15 is

$$\frac{1}{D}\left\{S \frac{dC_{N_\alpha}}{dx}\right\} = -\int_0^\pi \frac{C_p}{\alpha_t} \cos \phi \, d\phi \tag{A11}$$

where

$\alpha_t$ test angle of attack

$C_p$ pressure coefficient, $\frac{p - p_\infty}{q_\infty}$

$\phi$ angle between the lift plane and an inclined plane intersecting the lift plane along the vehicle axis of revolution

D local diameter of the cross section normal to the axis of revolution, $D = 2r$.

## APPENDIX A

### Spherical Segments

The loading function can be approximated for a spherical segment by use of equation (A11) and an approximate relationship for the pressure distribution.

In the following sketch, consider the point b on the spherical surface lying in the plane Oab which is inclined the angle $\phi$ with respect to the vertical plane and intercepts the vertical plane along the vehicle axis of revolution.

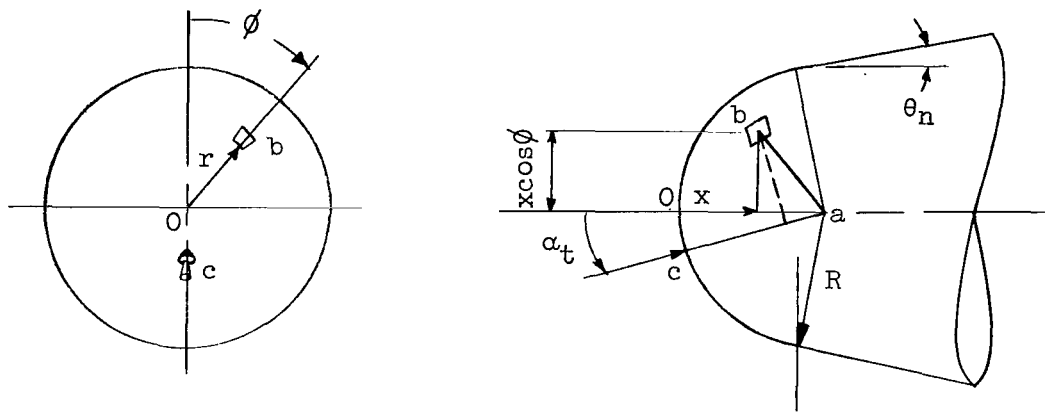


Defining $\beta$ as the angle between the normal to the surface at the stagnation point (ca) and the radius (ab = R) from the origin of the spherical surface to the point b, then the pressure coefficient $C_p$ can be approximated by the relationship

$$C_p = A \cos^2\beta + B \tag{A12}$$

If a transformation to the x, r, and $\phi$ body coordinates is made, equation (A12) becomes

$$C_p = A\left[\left(1 - \frac{x}{R}\right)\cos \alpha_t - \frac{r}{R} \sin \alpha_t \cos \phi\right]^2 + B \tag{A13}$$

where

R sphere radius; $R = D_o/2$

and

r local radius of the cross section at x normal to the vehicle axis of revolution; $r = D/2$

x coordinate along the axis of revolution of the vehicle and having its origin at the surface of the sphere

If equation (A13) is substituted into equation (A11) there will result

$$\frac{1}{D}\left\{S\,\frac{dC_{N_\alpha}}{dx}\right\} = -\int_0^\pi \frac{A\left[\left(1 - \frac{x}{R}\right)\cos\alpha_t - \frac{r}{R}\sin\alpha_t\cos\phi\right]^2 + B}{\alpha_t}\cos\phi\,d\phi \tag{A14}$$

For the spherical surface; r, x, and R are constrained by

$$\frac{r}{R} = 2\sqrt{\frac{x}{D_o}\left(1 - \frac{x}{D_o}\right)} \tag{A15}$$

Imposing the constraint of equation (A15) on equation (A14), integrating, and using the customary approximations for small angles of attack (i.e., $\cos\alpha = 1$, $\sin\alpha = \alpha$), equation (A14) yields

$$\frac{1}{D}\left\{S\,\frac{dC_{N_\alpha}}{dx}\right\} = 4\pi A\left(\frac{1}{2} - \frac{x}{D_o}\right)\sqrt{\frac{x}{D_o}\left(1 - \frac{x}{D_o}\right)} \tag{A16}$$

where the constant B vanished by virtue of

$$\int_0^\pi B\cos\phi\,d\phi = 0$$

Values for the undefined coefficient A are obtainable by comparing the maxima of equation (A16) with comparative maxima obtained from reference 15 for various Mach numbers.

Equation (A16) is valid within the bounds on positive x values given by the following condition

$$\frac{x}{D_o} \leqq \frac{1 - \sin\theta_n}{2} \tag{A17}$$

where $\theta_n$ is the semivertex angle of the nose cone. The preceding limit restricts the use of equation (A16) to x values from zero to the x position of the tangent of the nose cone to the spherical surface.

## APPENDIX B

## APPLICATION OF METHOD

The empirical method presented in the body of the report is utilized to determine the distributed aerodynamic loads for a typical launch-vehicle configuration. The configuration for which data are generated is shown in figure B1. Data will be developed only for Mach 2.4 whereas in actual practice distributed loads for a range of Mach numbers would be required.

The vehicle is first broken down into components for which data are available. For the configuration under consideration, there will be five components

(1) Spherical nose cap

(2) Cone following a spherical nose cap

(3) Cylinder following a cone

(4) Frustum following a cone-cylinder combination

(5) Cylinder following a frustum

### Spherical Nose Cap

For a spherical nose cap, the bluntness ratio of the conical nose is given as $b_n = 0.40$; the cone semivertex angle is given as $\theta_n = 22.5^{\circ}$; and the cylinder diameter $D_1$ is 2.17 meters. By using the relationships given in table B1, the local diameter at the various $x/D_o$ stations can be determined. It should be noted that $x/D_o = 0$ corresponds to the tip of the vehicle and $x/D_o = 0.309$ corresponds to the point at which the sphere meets the cone. For this component, $D_o$ is the sphere diameter. The appropriate curve from figure 2(b) is then used to determine the $\frac{1}{D}\left\{S \frac{dC_{N_\alpha}}{dx}\right\}$ values at the $x/D_o$ stations of interest. In this example, interpolation on Mach number is required. These values are then multiplied by the local diameters to yield the product of the reference area and the distributed normal-force-coefficient slope $\left\{S \frac{dC_{N_\alpha}}{dx}\right\}$ tabulated in table B1.

### Cone Following Spherical Nose Cap

The cone data in figure 3(a) are used to determine the load distribution on a blunted cone. Since the loading on a cone is a constant, only two values of

$\frac{1}{D}\left\{S\frac{dC_{N_\alpha}}{dx}\right\}$ are required: one at the tangency point and one at the cone-cylinder junction. A straight line is then drawn between them. The expression given in table B2 is used to calculate the diameter at the sphere-cone tangency point. For a sharp cone the diameter would be zero. The reference diameter for cones $D_o$ is taken to be the maximum diameter of the cone or $D_o = D_1 = 2.17$ meters. The appropriate value of $\frac{1}{D}\left\{S\frac{dC_{N_\alpha}}{dx}\right\}$ is obtained from figure 3(a). For this case interpolation is not required on cone semivertex angle. This value is then multiplied by the diameters at the tangency point, $D_T$, and the cone base, $D_o$, respectively, to obtain the two end points of the final curve of $\left\{S\frac{dC_{N_\alpha}}{dx}\right\}$ for the cone. The final curve for the complete blunted cone is shown in the following sketch:

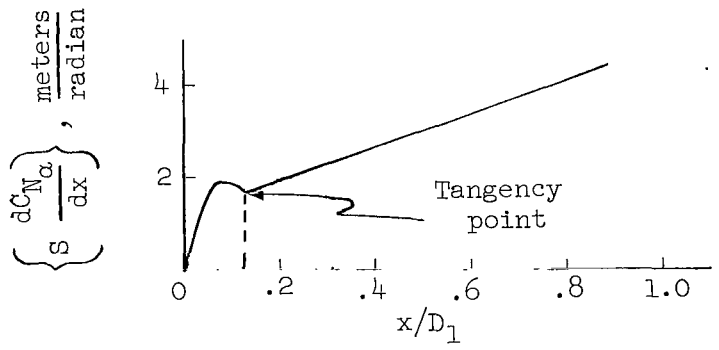


Sphere-Cone Combination

The curves of figure 5(d) are used to obtain the loading on a cylinder following a cone. The reference diameter for cylinders is the cylinder diameter or $D_o = D_1 = 2.17$ meters. The cylinder of this configuration has a fineness ratio of 4.87. The curves of figure 5 are for cylinders following sharp cones; however, since the effect of blunting on the cylinder loading is secondary, these curves are also used for cylinders following blunt cones. From figure 5(d), the values of $\frac{1}{D}\left\{S\frac{dC_{N_\alpha}}{dx}\right\}$ for a cylinder following a cone with semivertex angle $\theta_n = 22.5^\circ$ are obtained. Linear interpolation on $\theta_n$ is used to determine the appropriate values. These values are then multiplied by the cylinder diameter and tabulated in table B3. The final curve is shown in the following sketch:

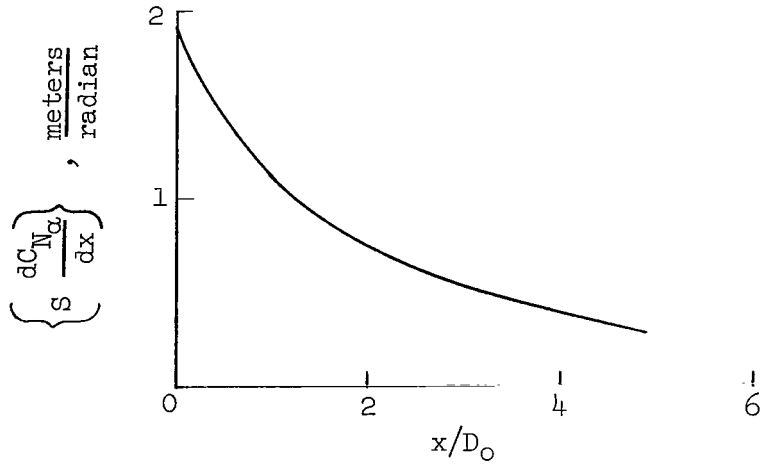


Cylinder Following Cone

The frustum data are presented in figures 6 and 7. The parameters which affect the loading on a frustum are the nose angle $\theta_n$, the preceding cylinder length $\left(f_{a,1}\right)$, the frustum angle $\left(\theta_f\right)$, and the Mach number (M). For the configuration under consideration, $\theta_n = 22.5$, $f_{a,1} = 4.87$, and $\theta_f = 5$. The reference diameter $D_o$ for a frustum is the minimum diameter; therefore, $D_o = D_1 = 2.17$ meters. The fineness ratio of a frustum $f_f$ and the local diameter D in terms of x/D stations can be obtained by using the formulas found in table B4 as follows, hence:

$$f_f = 2.42$$

$$D = 2.17\left(1 + 0.1750 \frac{x}{D_o}\right)$$

By using the foregoing equation the appropriate values of D can be calculated. Since $f_{a,1}$ is greater than 4.0, the loading on the frustum is no longer considered to be a function of $\theta_n$. Therefore, the only parameter for which interpolation of the available data is required is Mach number. The data of figure 6(g) and figure 6(i) were used with $f_{a,1} = 4.0$ and $\theta_f = 5^\circ$. From these curves, the values of $\frac{1}{D}\left\{S \frac{dC_{N_\alpha}}{dx}\right\}$ at the appropriate $x/D_o$ locations are read. These values are then multiplied by their respective local diameters to yield the final frustum loading curve. The desired data for Mach 2.4 are tabulated in the next to the last column on table B4.

## APPENDIX B

### Cylinder Following Frustum

The data figures 8(d) and 8(e) are used to determine the loading on a cylinder following a frustum. For the configuration under consideration, the parameters affecting the cylinder loading are the frustum angle $\left(\theta_f\right)$, the cylinder-diameter ratio $\left(D_1/D_o\right)$, and the Mach number (M). Since curves are available for a $5^o$ frustum angle, the only interpolations which are necessary are with respect to $D_1/D_o$ and Mach number. The reference diameter for this component is 3.09 meters. The fineness ratio is 6.98. The interpolated values of $\left\{S \frac{dC_{N_\alpha}}{dx}\right\}$ are given in table B5.

The normal-force-coefficient slope for the configuration shown in figure B1 has now been determined for Mach 2.40. All that remains is to combine the component data. It should be noted that the values of $x/D_o$ at which the data curves were read are completely arbitrary. The only criterion to be considered is the adequate description of the loading functions. When the component data are combined, discontinuities may exist in the final curve. This is a valid condition and these discontinuities are associated with the discontinuities which occur in the slope of a meridian section of the body. Where body-slope discontinuities do not exist, the loading function should be faired together to form a smooth curve. For this configuration this condition occurs at the sphere-cone interface. The reference point for plotting the final curve is also arbitrary, and, for this case, the nose of the vehicle has been chosen as the zero station for the $\mu$ coordinate of the combined system. To convert the component $x/D_o$ coordinates to the combined coordinates $\mu$, the component $x/D_o$ values are multiplied by the appropriate $D_o$ for each component and added to the final $\mu$ station of the previous component. The initial and final stations for each component are given in the $\mu$ columns of tables B1 to B5. As stated previously, the reference area term is also arbitrary and should it be desired to convert the final $\left\{S \frac{dC_{N_\alpha}}{dx}\right\}$ curve given in figure B1 to $\frac{dC_{N_\alpha}}{dx}$ form, all that is required is division by the selected reference area. This may be the maximum cross-sectional area of the cylinder or the configuration planform area, or in the event fins are used, the fin planform area.

APPENDIX B

TABLE B1.- APPLICATION OF METHOD TO SPHERICAL SEGMENTS

$\theta_n = 22.5^\circ$

$D_1 = 2.17$ meters

$b_n = D_s/D_1 = 0.40$

$D_o = D_s$ = Sphere diameter = 0.868 meter

$D = 2D_o\sqrt{x/D_o - \left(x/D_o\right)^2}$

$D_T = b_n D_1 \cos\theta_n = 0.802$ meter

$l = \left(D_o/2\right)\left(1 - \sin\theta_n\right) = 0.268$ meter

$\mu_o = 0$

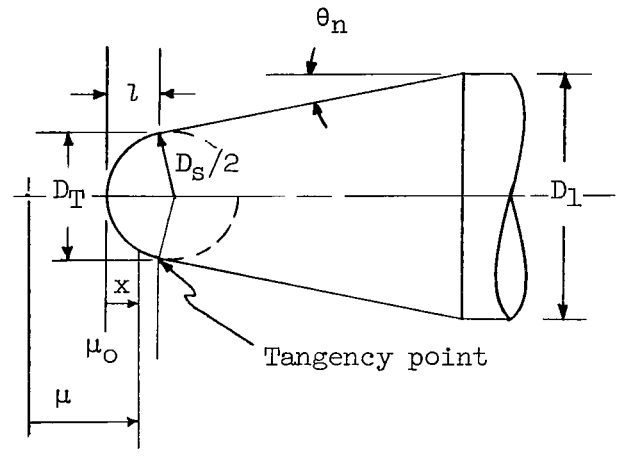


| $\mu$, meters | $x/D_o = \frac{\mu - \mu_o}{D_o}$ | D, meters | $\frac{1}{D}\left\{S\frac{dC_{N_\alpha}}{dx}\right\}$, 1/radian at M = 2.4 | $\left\{S\frac{dC_{N_\alpha}}{dx}\right\}$, meters/radian at M = 2.4 |
|---|---|---|---|---|
| 0 | 0 | 0 | 0 | 0 |
| .043 | .050 | .378 | 2.33 | .88 |
| .087 | .100 | .521 | 2.85 | 1.49 |
| .130 | .150 | .620 | 2.98 | 1.85 |
| .174 | .200 | .694 | 2.86 | 1.99 |
| .217 | .250 | .752 | 2.58 | 1.94 |
| .260 | .300 | .795 | 2.20 | 1.75 |
| .268 | .309 | .802 | 2.12 | 1.70 |

TABLE B2.- APPLICATION OF METHOD TO CONES

$D_o = D_1 = 2.17$ meters

$b_n = D_s/D_1 = 0.40$

$\theta_n = 22.5^o$

$D_T = b_n D_1 \cos \theta_n = 0.802$ meter

$$l = \frac{D_1 - D_T}{2 \tan \theta_n} = 1.652 \text{ meters}$$

$\mu_o = 0.268$ meter

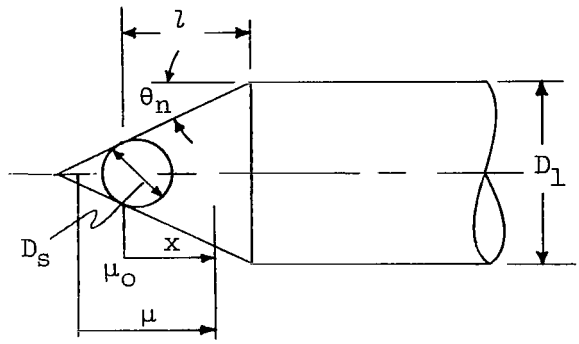


| $\mu$, meters | $\frac{x}{D_o} = \frac{\mu - \mu_o}{D_o}$ | D, meters | $S\left\{\frac{dC_{N_\alpha}}{dx}\right\}$, meters/radian at M = 2.4 |
|---|---|---|---|
| 0.268 | 0 | 0.802 | 1.67 |
| 1.920 | .761 | 2.17 | 4.51 |

TABLE B3.- APPLICATION OF METHOD TO CYLINDER FOLLOWING CONES

$D_o = D_1 = 2.17$ meters

$l = 10.579$ meters

$f_a = \frac{l}{D_1} = 4.875$

$\theta_n = 22.5^o$

$\mu_o = 1.920$ meters

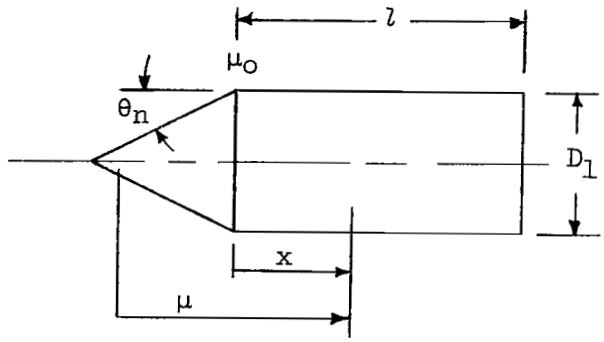


| $\mu$, meters | $\frac{x}{D_o} = \frac{\mu - \mu_o}{D_o}$ | D, meters | $\left\{S \frac{dC_{N_\alpha}}{dx}\right\}$, meters/radian at M = 2.4 |
|---|---|---|---|
| 1.920 | 0 | 2.17 | 1.90 |
| 2.353 | .2 | ↓ | 1.67 |
| 2.788 | .4 | | 1.50 |
| 3.222 | .6 | | 1.35 |
| 3.655 | .8 | | 1.22 |
| 4.090 | 1.0 | | 1.11 |
| 5.174 | 1.5 | | .88 |
| 6.260 | 2.0 | | .71 |
| 8.430 | 3.0 | | .54 |
| 10.600 | 4.0 | | .39 |
| 12.499 | 4.875 | | .28 |

TABLE B4.- APPLICATION OF METHOD TO FRUSTUMS FOLLOWING CONE-CYLINDERS

$D_o = D_1 = 2.17$ meters

$\theta_f = 5^o$

$\theta_n = 22.5^o$

$f_{a,1} = 4.875$

$D_2 = 3.09$ meters

$$f_f = \frac{D_2 - D_1}{2D_1 \tan \theta_f} = \frac{l}{D_1} = 2.423$$

$$D = D_o\left(1 + 2\frac{x}{D_o} \tan \theta_f\right)$$

$\mu_o = 12.499$ meters

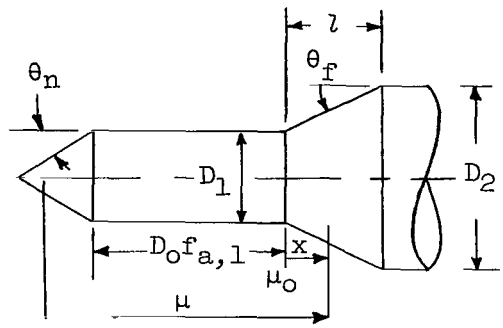


| $\mu$, meters | $\frac{x}{D_o} = \frac{\mu - \mu_o}{D_o}$ | D, meters | $\frac{1}{D}\left\{S \frac{dC_{N_\alpha}}{dx}\right\}$, 1/radian at - | | $\left\{S \frac{dC_{N_\alpha}}{dx}\right\}$, meters/radian at - | | |
|---|---|---|---|---|---|---|---|
| | | | M = 2.18 | M = 2.81 | M = 2.18 | M = 2.4 | M = 2.81 |
| 12.499 | 0 | 2.17 | 0.23 | 0.20 | 0.50 | 0.48 | 0.43 |
| 13.584 | .5 | 2.36 | .37 | .12 | .87 | .66 | .28 |
| 14.669 | 1.0 | 2.55 | .50 | .13 | 1.28 | .95 | .33 |
| 15.754 | 1.5 | 2.74 | .60 | .17 | 1.64 | 1.23 | .47 |
| 16.839 | 2.0 | 2.93 | .66 | .23 | 1.93 | 1.49 | .67 |
| 17.757 | 2.423 | 3.09 | .70 | .31 | 2.16 | 1.74 | .96 |

TABLE B5.- APPLICATION OF METHOD TO CYLINDERS FOLLOWING FRUSTUMS

$D_o = D_2 = 3.09$ meters

$D_1/D_o = 0.70$

$\theta_f = 5^o$

$f_{a,2} = \frac{l}{D_2} = 6.98$

$\mu_o = 17.757$ meters

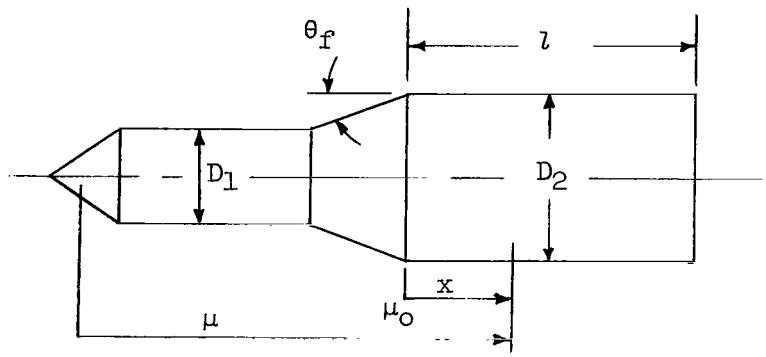


| $\mu$, meters | $\frac{x}{D_o} = \frac{\mu - \mu_o}{D_o}$ | D, meters | $\left\{S \frac{dC_{N_\alpha}}{dx}\right\}$, meters/radian at - | | |
|---|---|---|---|---|---|
| | | | M = 1.5 | M = 2.4 | M = 2.5 |
| 17.757 | 0 | 3.09 | 0.700 | 0.597 | 0.586 |
| 19.302 | .5 | ↓ | .552 | .507 | .502 |
| 20.847 | 1.0 | | .453 | .436 | .434 |
| 22.392 | 1.5 | | .360 | .371 | .377 |
| 23.937 | 2.0 | | .291 | .313 | .316 |
| 27.027 | 3.0 | | .202 | .233 | .236 |
| 30.117 | 4.0 | | .143 | .182 | .186 |
| 33.207 | 5.0 | | .109 | .150 | .155 |
| 39.409 | 6.98 | | .049 | .111 | .117 |

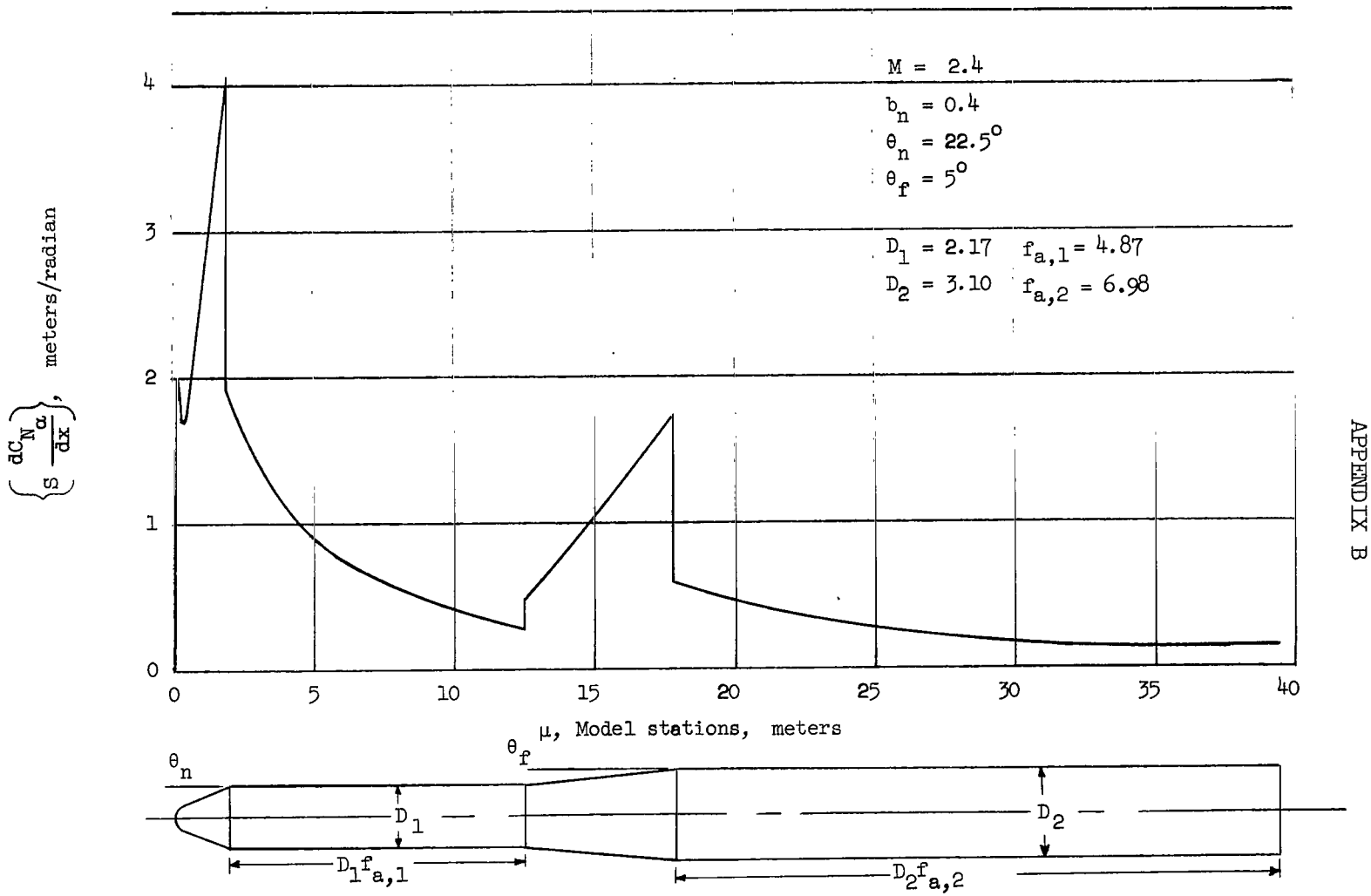


Figure B1.- Product of reference area and the distributed normal-force-coefficient slope for typical launch-vehicle configuration.

## REFERENCES


1. Kelly, A. H.; and Ross, F. W.: A Supersonic Body Profile Developmental Study. UMM-58 (USAF Contract W-33-038-ac-14222), Aeron. Res. Center, Univ. of Michigan, July 31, 1950.

2. Van Dyke, Milton D.: First- and Second-Order Theory of Supersonic Flow Past Bodies of Revolution. J. Aeron. Sci., vol. 18, no. 3, Mar. 1951, pp. 161-178.

3. Ross, F. W.; and Dorrance, W. H.: An Introduction to a Supersonic Body Developmental Study. UMM-40 (USAF Contract W33-038-ac-14222), Aeron. Res. Center, Univ. of Michigan, Dec. 1949.

4. Anon.: Handbook of Supersonic Aerodynamics. Section 8 - Bodies of Revolution, NAVWEPS Report 1488 (Vol. 3), U.S. Govt. Printing Office, Oct. 1961.

5. Nielson, Jack N.: Missile Aerodynamics. McGraw-Hill Book Co., Inc., 1960.

6. Truitt, Robert Wesley: Hypersonic Aerodynamics. The Ronald Press Co., c.1959.

7. Syvertson, Clarence A.; and Dennis, David H.: A Second-Order Shock-Expansion Method Applicable to Bodies of Revolution Near Zero Lift. NACA Rept. 1328, 1957. (Supersedes NACA TN 3527.)

8. Phythian, J. E.; and Dommett, R. L.: Semi-Empirical Methods of Estimating Forces on Bodies at Supersonic Speeds. J. Roy. Aeron. Soc., vol. 62, no. 571, July 1958, pp. 520-524.

9. Kelly, Howard R.: The Estimation of Normal Force and Pitching Moment Coefficients for Blunt-Based Bodies of Revolution at Large Angles of Attack. TM-988, U.S. Naval Ord. Test Station, May 27, 1953.

10. Grimminger, G.; Williams, E. P.; and Young, G. B. W.: Lift on Inclined Bodies of Revolution in Hypersonic Flow. J. Aeron. Sci., vol. 17, no. 11, Nov. 1950, pp. 675-690.

11. Morrison, D. F.: Experimental Normal Force and Centre-of-Pressure Data for a Series of Cone-Cylinder Combinations at Mach Numbers 1.6 to 2.8. Tech. Note HSA 82, Weapons Res. Estab., Australian Defence Sci. Serv., Feb. 1962.

12. Rittenhouse, L. E.; and Kaupp, H., Jr.: Influence of Several Shape Parameters on the Aerodynamics of Ballistic Re-Entry Configurations. AEDC TR-60-13, U.S. Air Force, Dec. 1963.

13. Norell, R. G.: Normal Force, Pitching Moment and Normal Force Distributions of Cone-Cylinders at Supersonic Speeds. Rept. ZA-7-010, Consolidated Vultee Aircraft Corp., Apr. 2, 1954.

14. Salzer, Herbert E.: Table of Coefficients for Obtaining the First Derivative Without Differences. Natl. Bur. Std. Appl. Math. Ser. 2, U.S. Dept. Com., Apr. 22, 1948.

15. Muraca, Ralph J.: Aerodynamic Load Distributions for the Project Fire Configurations at Mach Numbers From 0.25 to 4.63. NASA TN D-2604, 1965.

16. Sims, Joseph L.: Tables for Supersonic Flow Around Right Circular Cones at Small Angles of Attack. NASA SP-3007, 1964.

17. Geudtner, W. J., Jr.: Sharp and Blunted Cone Force Coefficients and Centers of Pressure From Wind Tunnel Tests at Mach Numbers From 0.50 to 4.06. Rept. No. ZA-7-017, Convair/Astronaut., June 16, 1955.

18. Tinling, Bruce E.; and Allen, Clyde Q.: An Investigation of the Normal-Force and Vortex-Wake Characteristics of an Ogive-Cylinder Body at Subsonic Speeds. NASA TN D-1297, 1962.

19. Swihart, John M.; and Whitcomb, Charles F.: Pressure Distributions on Three Bodies of Revolution To Determine the Effect of Reynolds Number up to and Including the Transonic Speed Range. NACA RM L53H04, 1953.

20. Eckstrom, D. J.; French, N. J.; and Navone, M. V.: Analysis of Aerodynamic Characteristics of the NASA Mariner C Ascent Vehicle From Static Stability and Static Pressure Wind Tunnel Tests. TM 53-41-15, Lockheed Missiles and Space Co., Sept. 1963.

21. Kelly, Thomas C.: Investigation at Transonic Mach Numbers of the Effects of Configuration Geometry on Surface Pressure Distributions for a Simulated Launch Vehicle. NASA TM X-845, 1963.

22. Sims, Joseph L.; and Henderson, James H.: Normal Force, Pitching Moment, and Center of Pressure of Eighty Cone-Cylinder-Frustum Bodies of Revolution at Mach Number 2.81. Rept. 6R3N2, Ordnance Missile Labs., Redstone Arsenal, Mar. 28, 1956.

23. Wakefield, Roy M.; and Knechtel, Earl D.: Transonic Static Aerodynamic Characteristics of a Blunt Cone-Cylinder Body With Flared Afterbodies of Various Angles and Base Areas. NASA TM X-106, 1959.

24. Lavender, Robert E.: Normal Force, Pitching Moment, and Center of Pressure of Eighty Cone-Cylinder-Frustum Bodies of Revolution at Mach Number 1.50. Rept. 6R3N3, Ordnance Missile Labs., Redstone Arsenal, Apr. 5, 1956.

25. Henderson, James H.; and Sims, Joseph L.: Normal Force, Pitching Moment, and Center of Pressure of Eighty Cone-Cylinder-Frustum Bodies of Revolution at Mach Number 4.04. Rept. 6R3N1, Ordnance Missile Labs., Redstone Arsenal, Mar. 1, 1956.

26. Kelly, Thomas C.: Aerodynamic Loading Characteristics at Mach Numbers From 0.80 to 1.20 of a 1/10-Scale Three-Stage Scout Model. NASA TN D-945, 1961.

27. Jernell, Lloyd S.: Aerodynamic Loading Characteristics of a 1/10-Scale Model of the Three-Stage Scout Vehicle at Mach Numbers From 1.57 to 4.65. NASA TN D-1930, 1963.

28. Jorgensen, Leland H.; Spahr, J. Richard; and Hill, William A., Jr.: Comparison of the Effectiveness of Flares With That of Fins for Stabilizing Low-Fineness-Ratio Bodies at Mach Numbers From 0.6 to 5.8. NASA TM X-653, 1962.

29. Wakefield, Roy M.; Treon, Stuart L.; and Knechtel, Earl D.: Effects of Centerbody Length and Nose Shape on the Transonic Characteristics of Low-Fineness-Ratio Bodies of Revolution With a Flared Afterbody. NASA TM X-366, 1960.

30. Glover, Warren G.: Investigation of the Aerodynamics of Basic Multistage Missile Shapes at Mach Numbers 1.5 to 5.0. AEDC-TR-61-3, U.S. Air Force, July 1961.

31. Tempelmeyer, K. E.; and Glover, W. G.: Generalization of the Aerodynamic Performance of Multistage Missile Configurations at Supersonic Speeds. AEDC-TR-61-5, U.S. Air Force, July 1961.

32. Cartwright, Edgar M., Jr.; and Schroeder, Albert H.: Investigation at Mach Number 1.91 of Side and Base Pressure Distributions Over Conical Boattails Without and With Jet Flow Issuing From Base. NACA RM E51F26, 1951.

33. Maxwell, N. E.; and Shutts, W. H.: Aerodynamic Effects of Boattailing on a Body of Revolution - Mach Numbers 1.5, 2.0 & 2.5. Rept. No. CM-645 (Contract No. NORD 9028), Consolidated Vultee Aircraft Corp., Mar. 15, 1951.

34. Staylor, W. Frank; and Goldberg, Theodore J.: Afterbody Pressures on Two-Dimensional Boattailed Bodies Having Turbulent Boundary Layers at Mach 5.98. NASA TN D-2350, 1964.

35. Mello, John F.: Investigation of Normal-Force Distributions and Wake Vortex Characteristics of Bodies of Revolution at Supersonic Speeds. Rept. 4666 (Contract No. NOrd 12826), McDonnell Aircraft Corp., Apr. 2, 1956.

36. Hertler, E. G.: Pressure Tests on Circular Cone Cylinders at Mach 4.22 and 5.05. Rept. ZA-7-008, Consolidated Vultee Aircraft Corp., Aug. 1, 1952.

37. Buford, W. E., and Shatunoff, S.: The Effects of Fineness Ratio and Mach Number on the Normal Force and Center of Pressure of Conical and Ogival Head Bodies. Mem. Rept. No. 760, Ballistic Res. Labs., Aberdeen Proving Ground, Feb. 1954.

38. Chaplin, H.; and DeMeritte, F. J.: Static Stability and Axial Force Measurements on Cone-Cylinders. NAVORD Rept. 2882, U.S. Naval Ord. Lab., May 26, 1953.

39. Marks, A. S.: Normal Force, Pitching Moment, and Center of Pressure on Several Spherically Blunted Cones at Mach Numbers of 1.5, 2.18, 2.81, and 4.04. Ordnance Missile Laboratories Report 6R8F, April 1958.

40. Lavender, Robert E.; Henderson, James H.; and Deep, Raymond A.: Normal Force, Pitching Moment, and Center of Pressure of Eighty Cone-Cylinder-Frustum Bodies of Revolution at Mach Number 2.18. Rept. 6R3P, Ordnance Missile Labs., Redstone Arsenal, Jan. 23, 1956.

41. Jaeger, B. F.; and Morgan, A. J. A.: A Review of Experiment and Theory Applicable to Cone-Cylinder and Ogive-Cylinder Bodies of Revolution in Supersonic Flow. NAVORD Rept. 5239 (NOTS 1438), U.S. Naval Ord. Test Station, June 12, 1956.

42. Dennis, David H.; and Cunningham, Bernard E.: Forces and Moments on Pointed and Blunt-Nosed Bodies of Revolution at Mach Numbers From 2.75 to 5.00. NACA RM A52E22, 1952.

43. Perkins, Edward W.; and Jorgensen, Leland H.: Comparison of Experimental and Theoretical Normal-Force Distributions (Including Reynolds Number Effects) on an Ogive-Cylinder Body at Mach Number 1.98. NACA TN 3716, 1956. (Supersedes NACA RM A54H23.)

44. Katz, Jerome R.: Pressure and Wave Drag Coefficients for Hemispheres, Hemisphere-Cones, and Hemisphere-Ogives. NAVORD Rept. 5849, Mar. 21, 1958.

45. Smith, Fred M.: A Wind-Tunnel Investigation of the Effects of Nose Bluntness, Face Shape, and Afterbody Length on the Aerodynamic Characteristics of Bodies of Revolution at Mach Numbers of 2.37, 2.98, and 3.90. NASA TM X-230, 1960.

46. Leach, R. N.: Presentation and Discussion of the Nimbus-Atlas Vehicle Transonic and Supersonic Force and Pressure Test Data. TM-57-15-04 (Contract AF 04(647)-787), Lockheed Missiles and Space Co., Apr. 30, 1962.

47. Reding, J. P.: Separated Flow Effects on the Static Stability of Cone-Cylinder-Flare Bodies. TM 53-40-119 (LMSC/802336), Lockheed Missiles and Space Co., [1962].

48. Wuerer, J. E.; and Clayton, F. I.: Flow Separation in High Speed Flight - A Review of the State-of-the-Art. Rept. SM-46429, Missile & Space Systems Div., Douglas Aircraft Co., Apr. 1965.

TABLE I

COMPONENTS FOR WHICH LOADING FUNCTIONS ARE AVAILABLE AND

THE PARAMETER RANGES COVERED

| Component | Parameter ranges | Mach number |
|---|---|---|
| 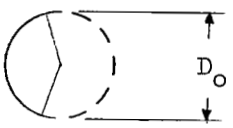  | | 0.25 to 4.63 |
| 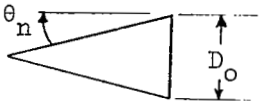  | $2.5^\circ < \theta_n < 50^\circ$ | 0.7 to 8.0 |
| 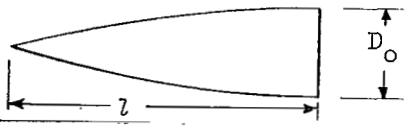  | $1.4 < f_n = l/D_o < 6.0$ | 0.8 to 5.0 |
| | $3.5^\circ < \theta_n < 35^\circ$ | 0.8 to 6.9 |
| | $3.0 < f_n = l/D_o < 7.0$ | 0.8 to 6.3 |
| 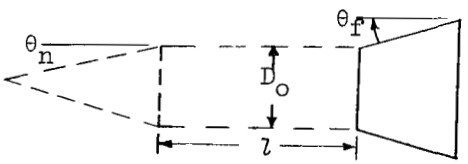  | $14.2^\circ < \theta_n < 30^\circ$<br>$0 < f_{a,1} = l/D_o < 4.0$<br>$5^\circ < \theta_f < 30^\circ$ | 0.8 to 4.0 |
| 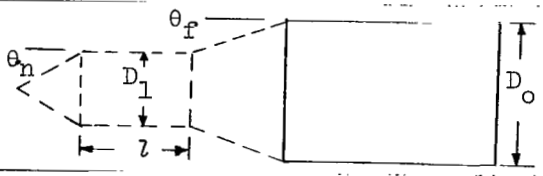  | $f_{a,1} = l/D_1 > 4.0$<br>$5^\circ < \theta_f < 30^\circ$<br>$0 < D_1/D_o < .75$ | 0.8 to 5.0 |
| 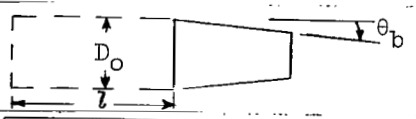  | $4^\circ < \theta_b < 18^\circ$<br>$2.0 < f_{a,1} = l/D_o < \infty$ | 0.8 to 6.0 |
| 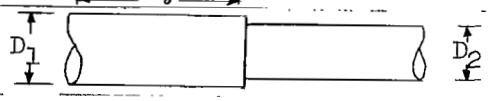  | $D_1/D_2 = 1.08$ | 0.8 to 5.0 |

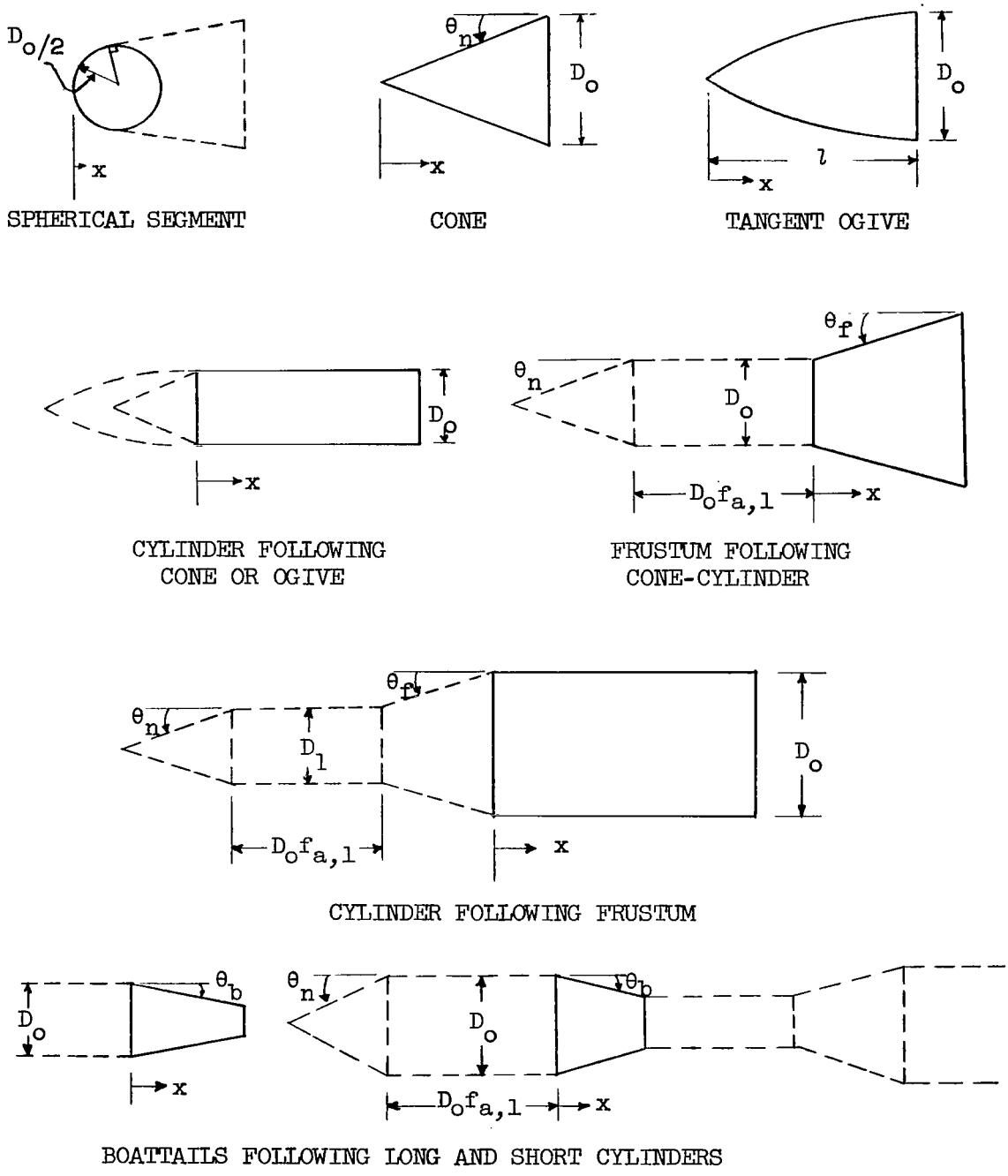


Figure 1.- Parameters used to define geometrical components.

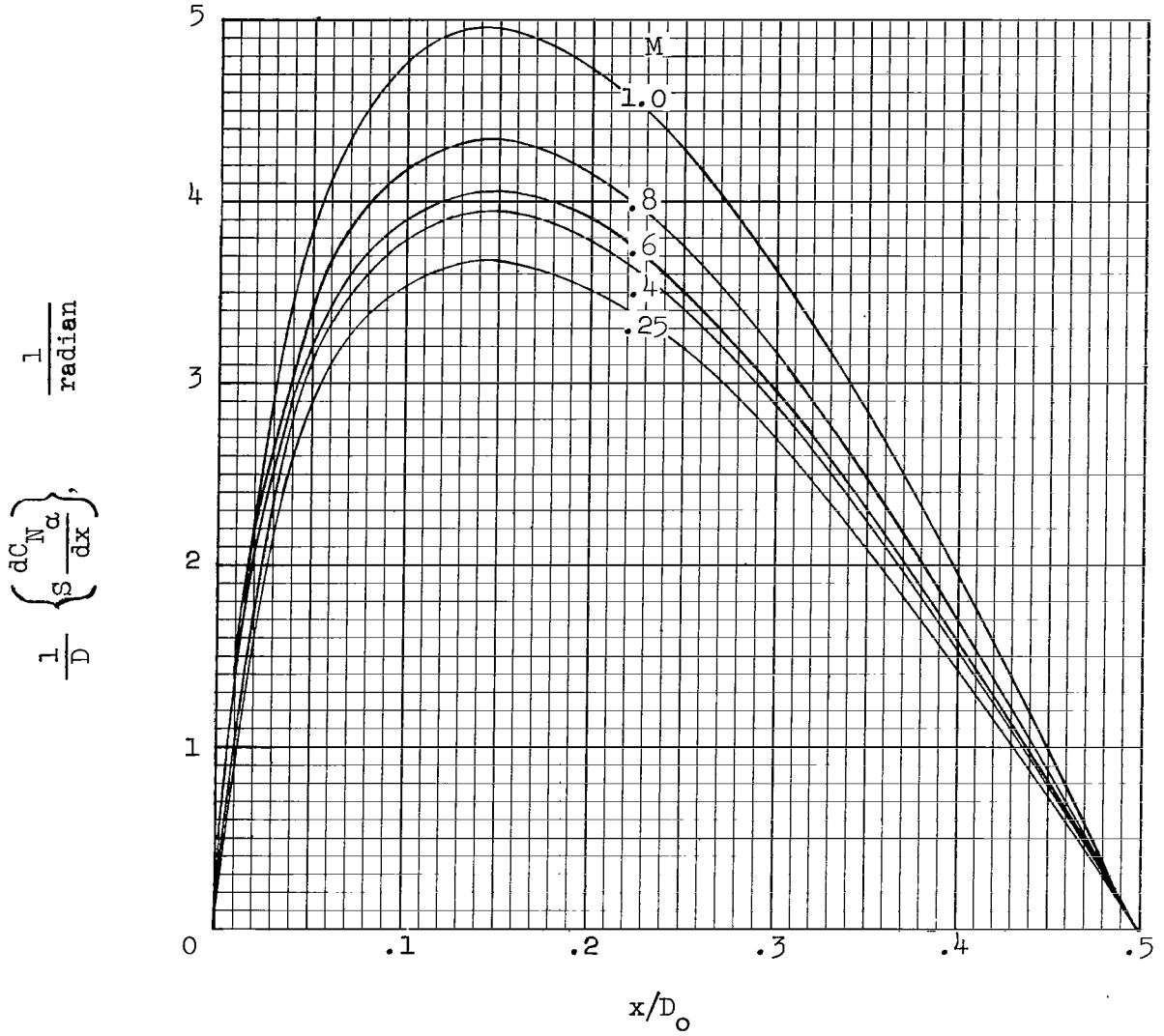


(a) M = 0.25 to 1.

Figure 2.- Loading functions for spherical segments for various Mach numbers.

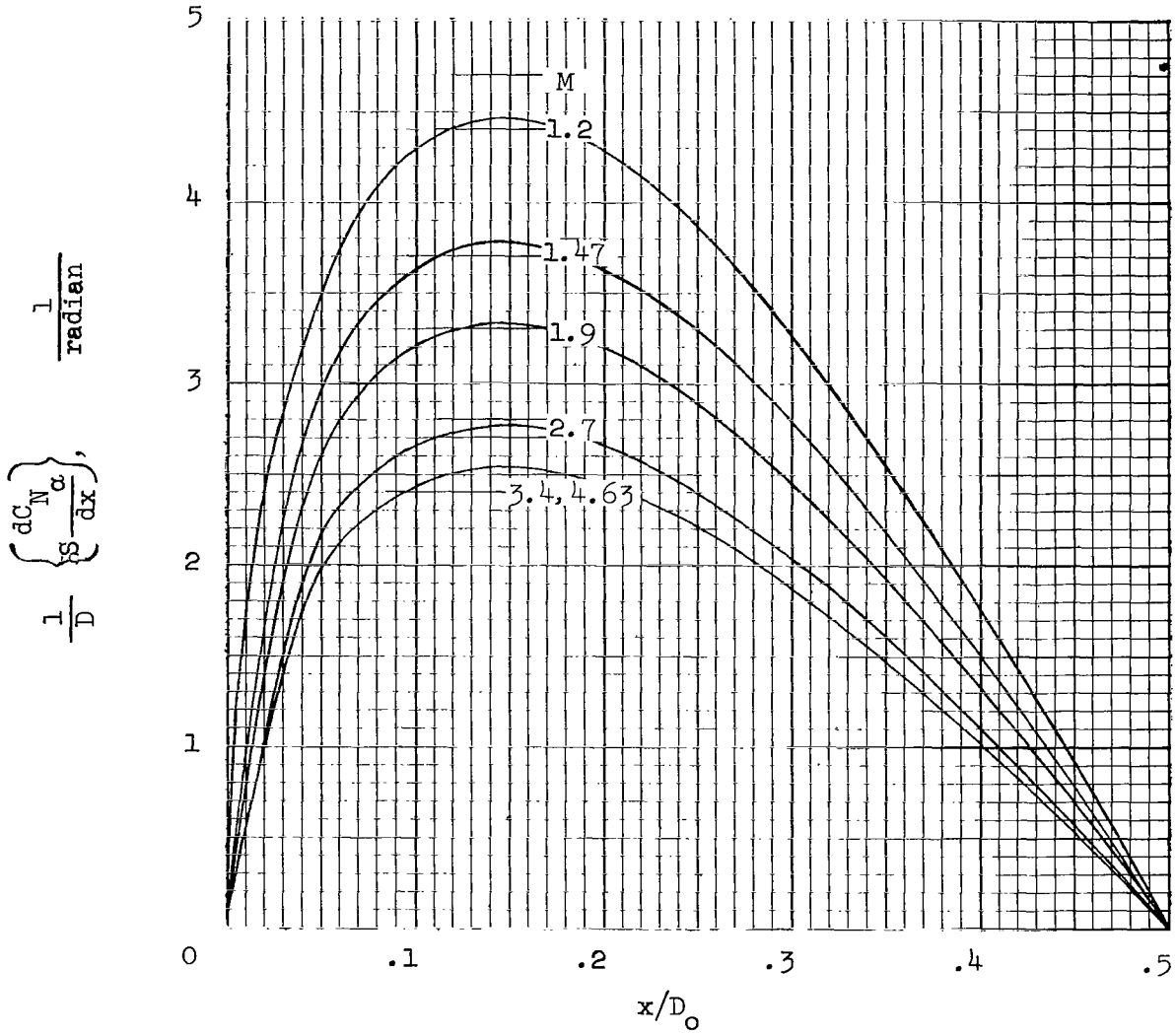


(b) M = 1.2 to 4.63.

Figure 2.- Concluded.

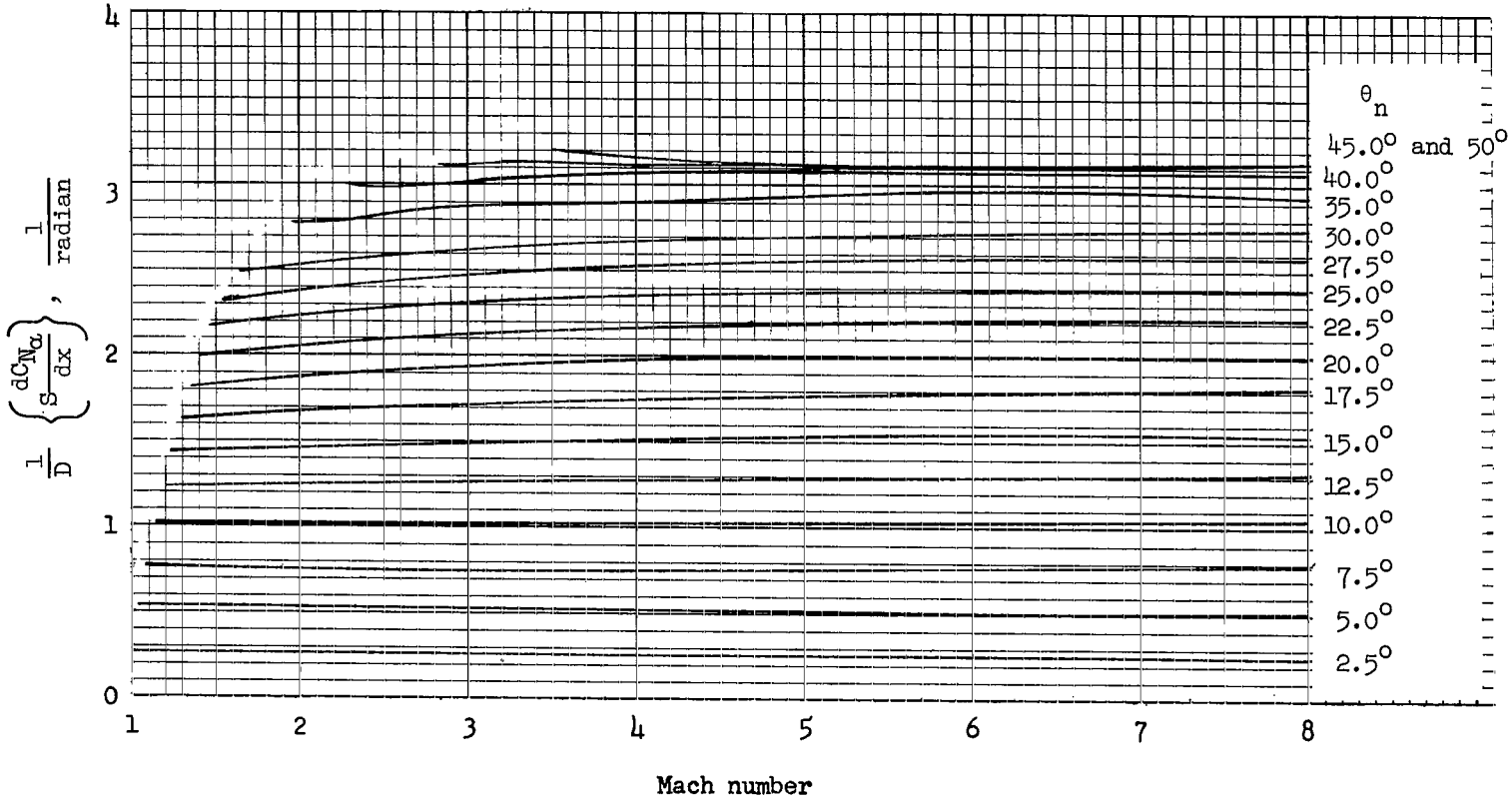


(a) Analytical results.

Figure 3.- Loading functions for cones of various semivertex angles.

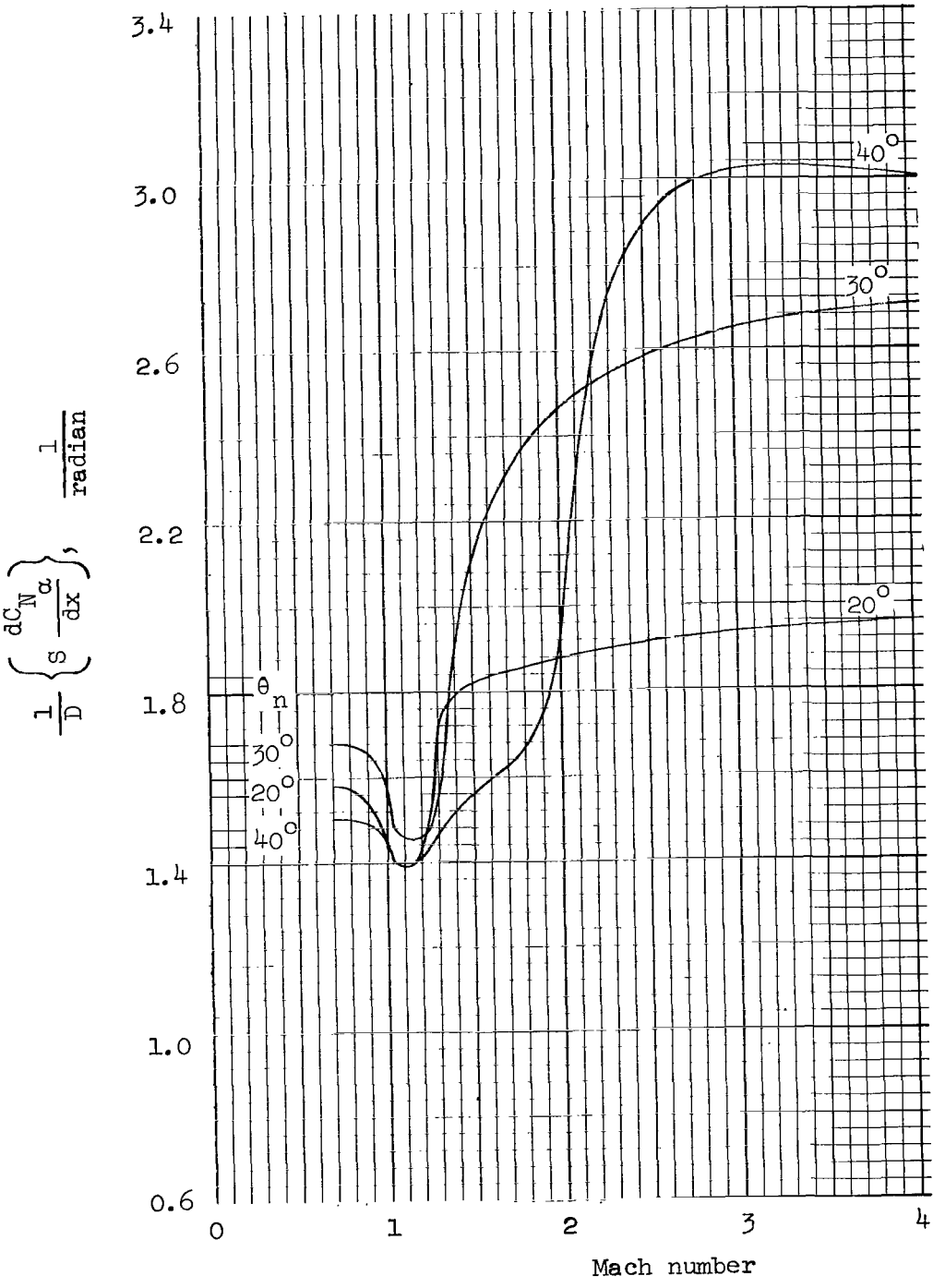


(b) Experimental results.

Figure 3.- Concluded.

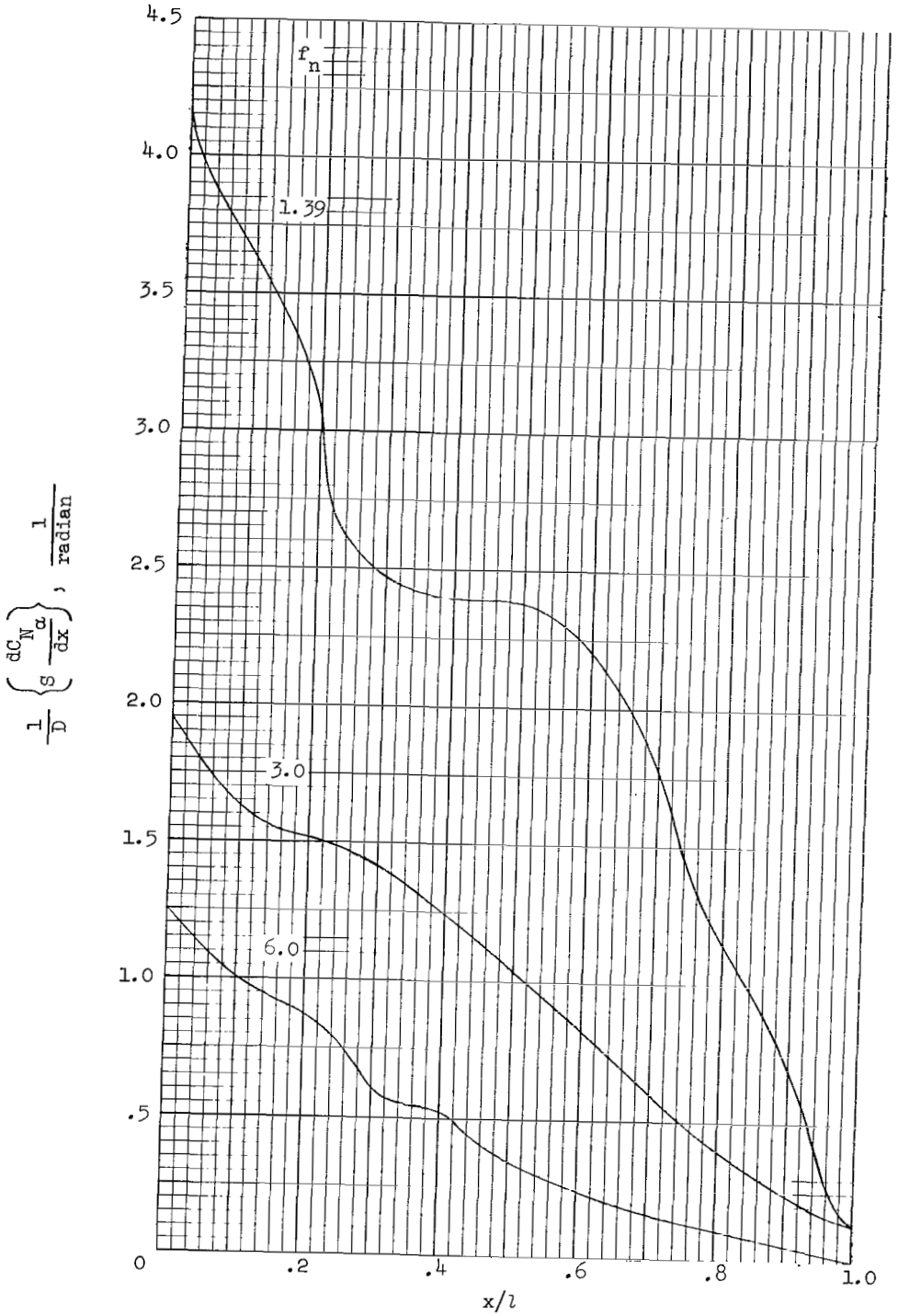


(a) M = 0.8.

Figure 4.- Loading functions for tangent ogives.

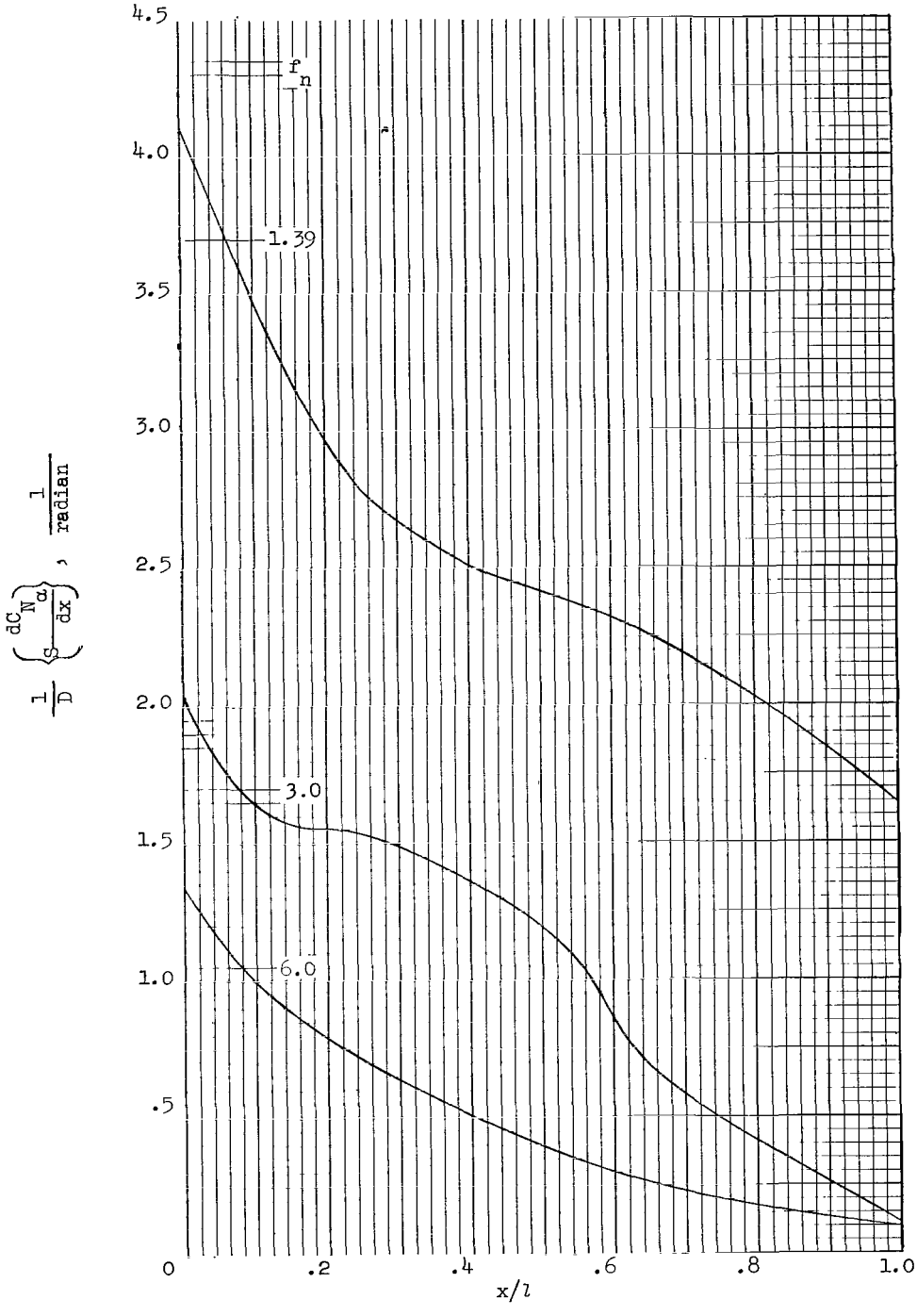


(b) M = 1.0.

Figure 4.- Continued.

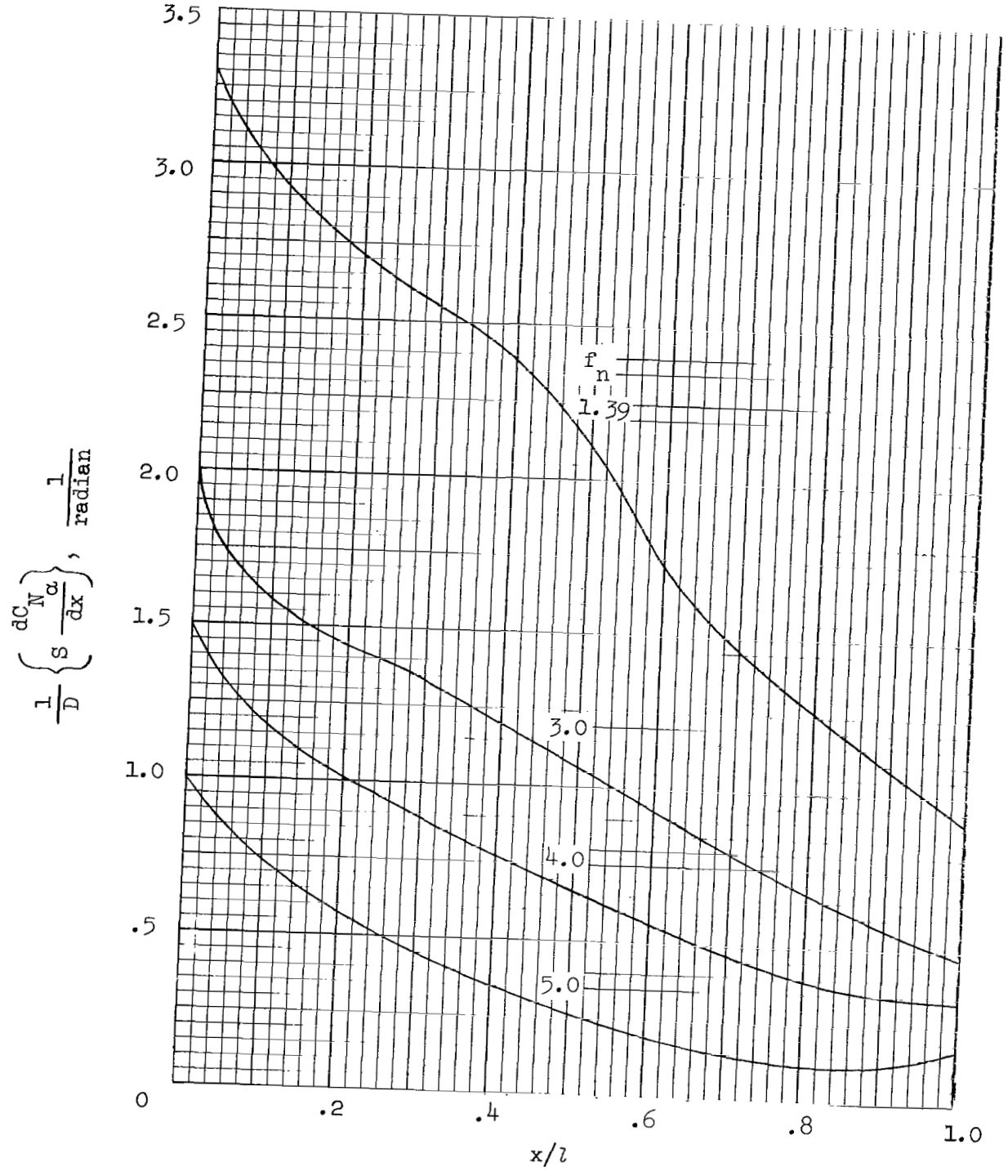


(c) M = 2.0.

Figure 4.- Continued.

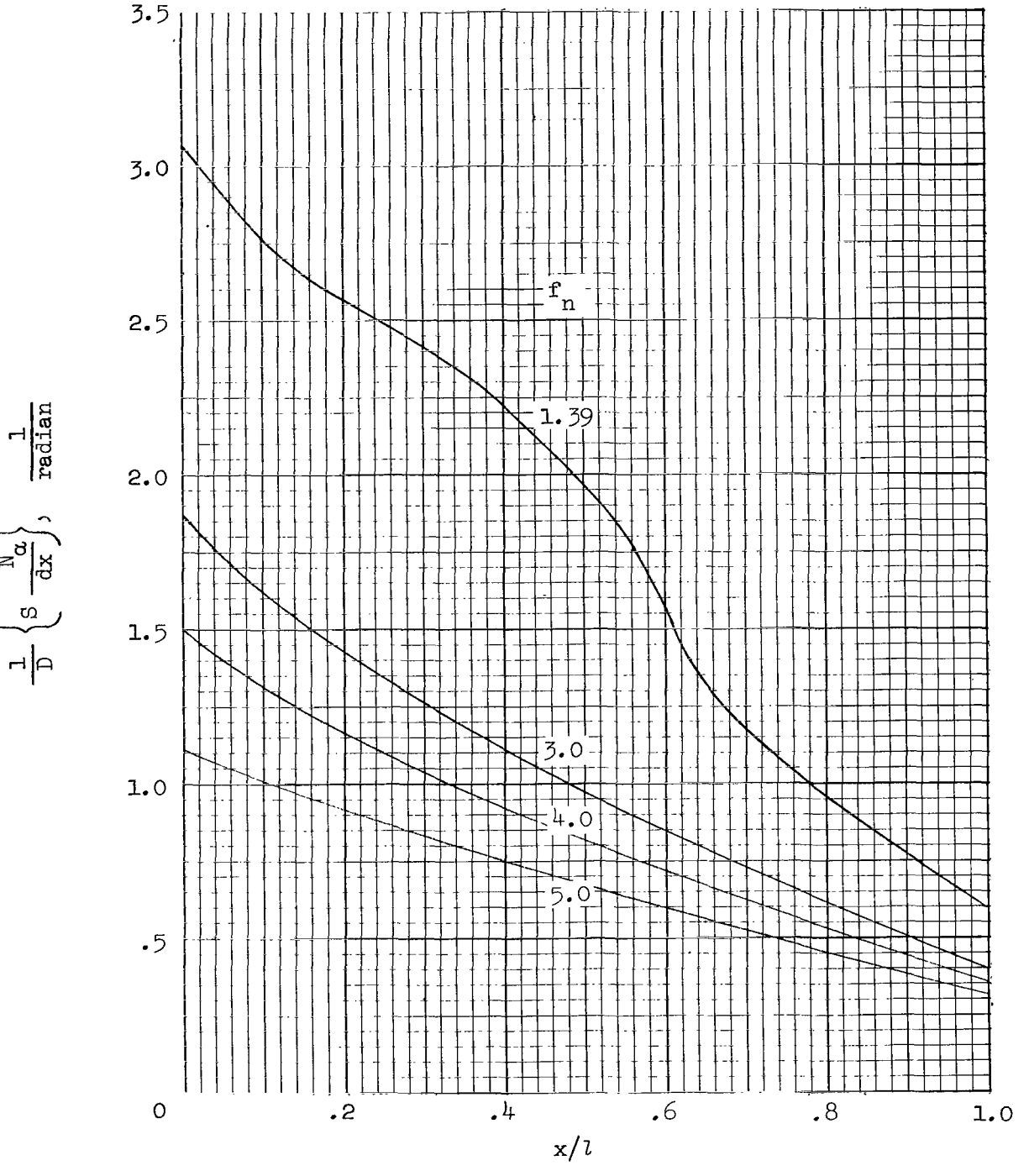


(d) M = 3.0.

Figure 4.- Continued.

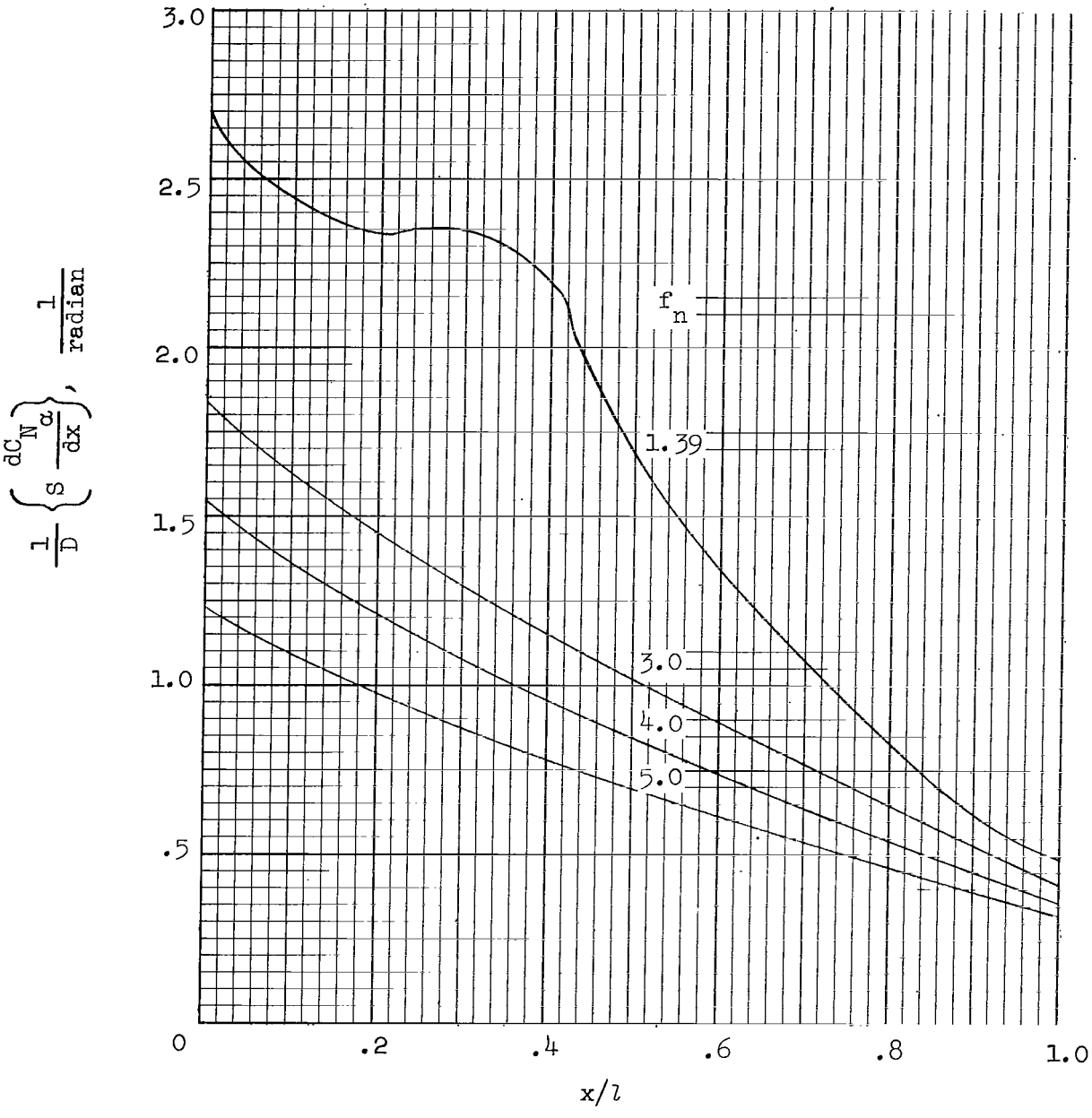


(e) M = 4.25.

Figure 4.- Continued.

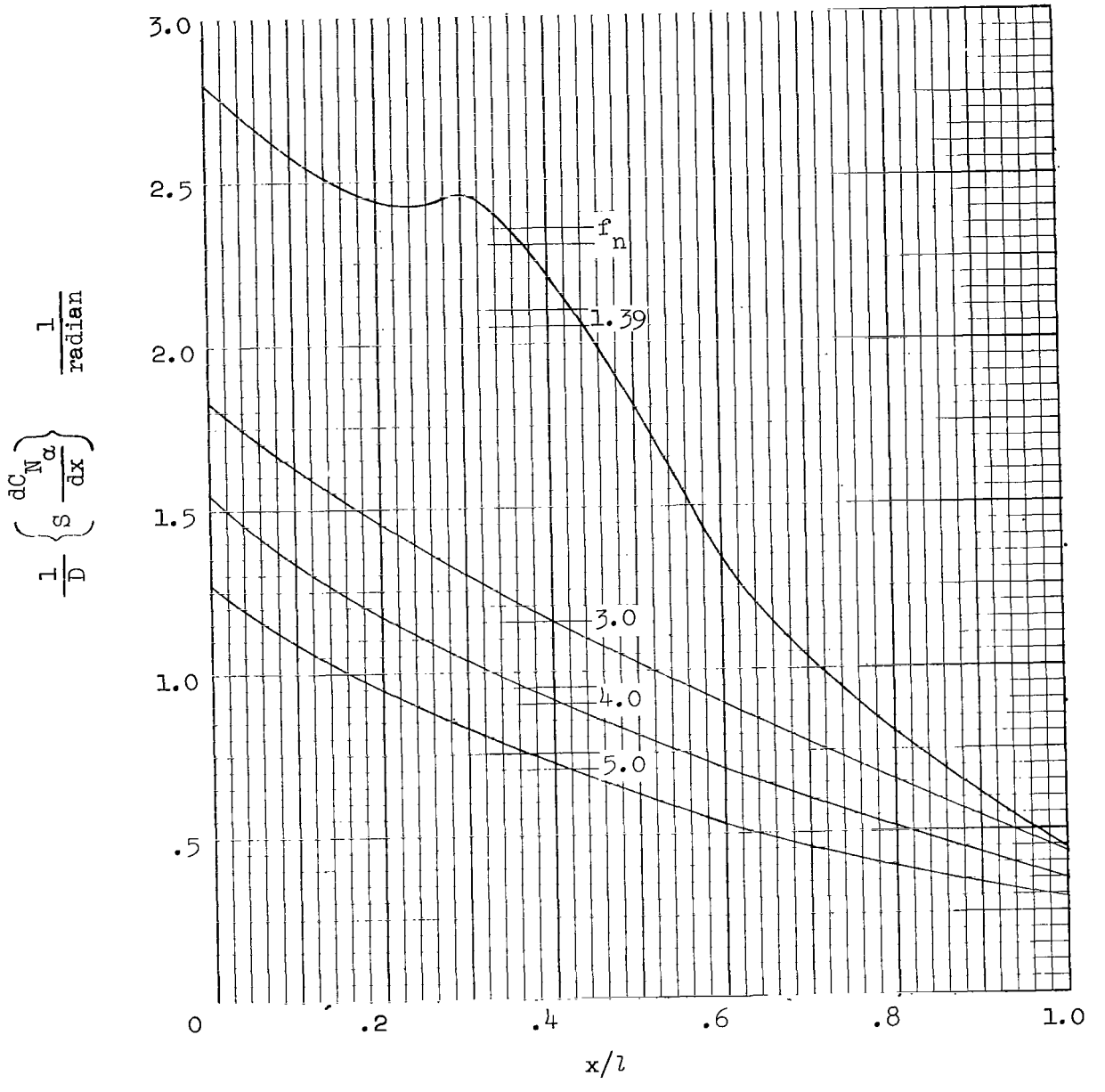


(f) M = 5.05.

Figure 4.- Concluded.

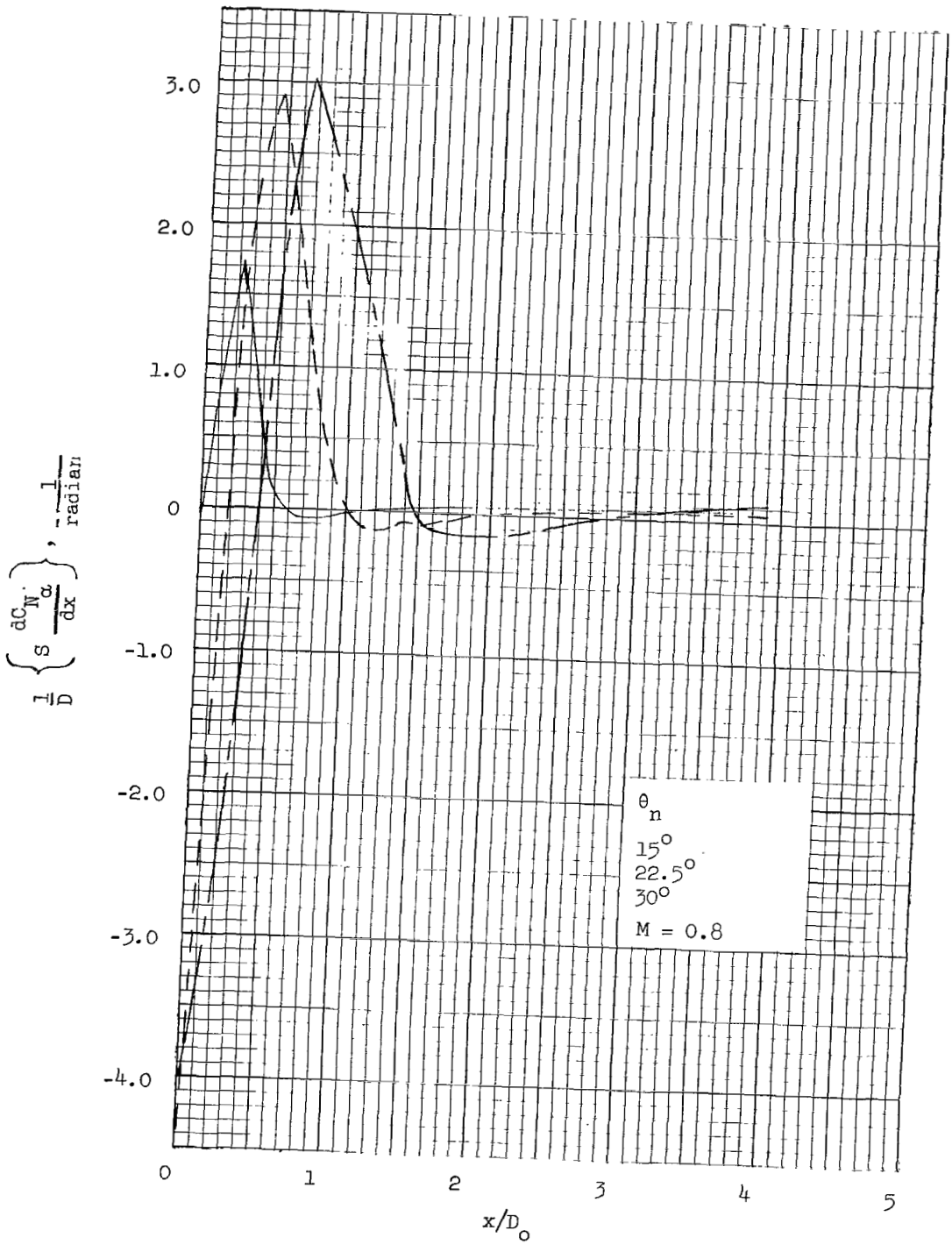


(a) Cylinder following cones; M = 0.8.

Figure 5.- Loading functions for cylinders following cones and tangent ogives.

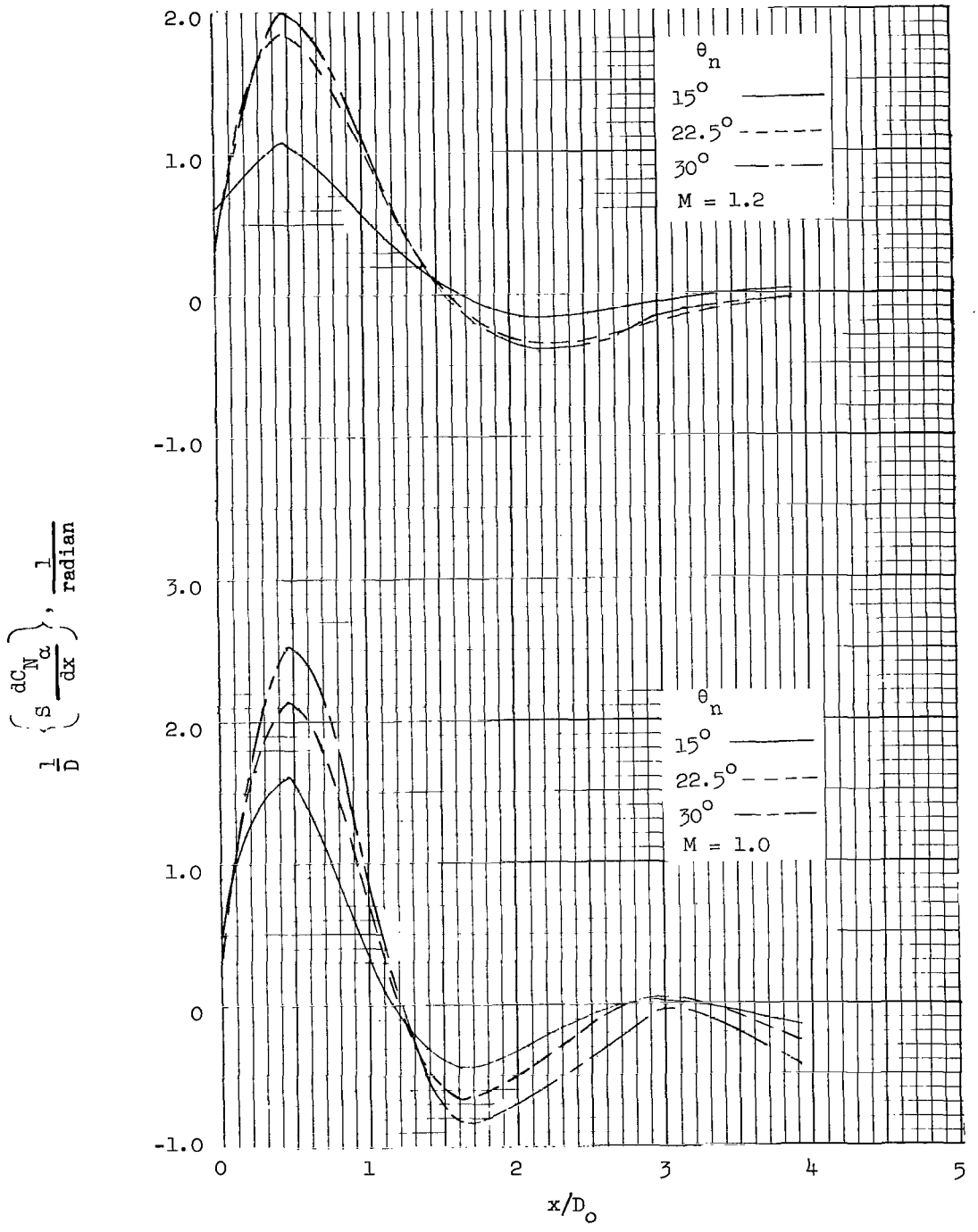


(b) Cylinders following cones; M = 1.0 and 1.2.

Figure 5.- Continued.

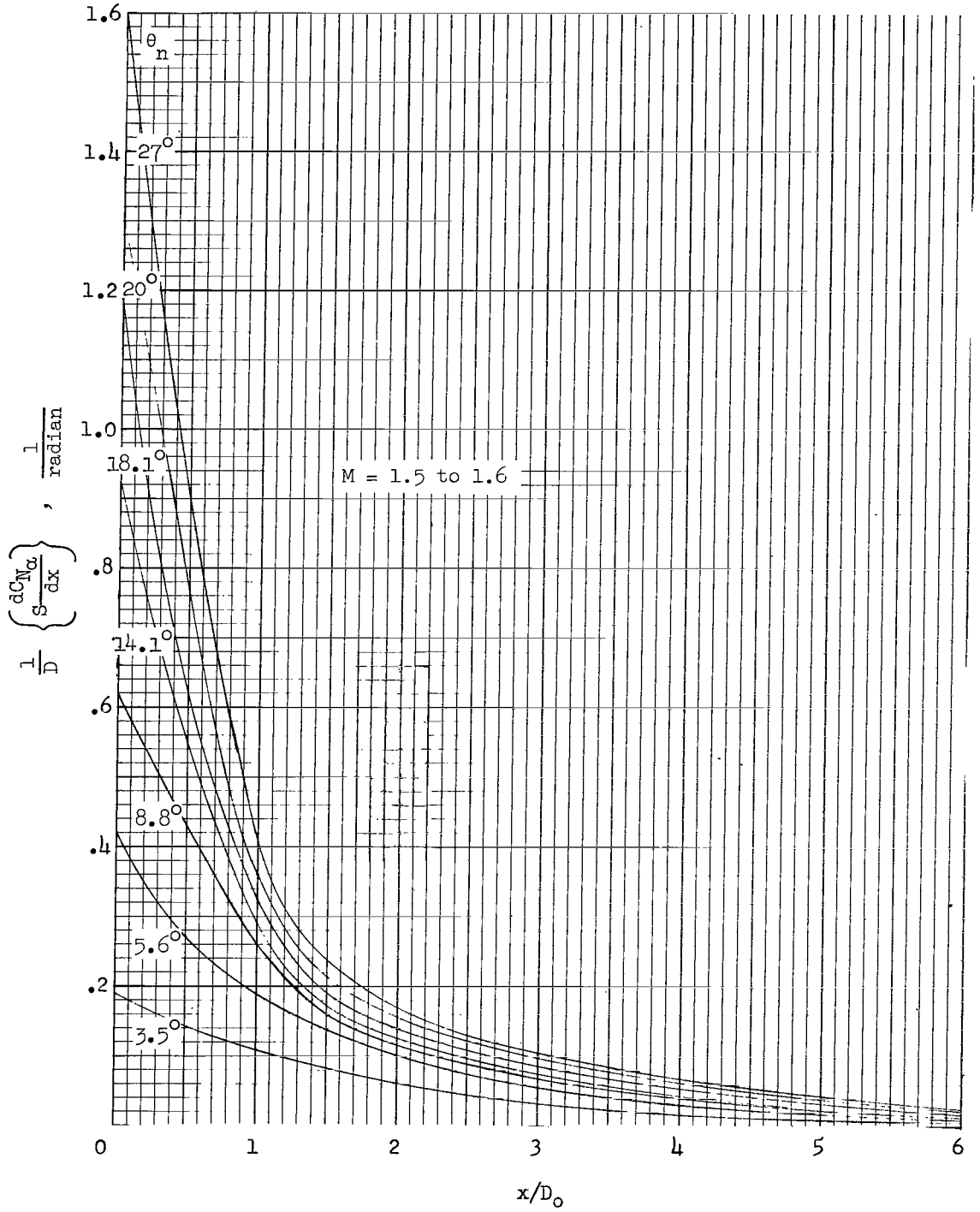


(c) Cylinders following cones; M = 1.5 to 1.6.

Figure 5.- Continued.

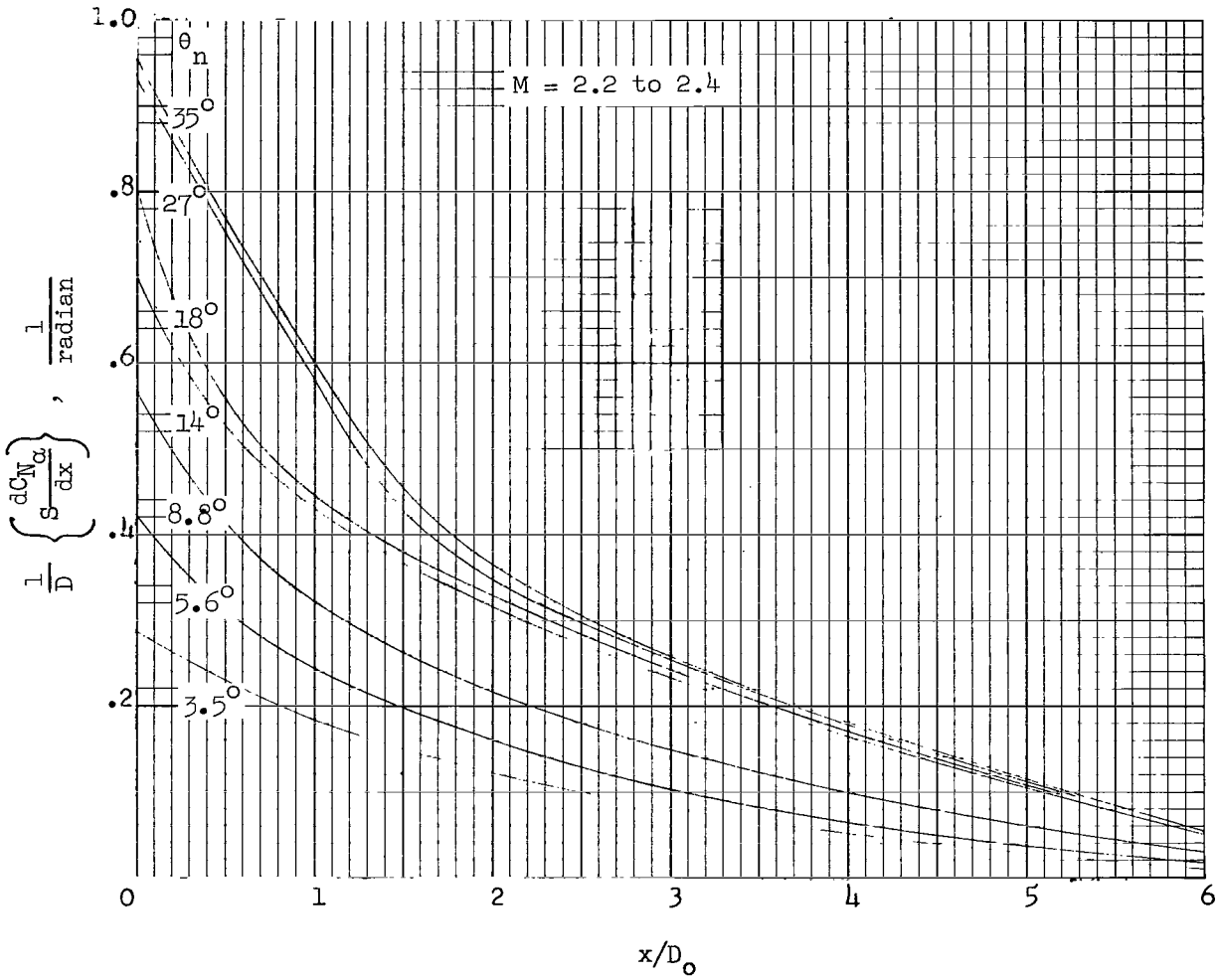


(d) Cylinders following cones; M = 2.2 to 2.4.

Figure 5.- Continued.

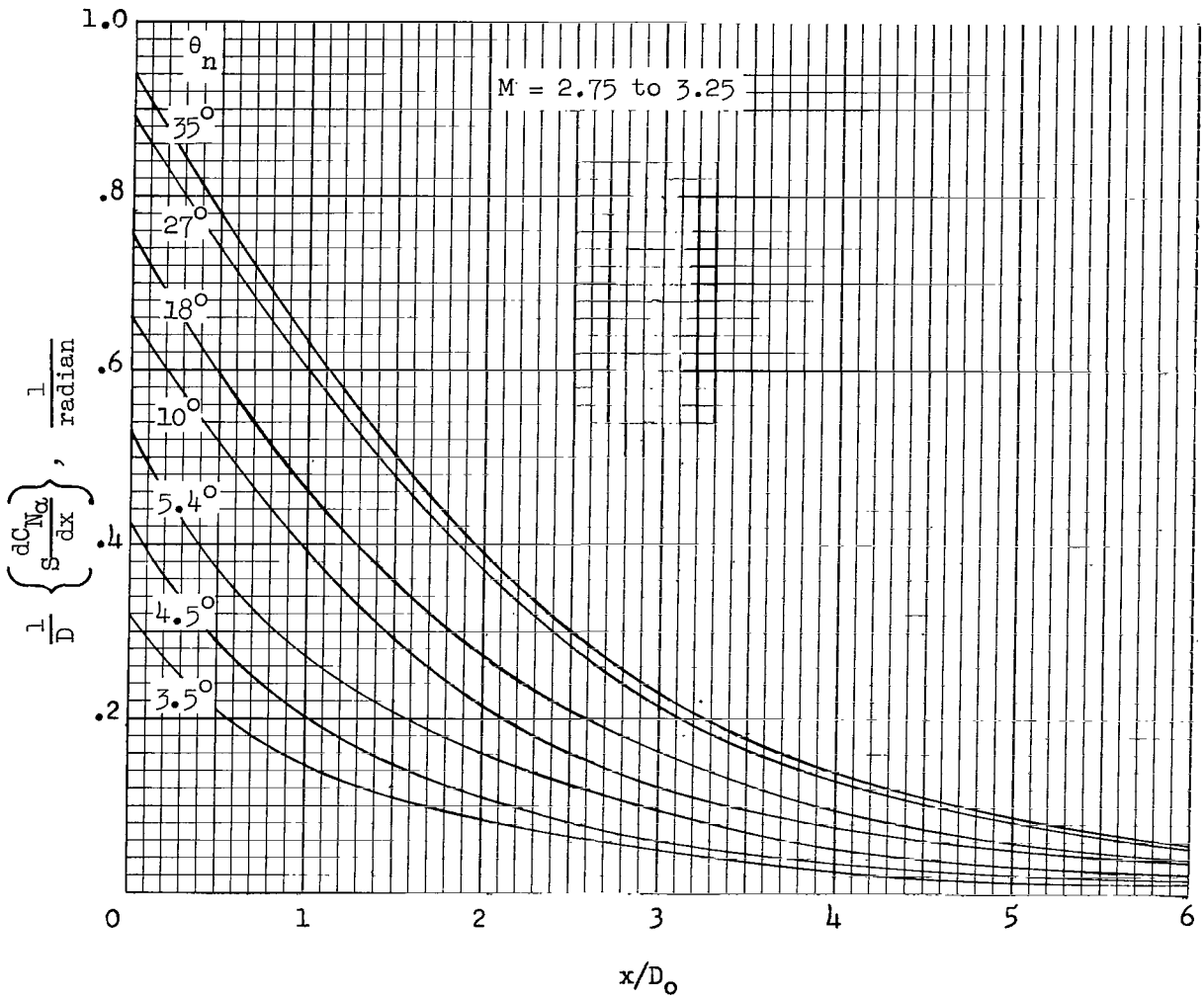


(e) Cylinders following cones; M = 2.75 to 3.25.

Figure 5.- Continued.

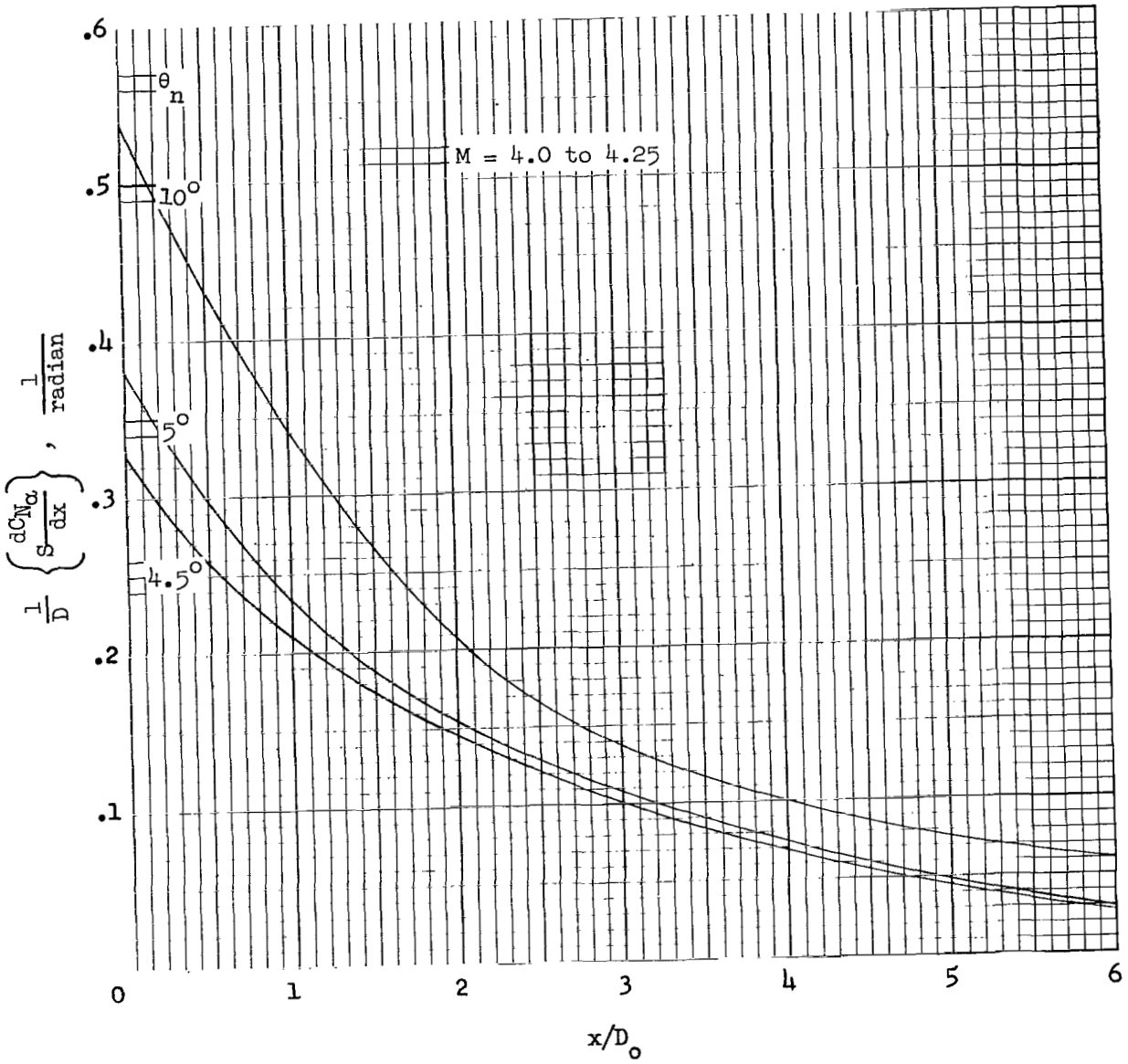


(f) Cylinders following cones; M = 4.0 to 4.25.

Figure 5.- Continued.

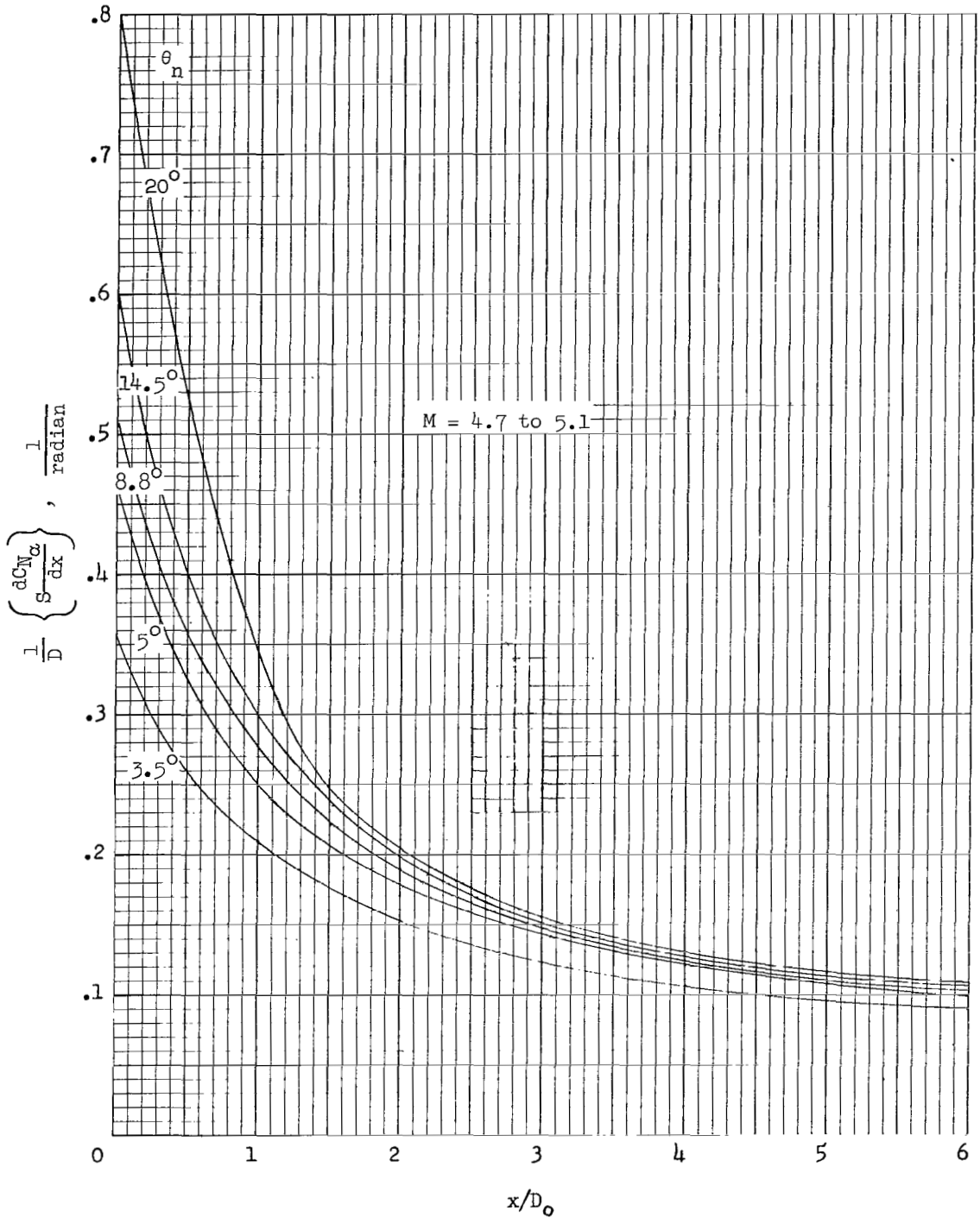


(g) Cylinders following cones; M = 4.7 to 5.1.

Figure 5.- Continued.

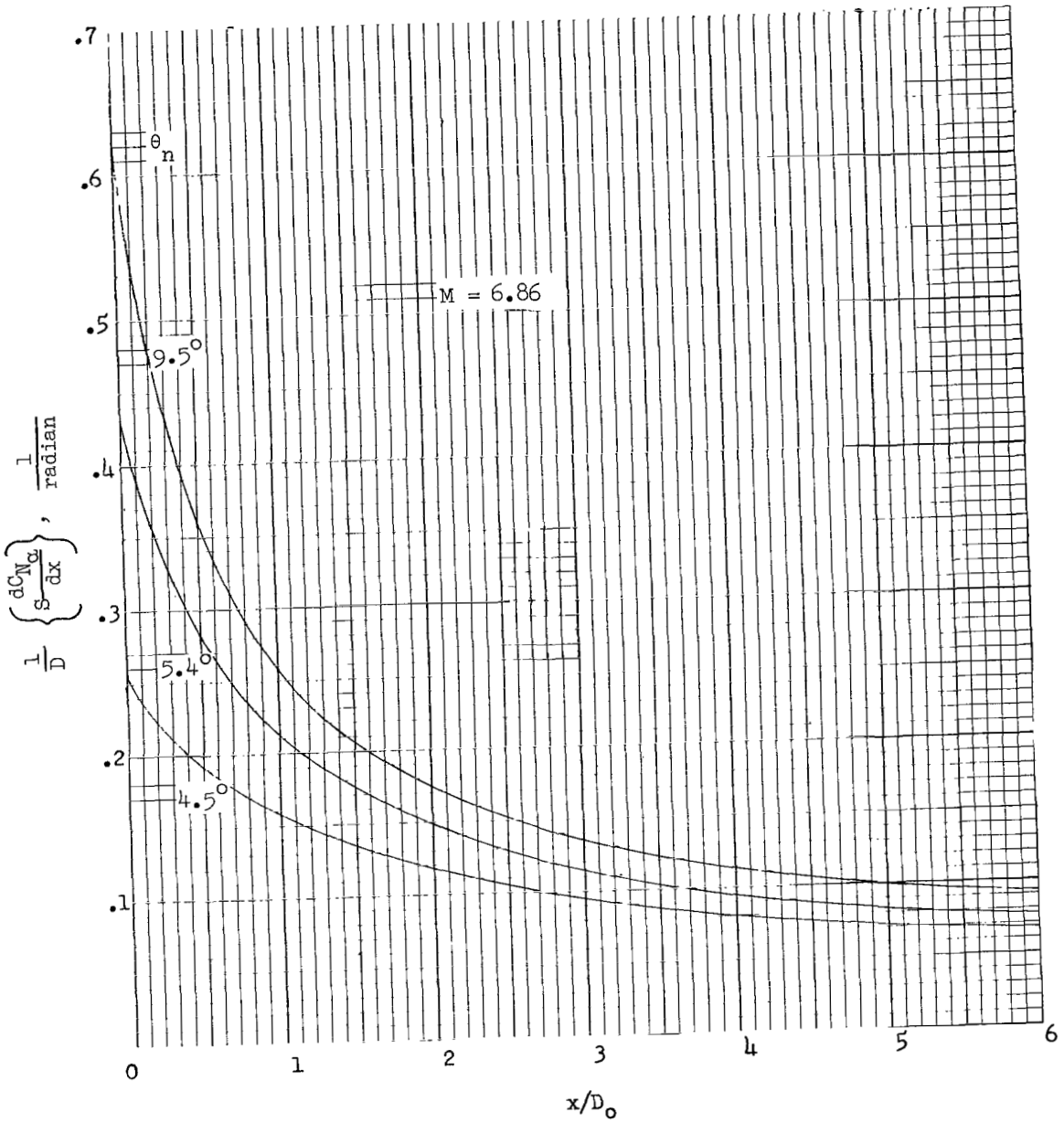


(h) Cylinders following cones; M = 6.86.

Figure 5.- Continued.

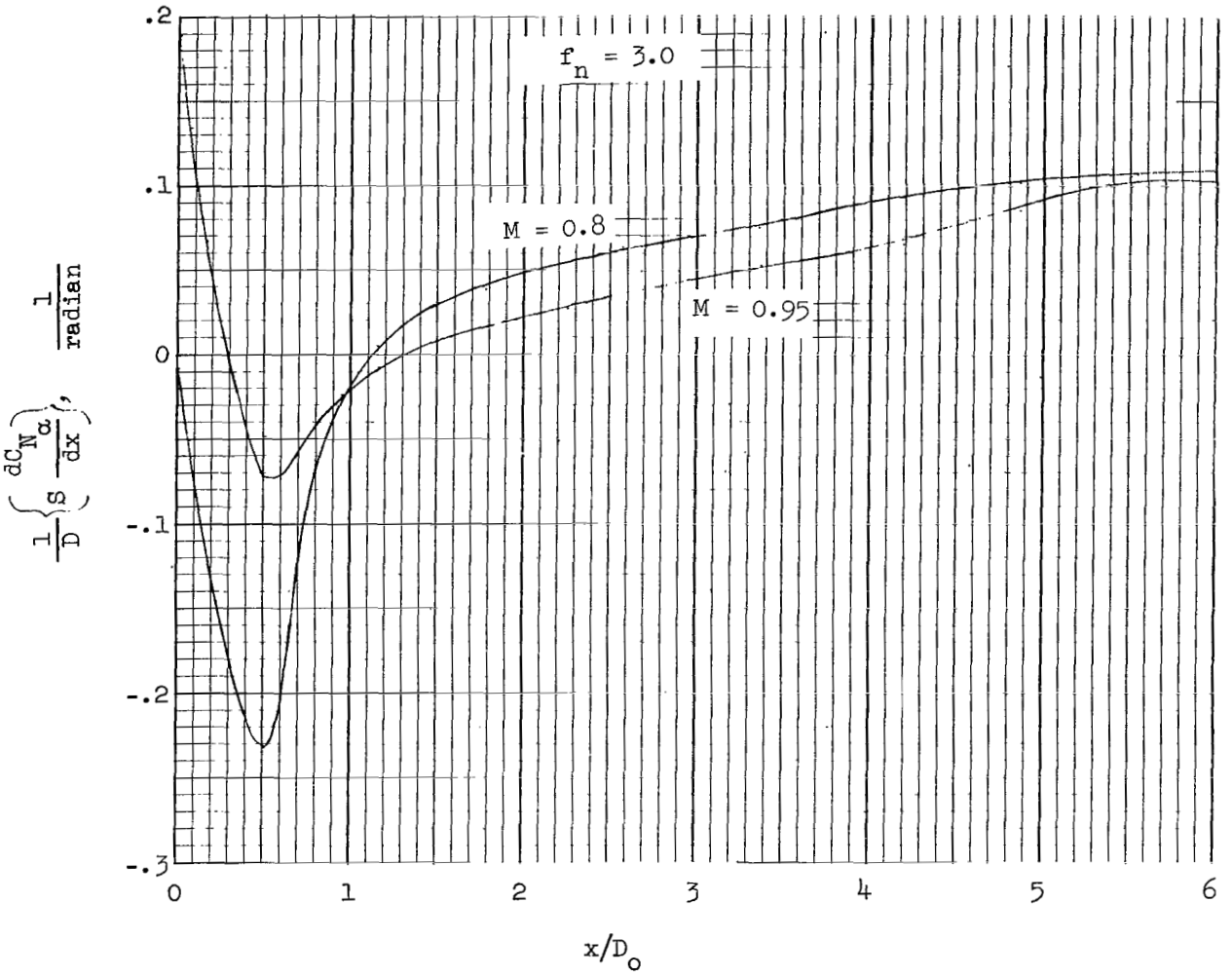


(i) Cylinders following ogives; M = 0.8 and 0.95.

Figure 5.- Continued.

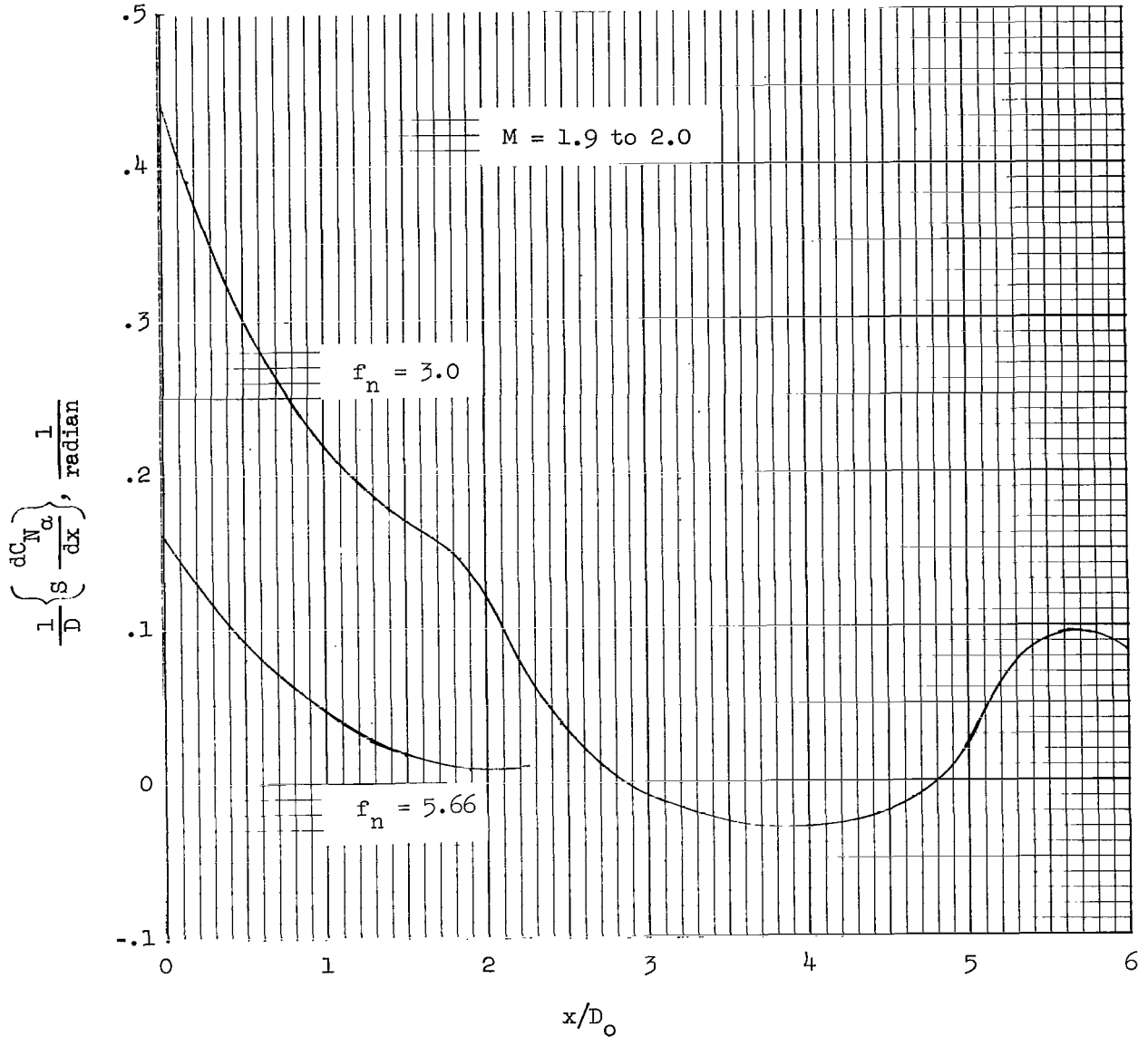


(j) Cylinders following ogives; M = 1.9 to 2.0.

Figure 5.- Continued.

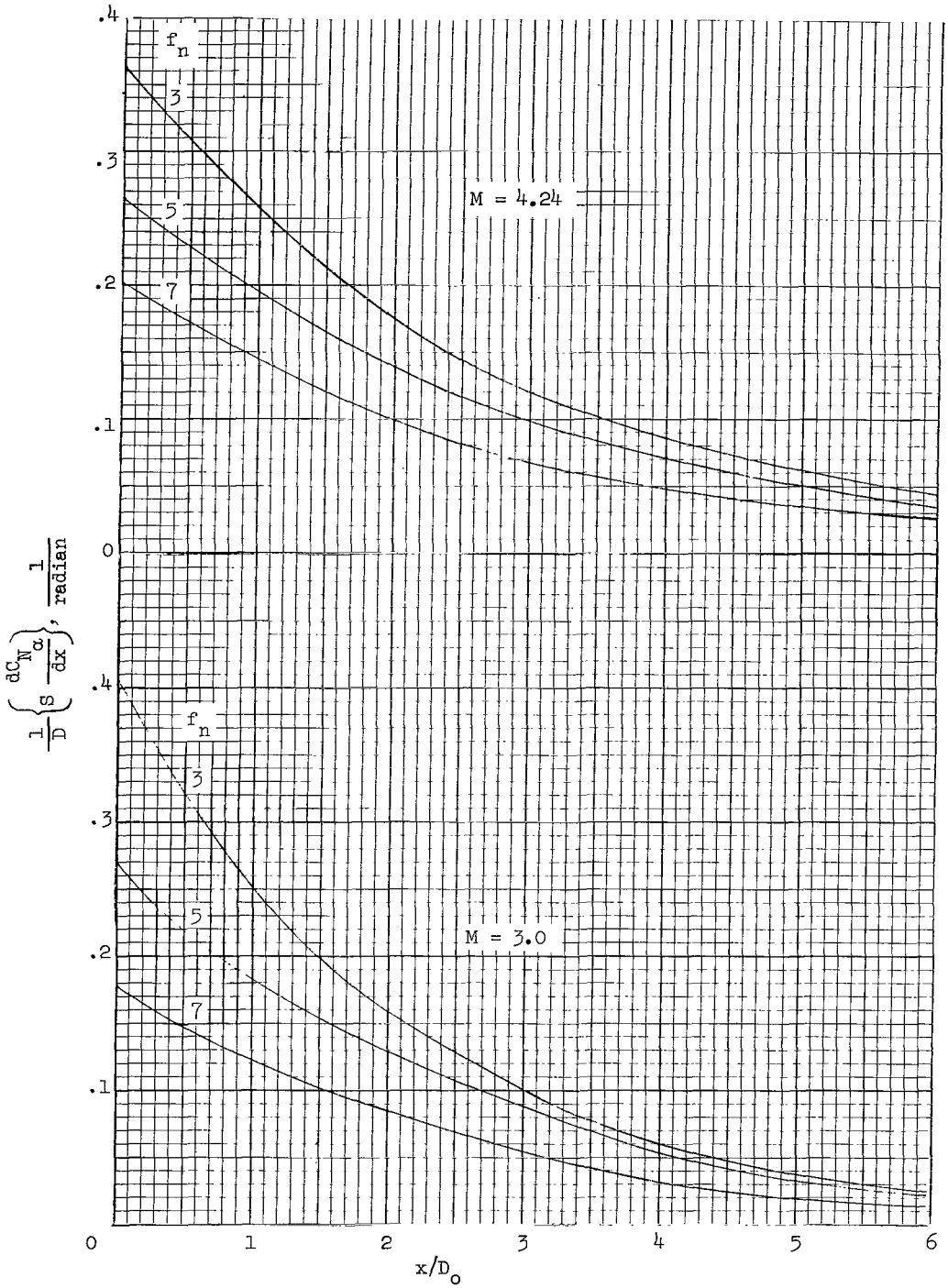


(k) Cylinders following ogives; M = 3.0 and 4.24.

Figure 5.- Continued.

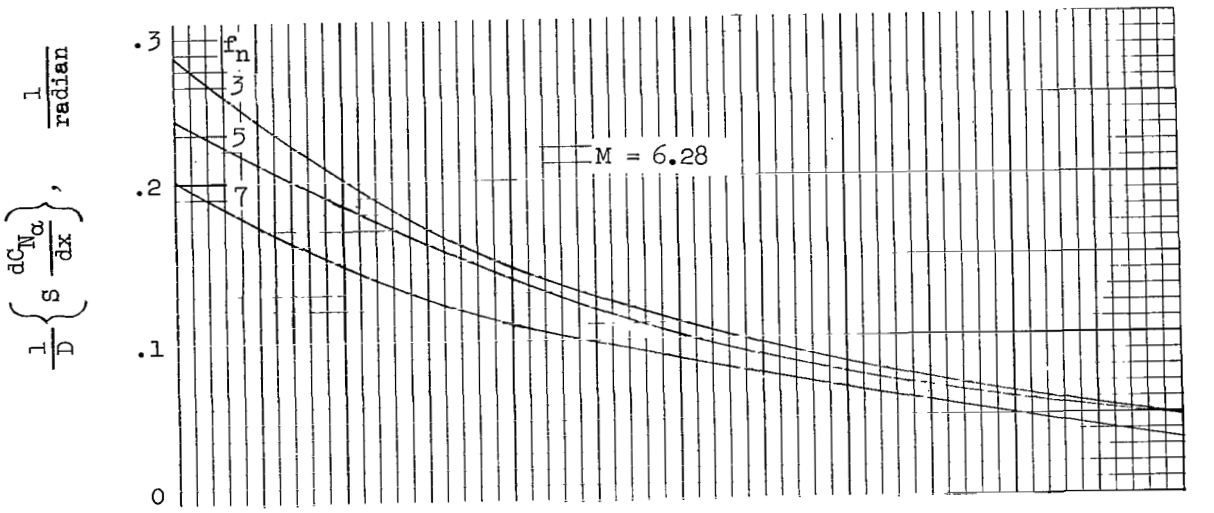


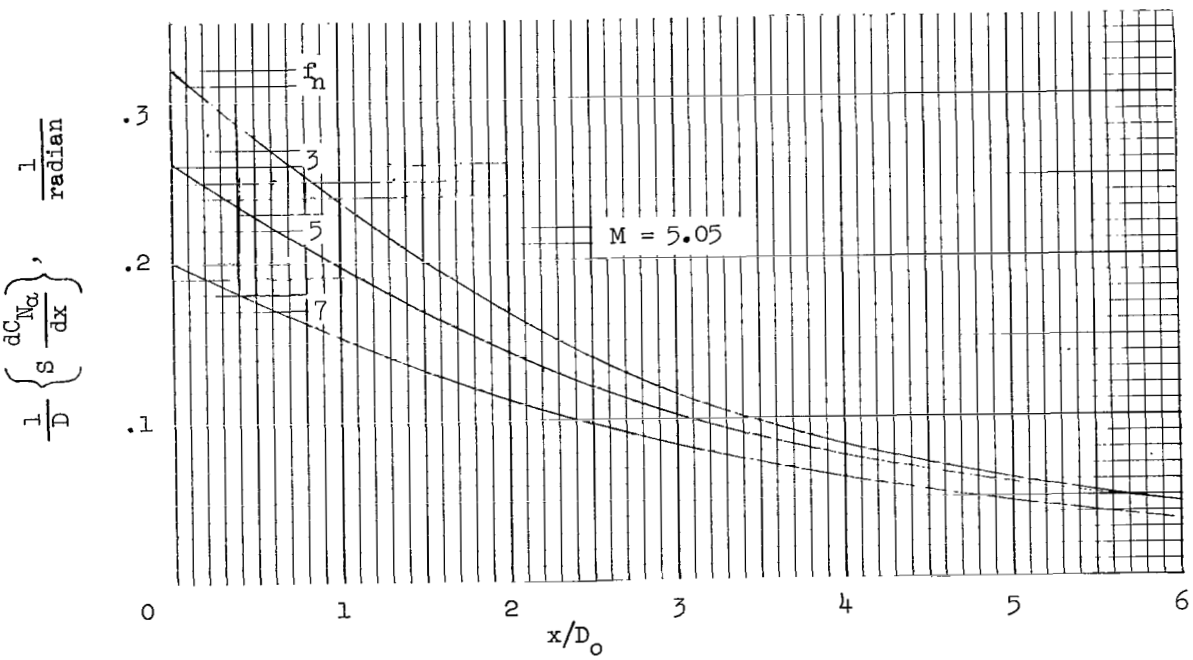


(l) Cylinders following ogives; M = 5.05 and 6.28.

Figure 5.- Concluded.

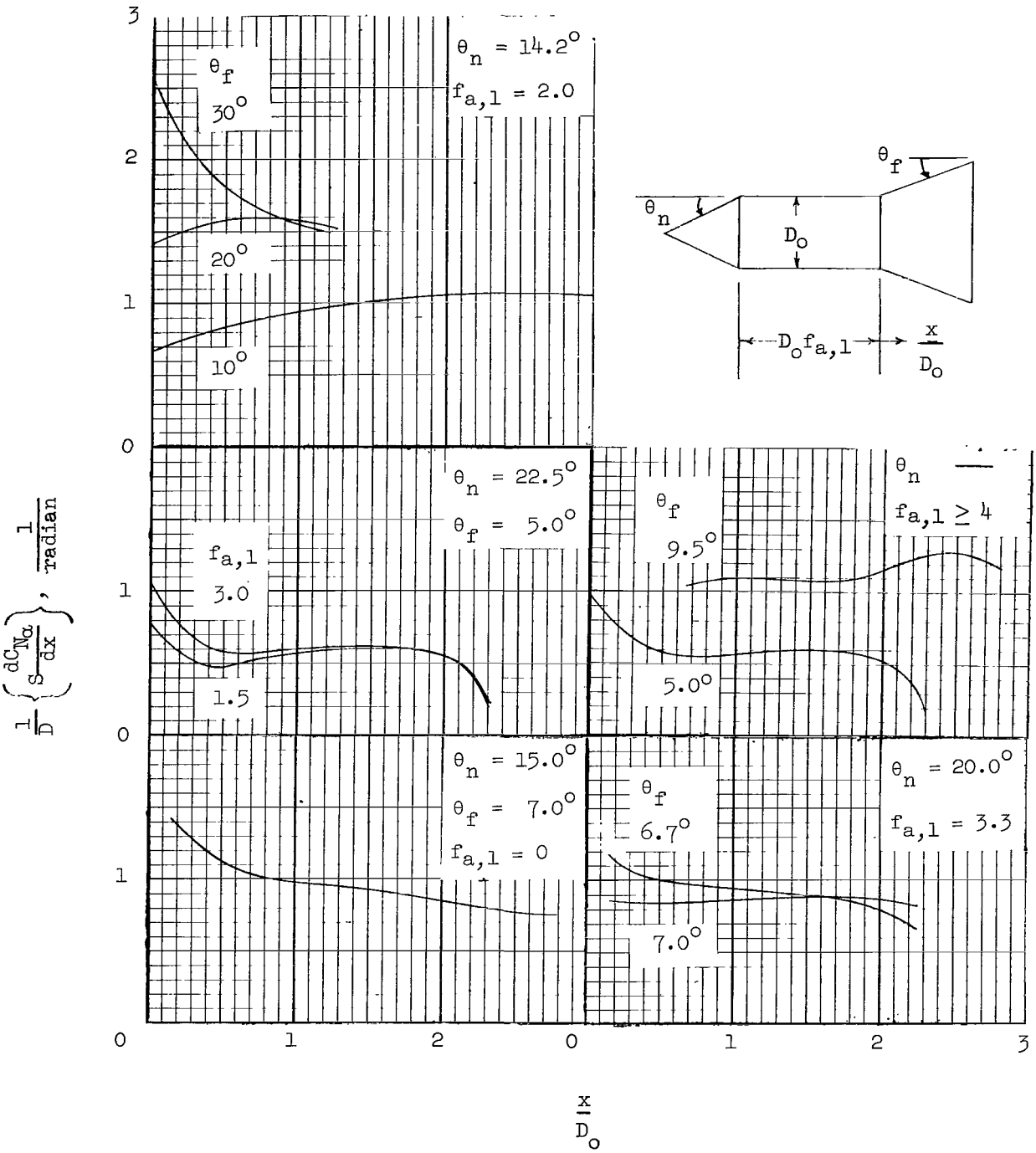


(a) M = 0.8.

Figure 6.- Loading functions for frustums following cone-cylinders.

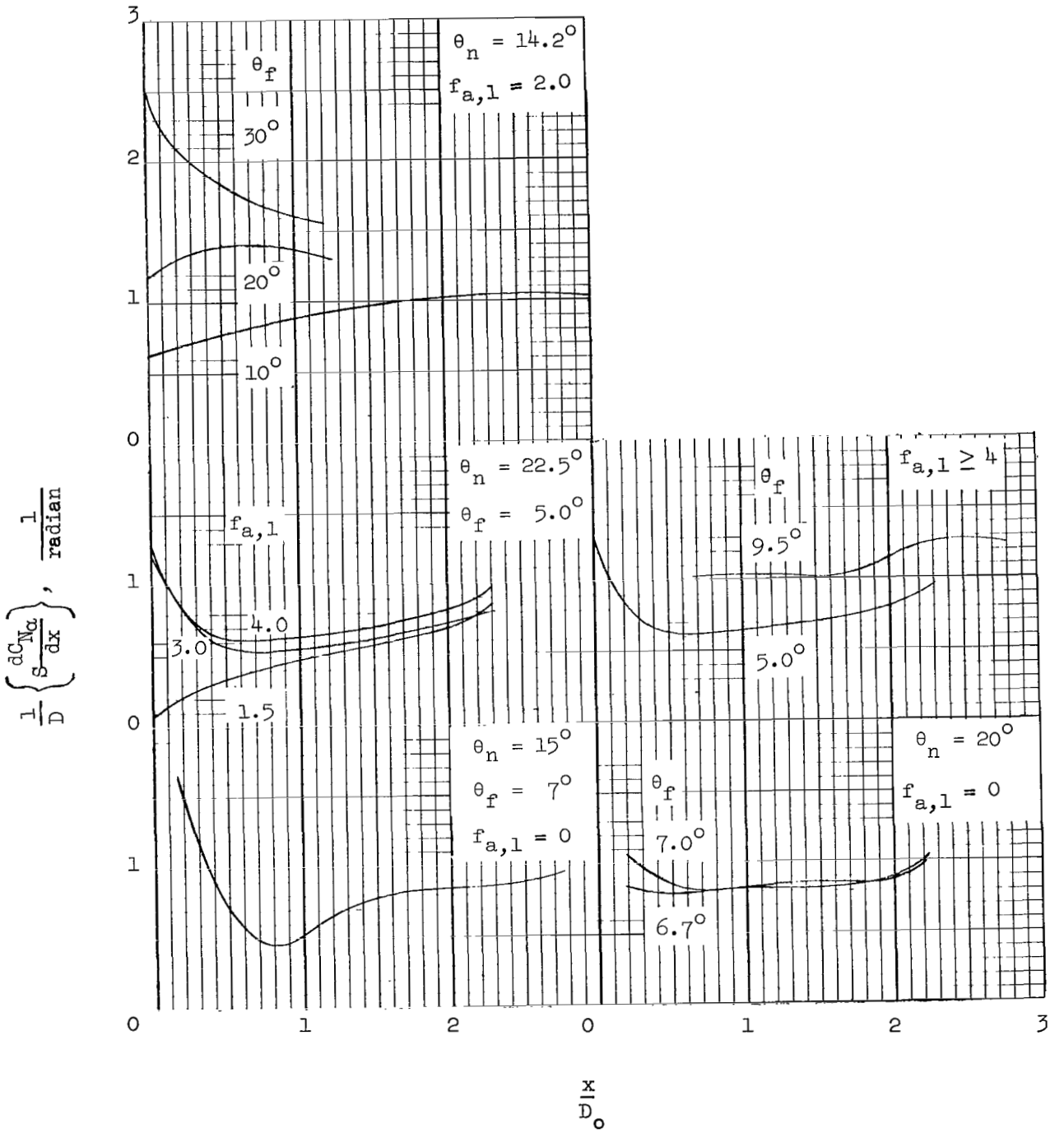


(b) M = 1.0.

Figure 6.- Continued.

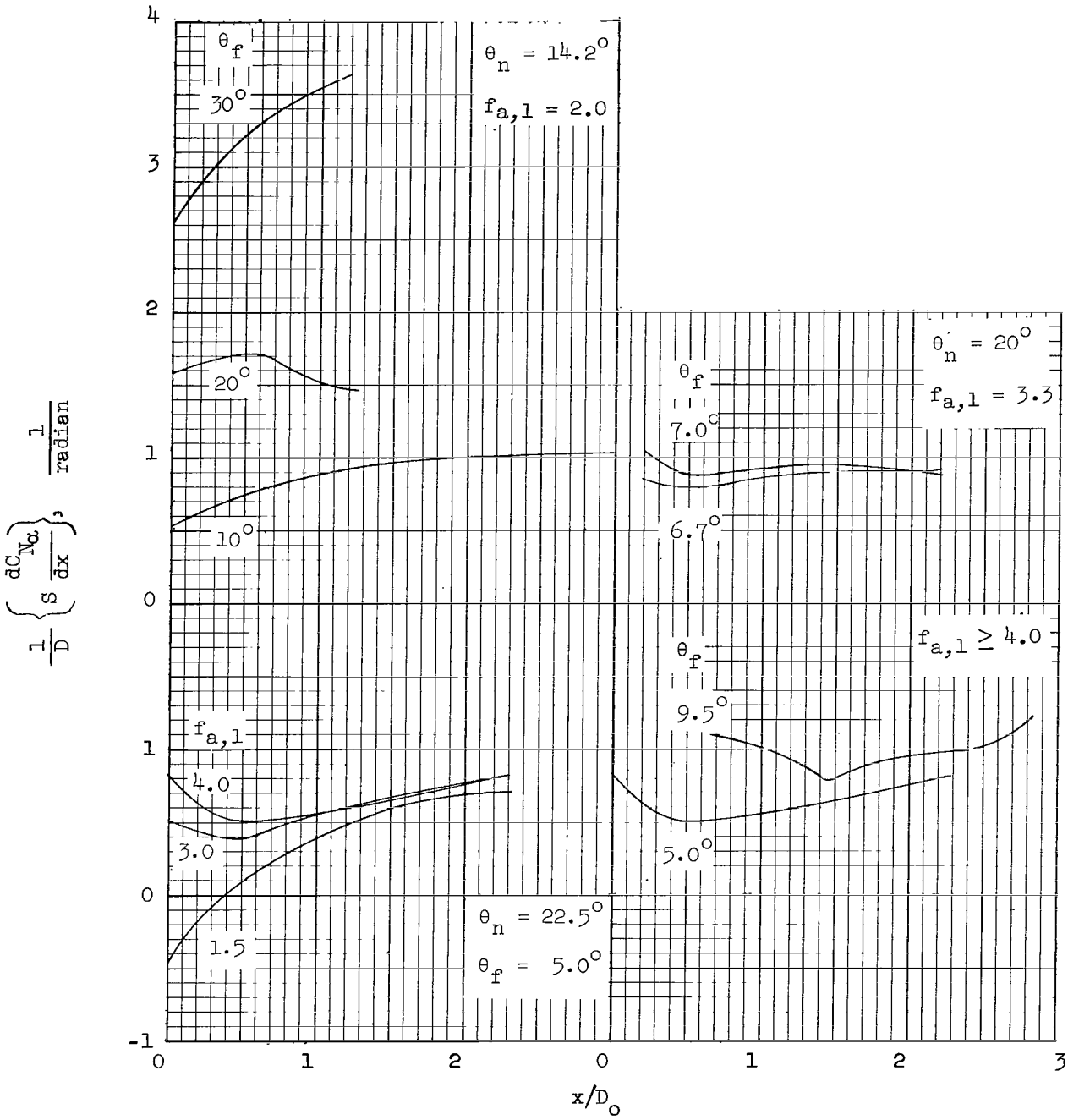


(c) M = 1.2.

Figure 6.- Continued.

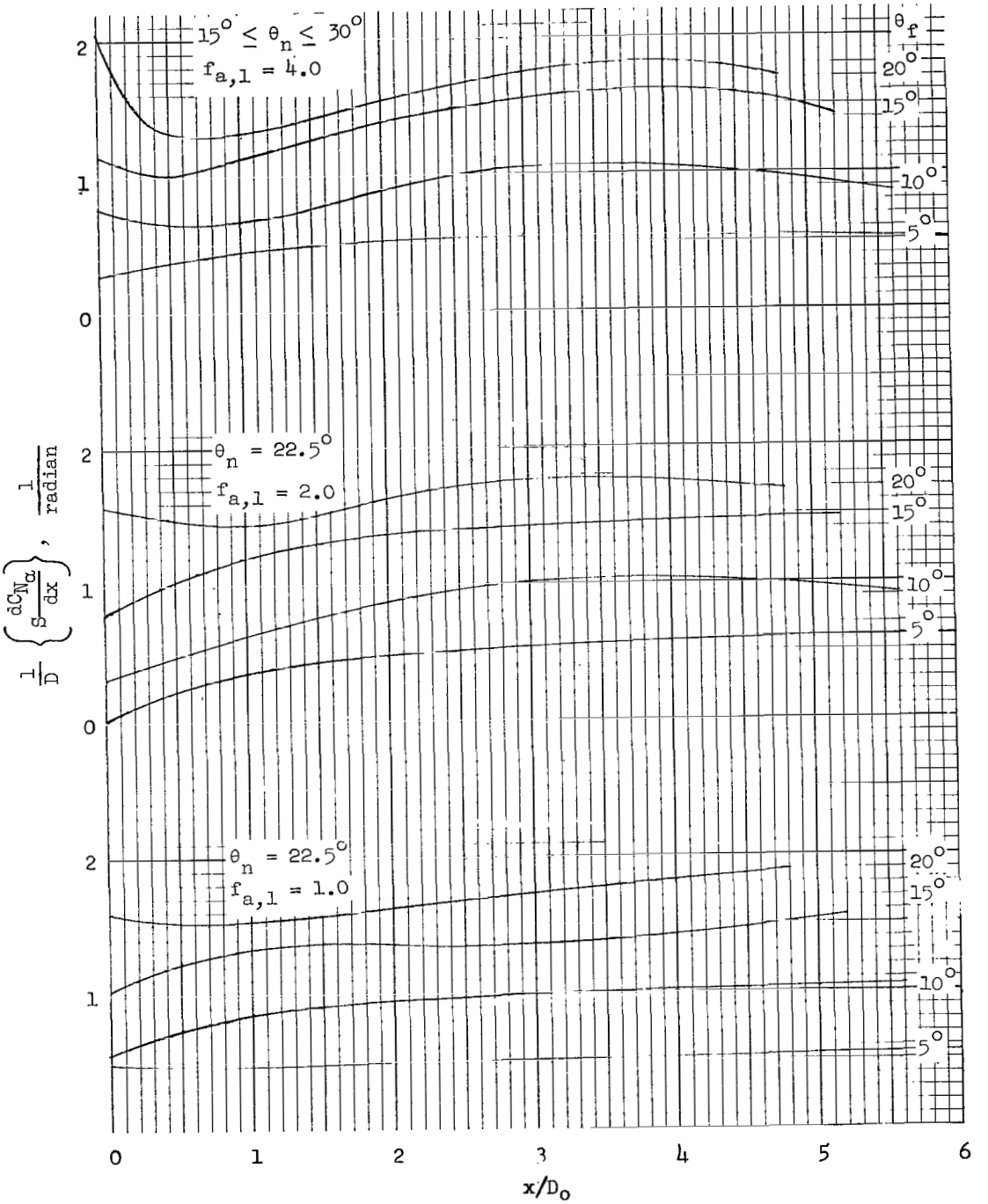


(d) M = 1.5.

Figure 6.- Continued.

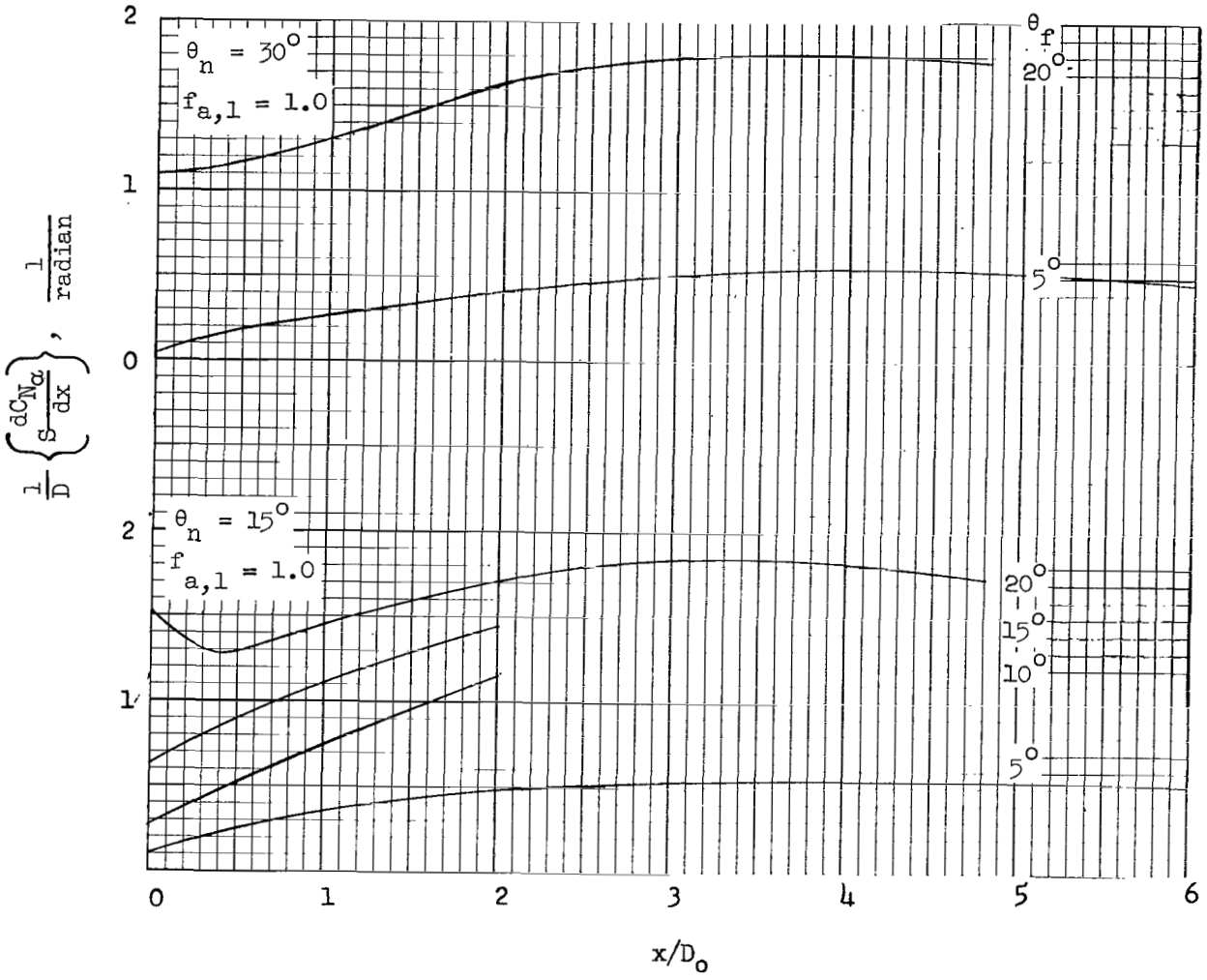


(e) M = 1.5.

Figure 6.- Continued.

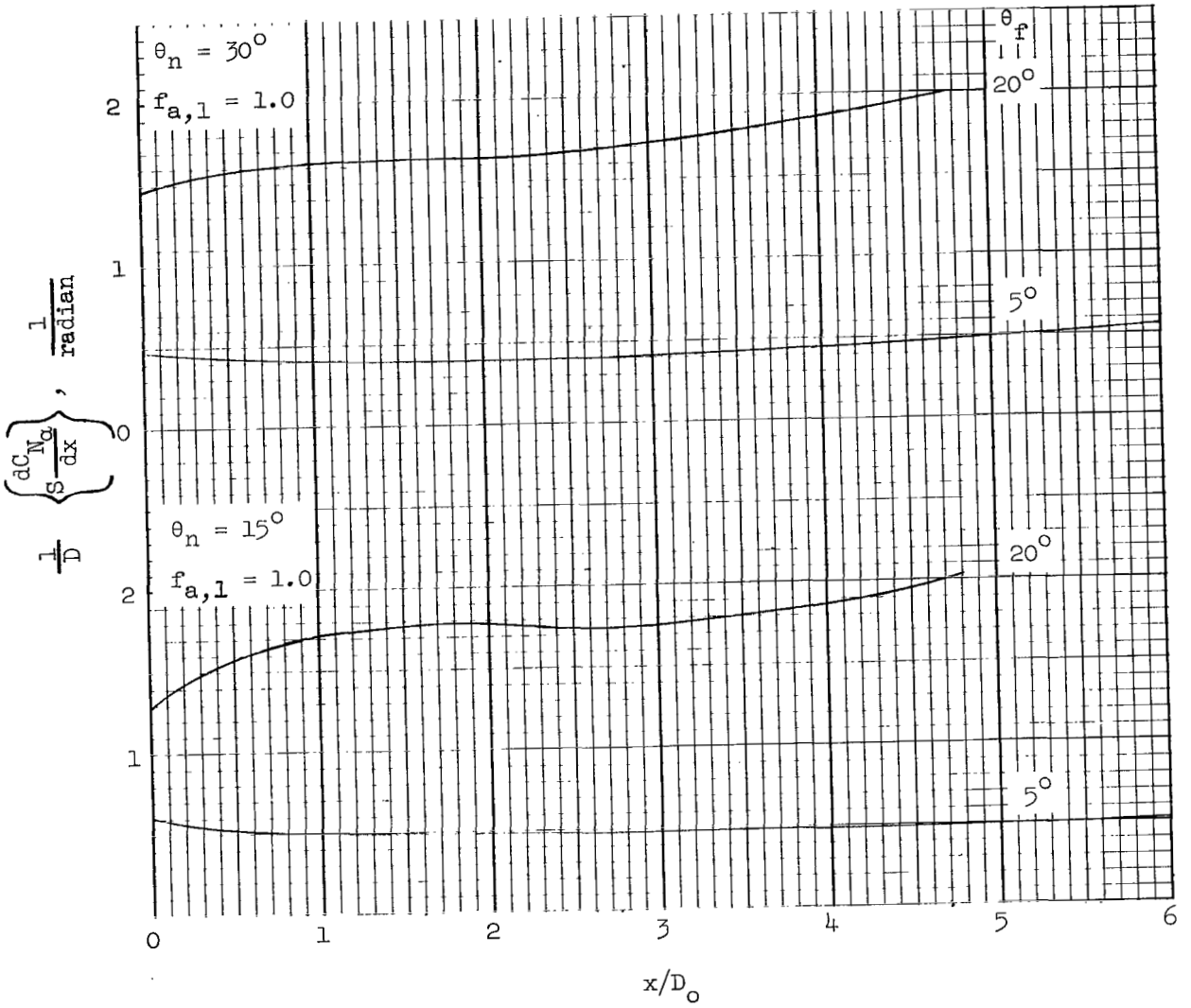


(f) M = 2.18.

Figure 6.- Continued.

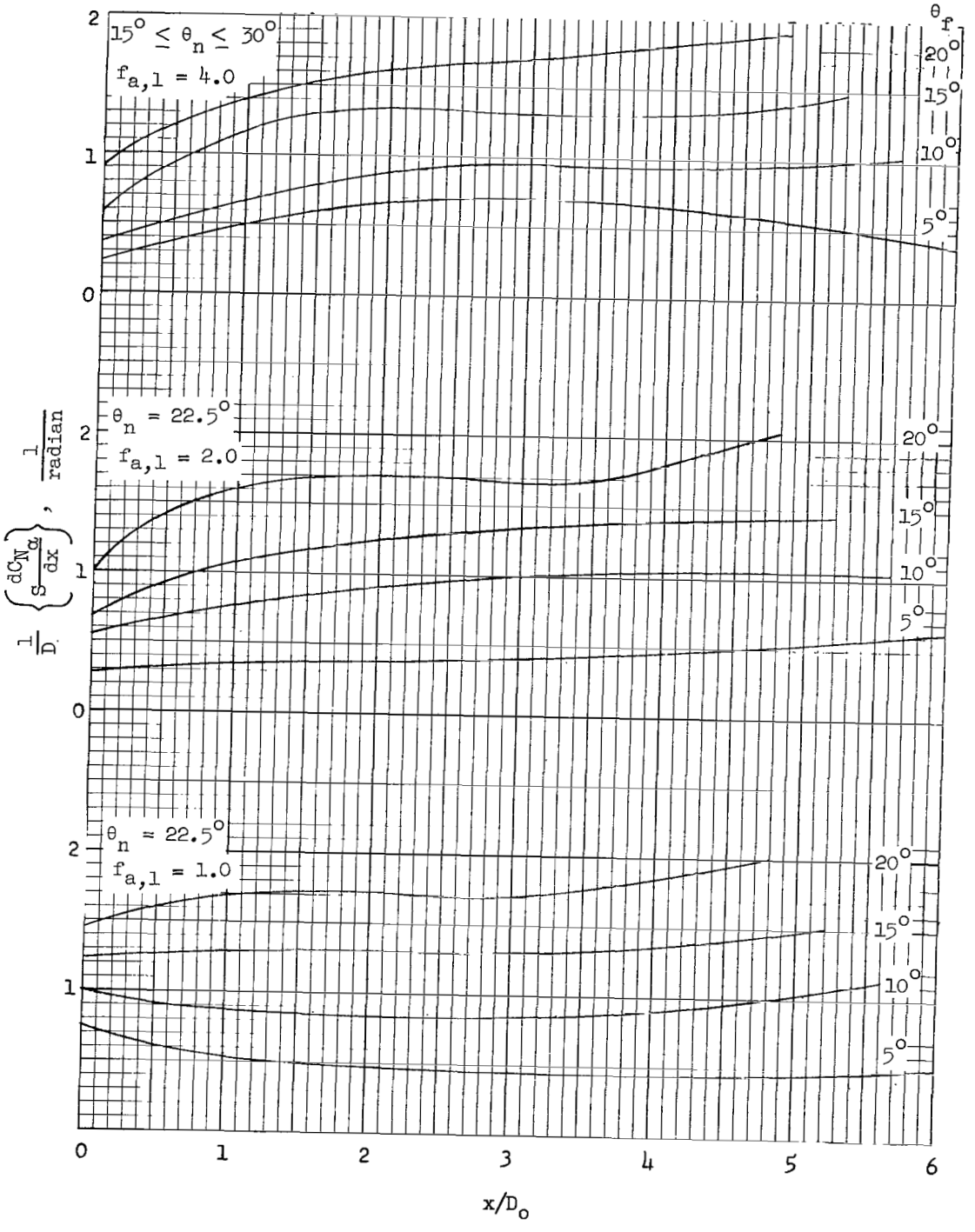


(g) M = 2.18.

Figure 6.- Continued.

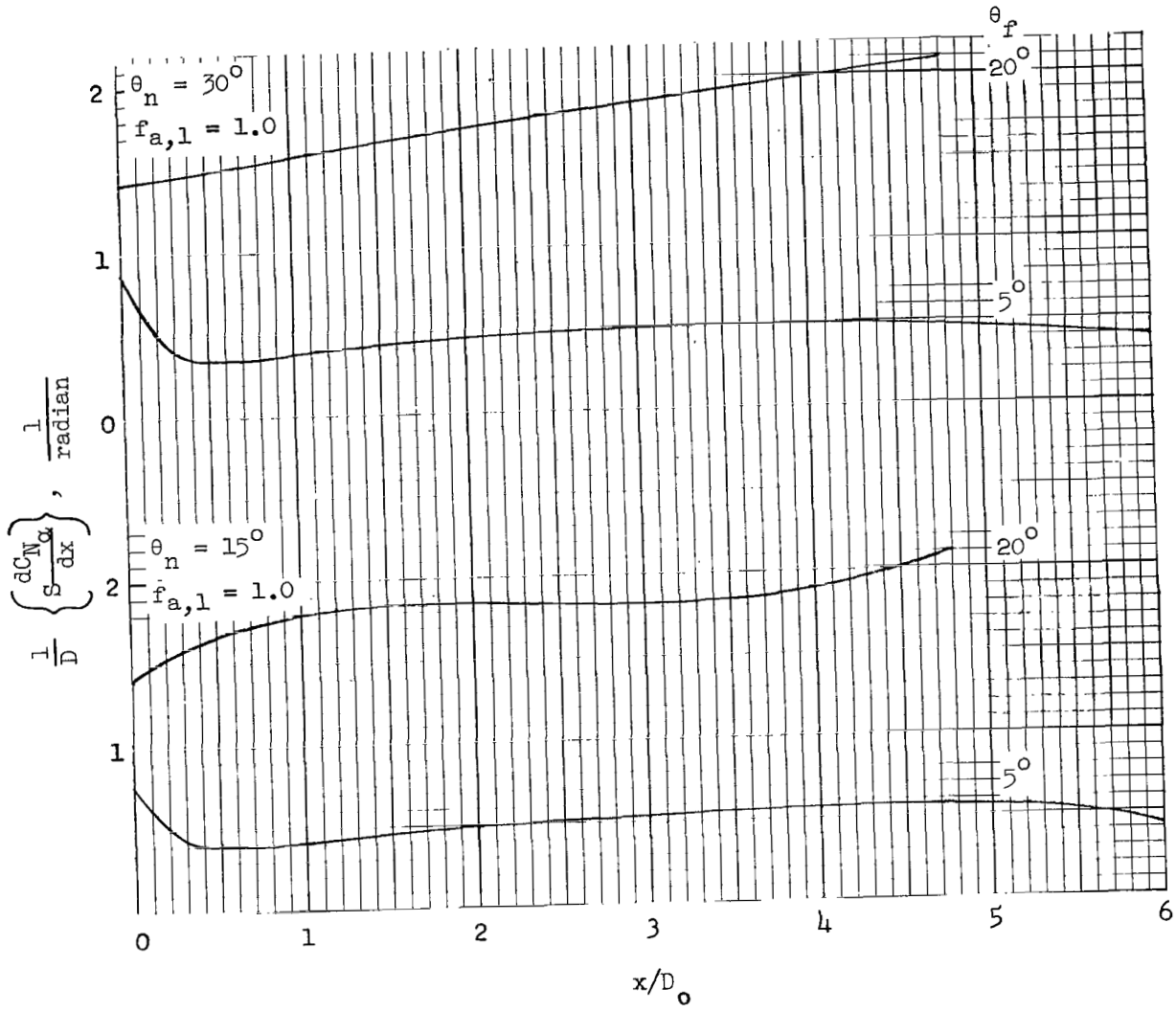


(h) M = 2.81.

Figure 6.- Continued.

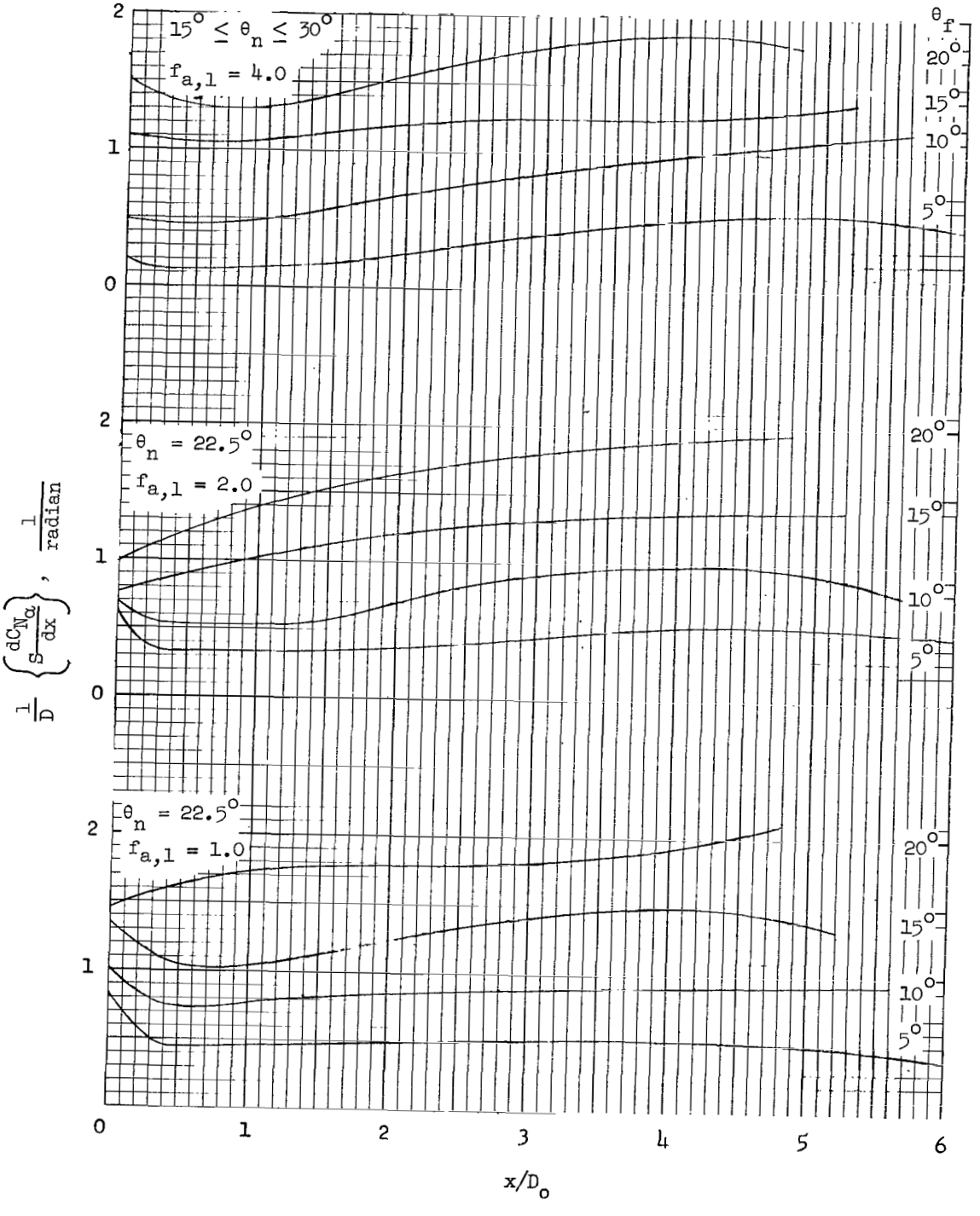


(i) M = 2.81.

Figure 6.- Continued.

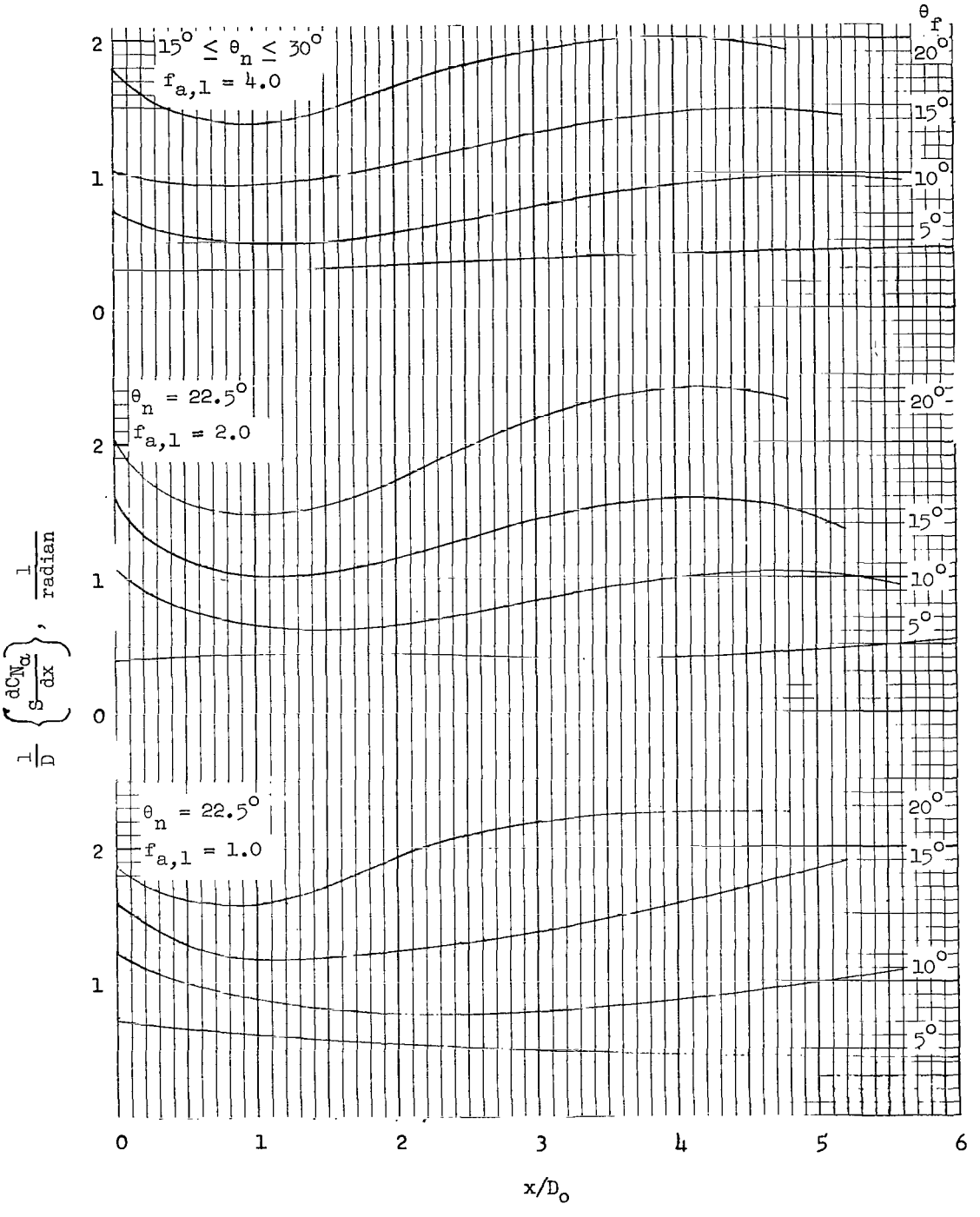


(j) M = 4.04.

Figure 6.- Continued.

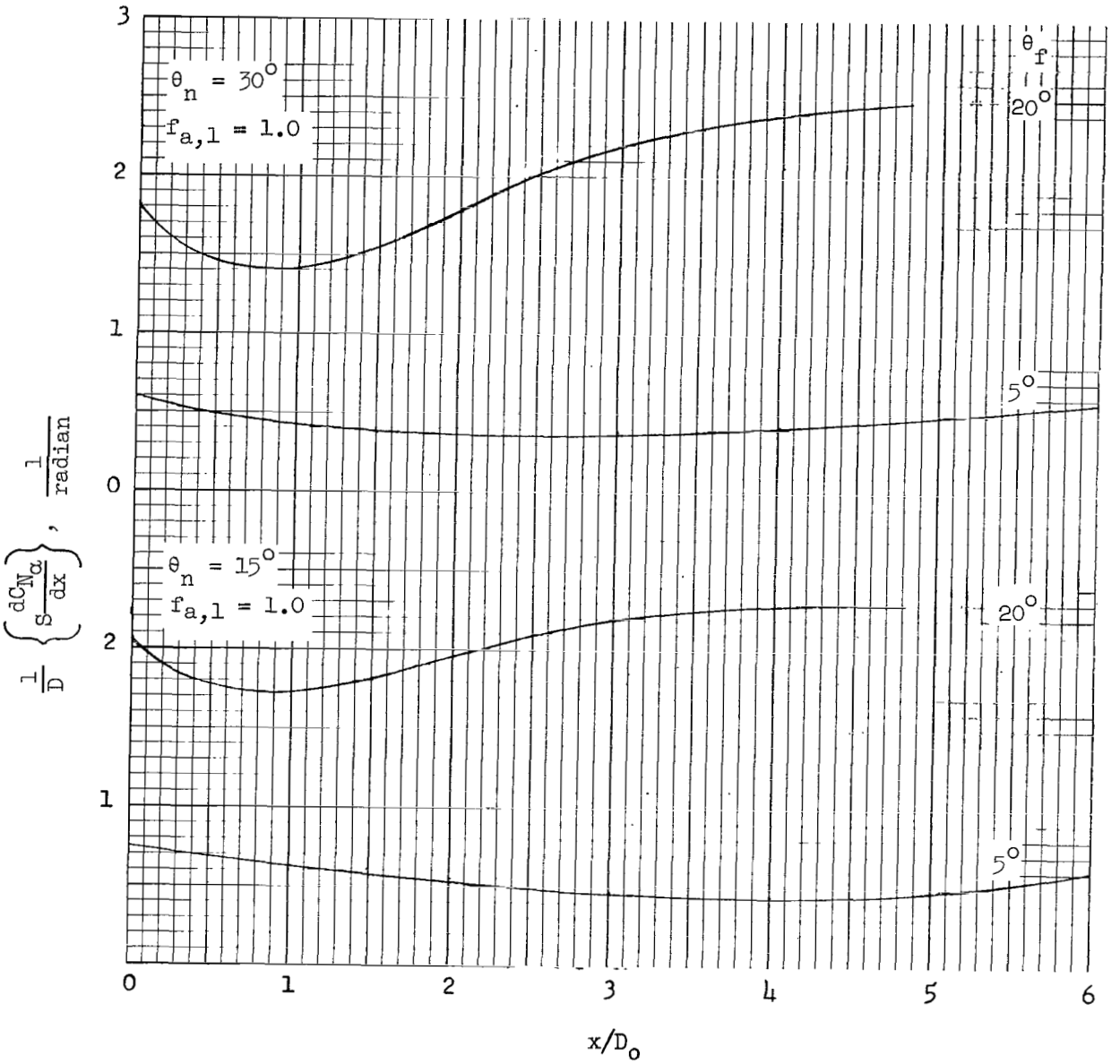


(k) M = 4.04.

Figure 6.- Concluded.

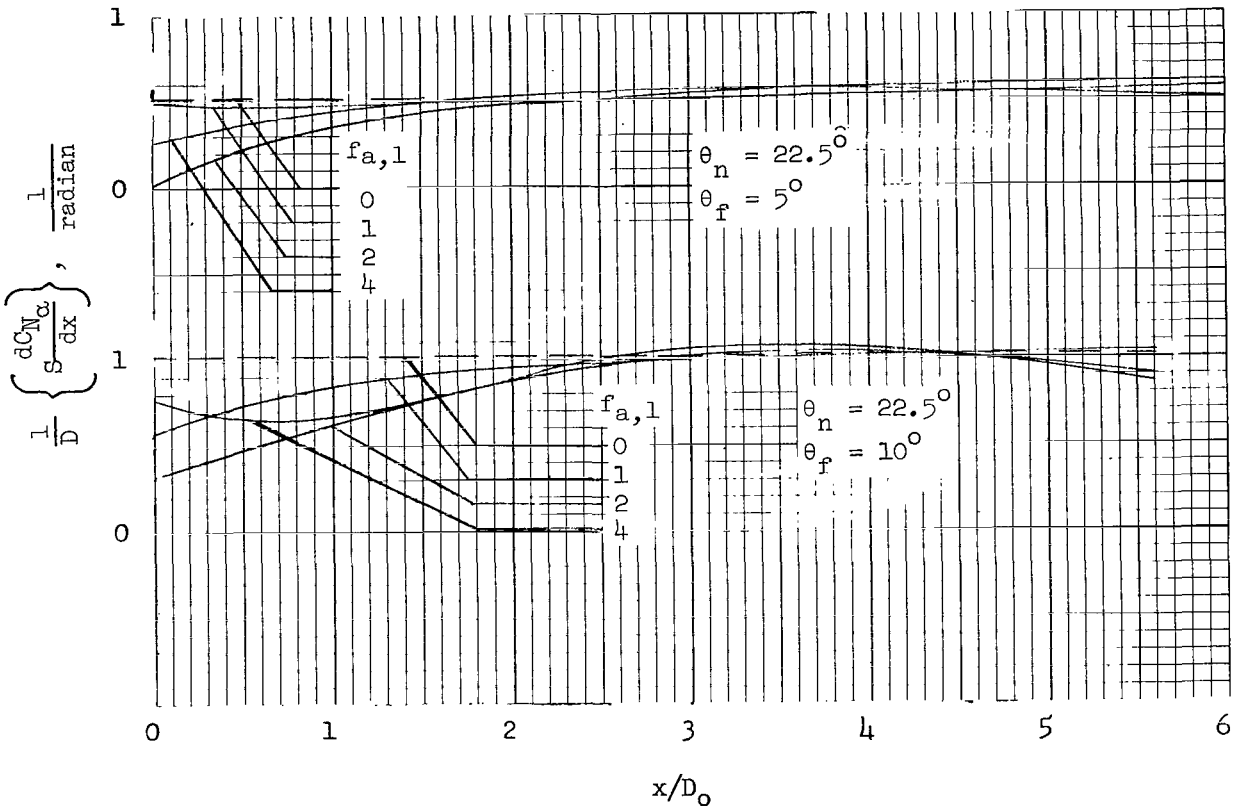


(a) M = 1.5.

Figure 7.- Loading functions for frustums following cone-cylinders. (Cross-plots from fig. 6.)

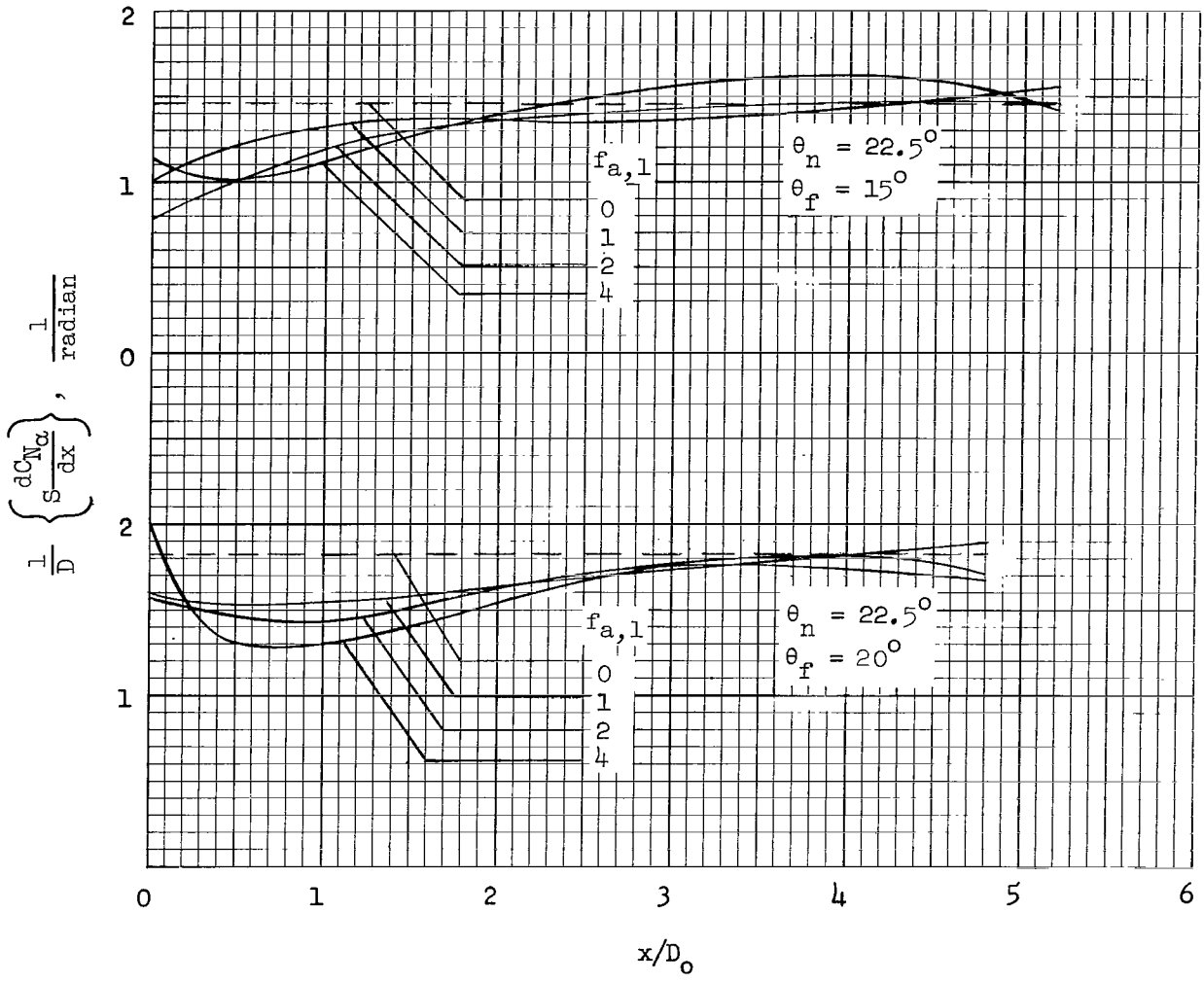


(b) M = 1.5.

Figure 7.- Continued.

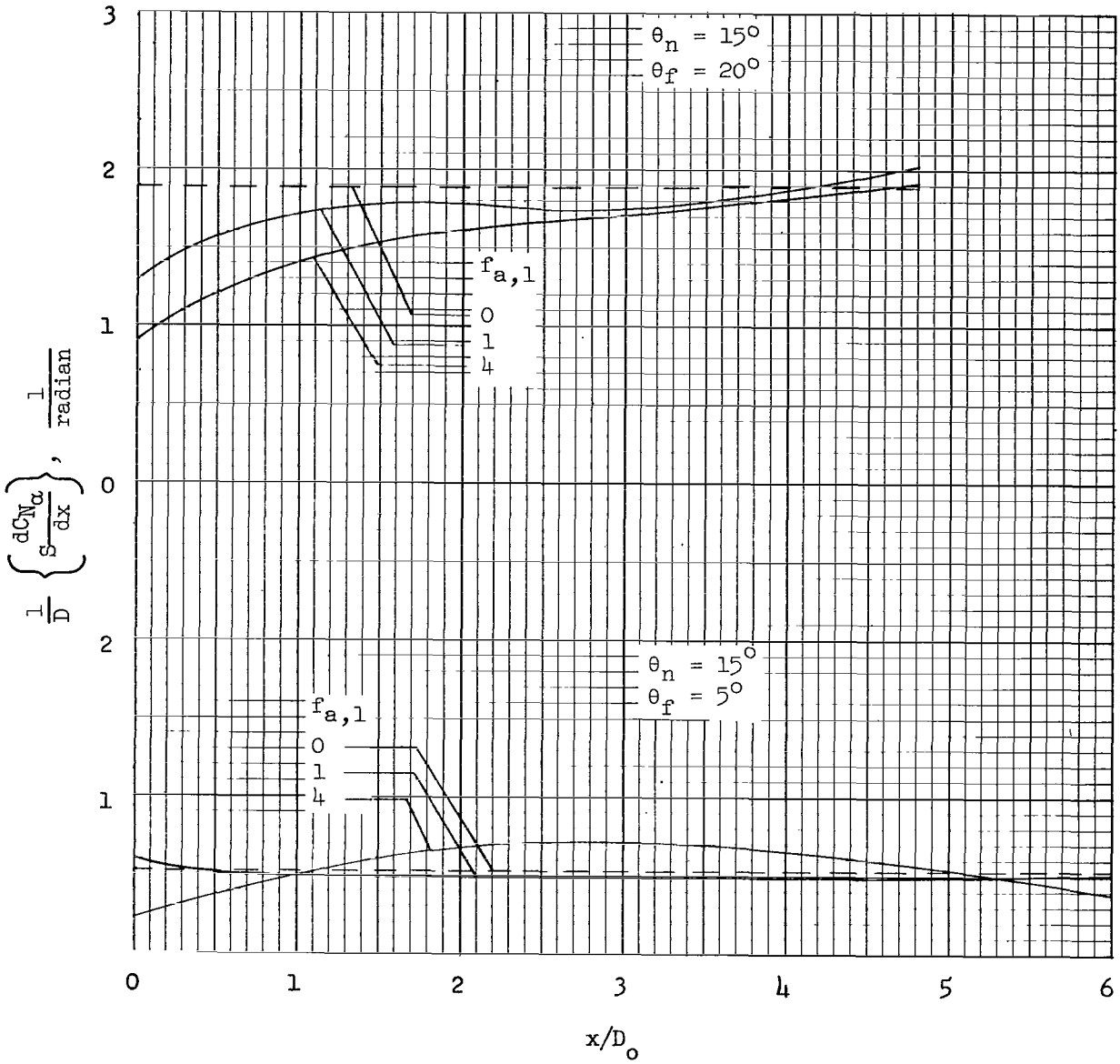


(c) M = 2.18.

Figure 7.- Continued.

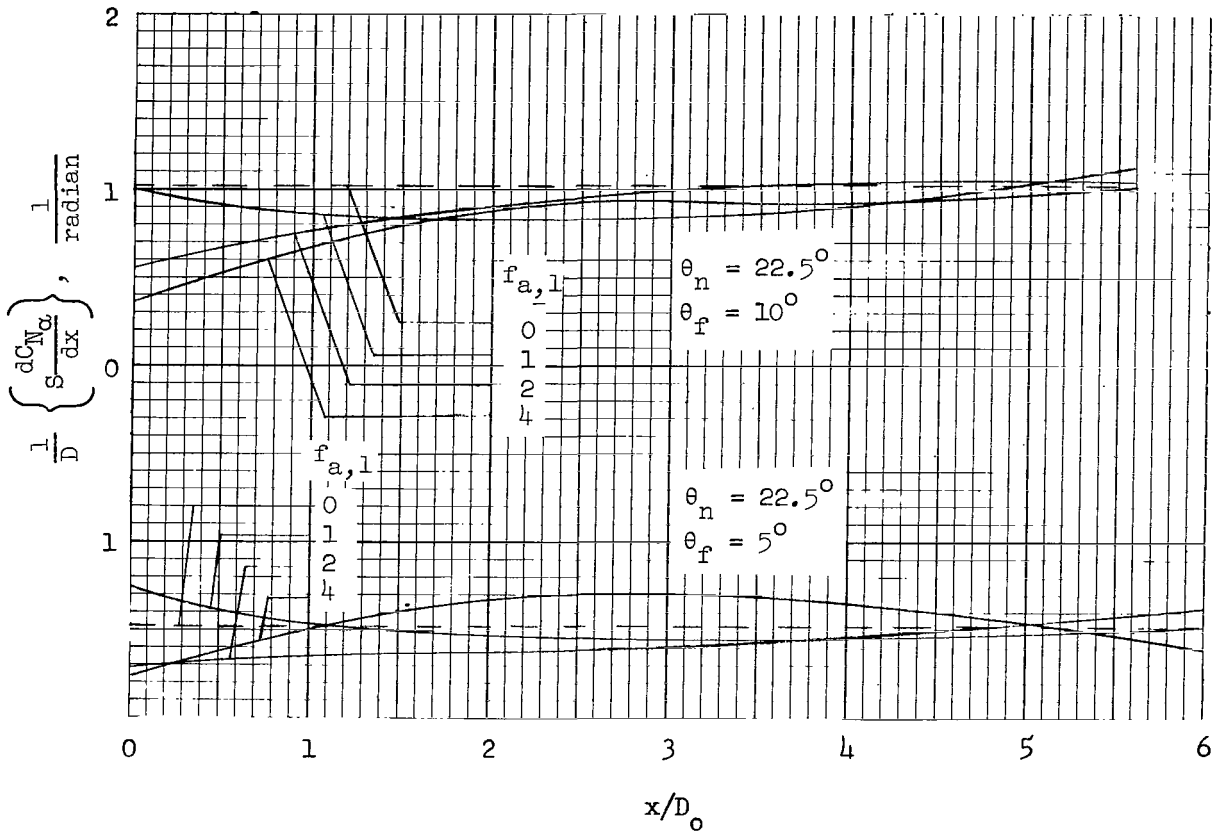


(d) M = 2.18.

Figure 7.- Continued.

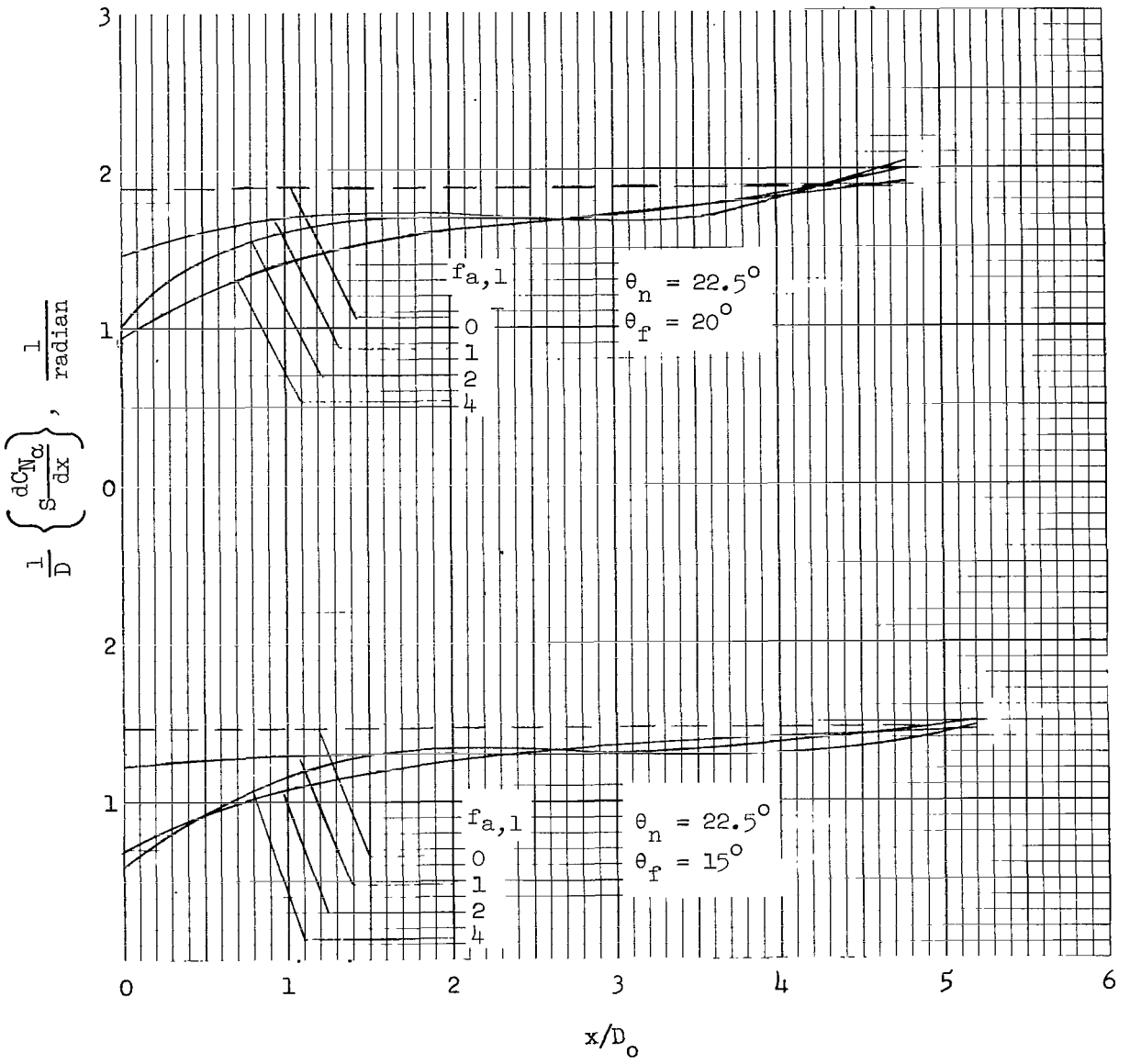


(e) M = 2.18.

Figure 7.- Continued.

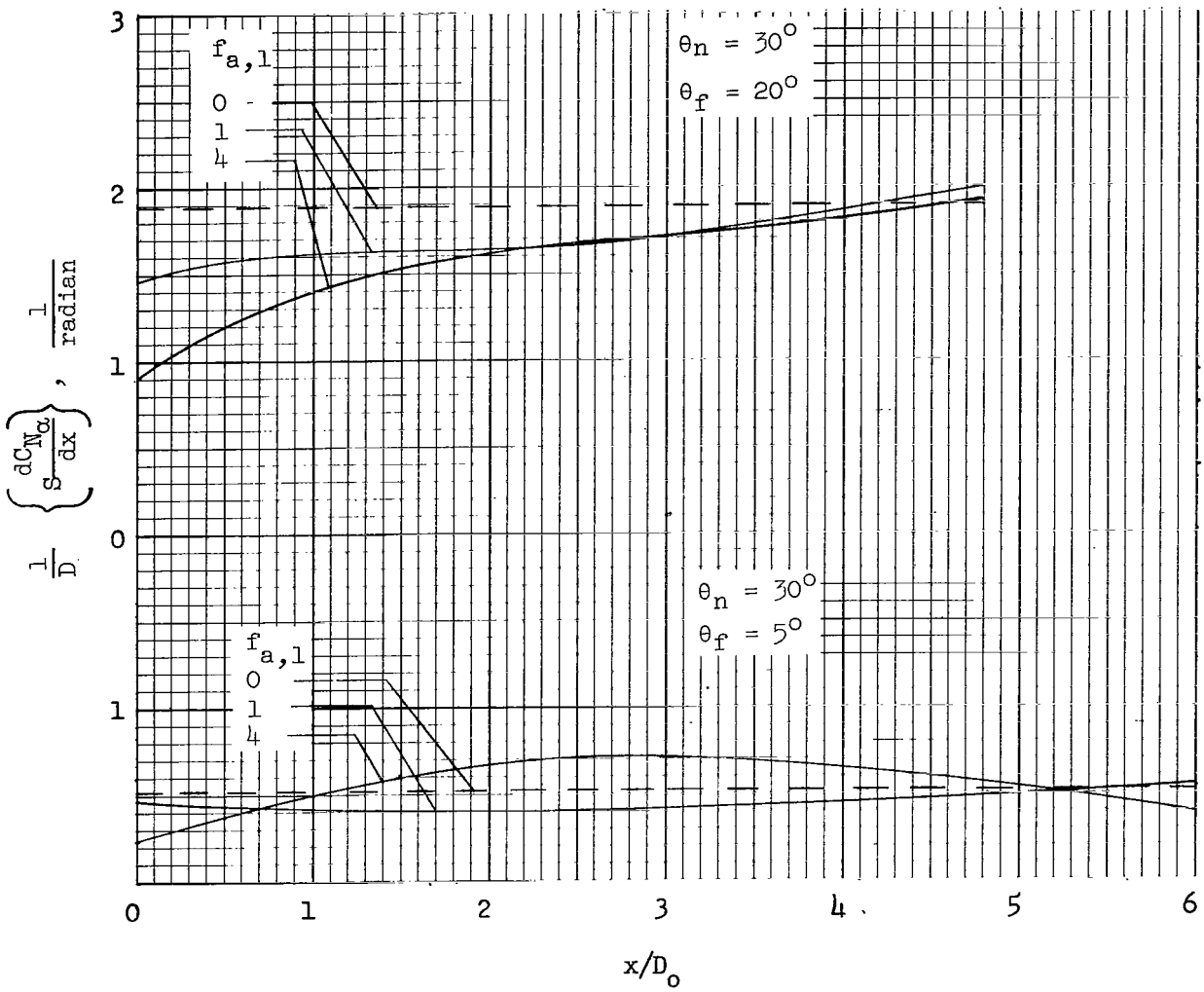


(f) M = 2.18.

Figure 7.- Continued.

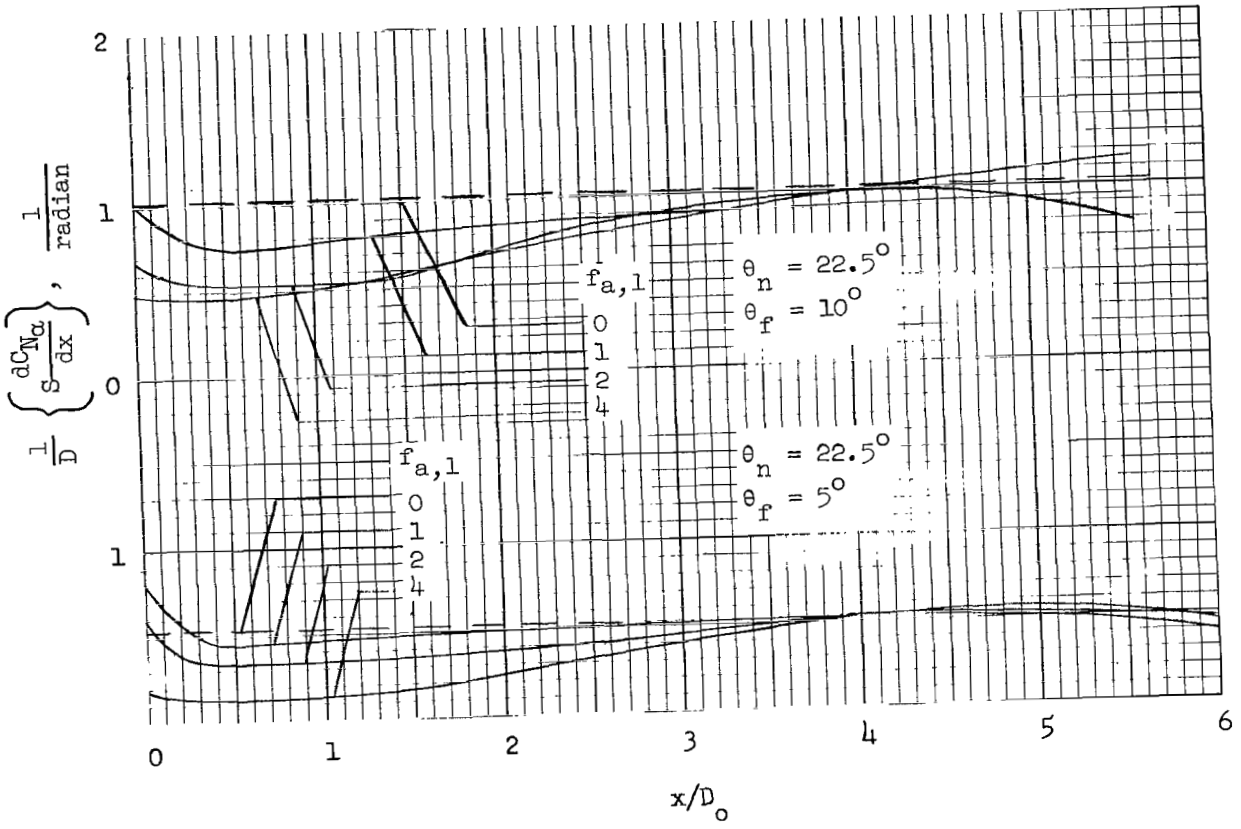


(g) M = 2.81.

Figure 7.- Continued.

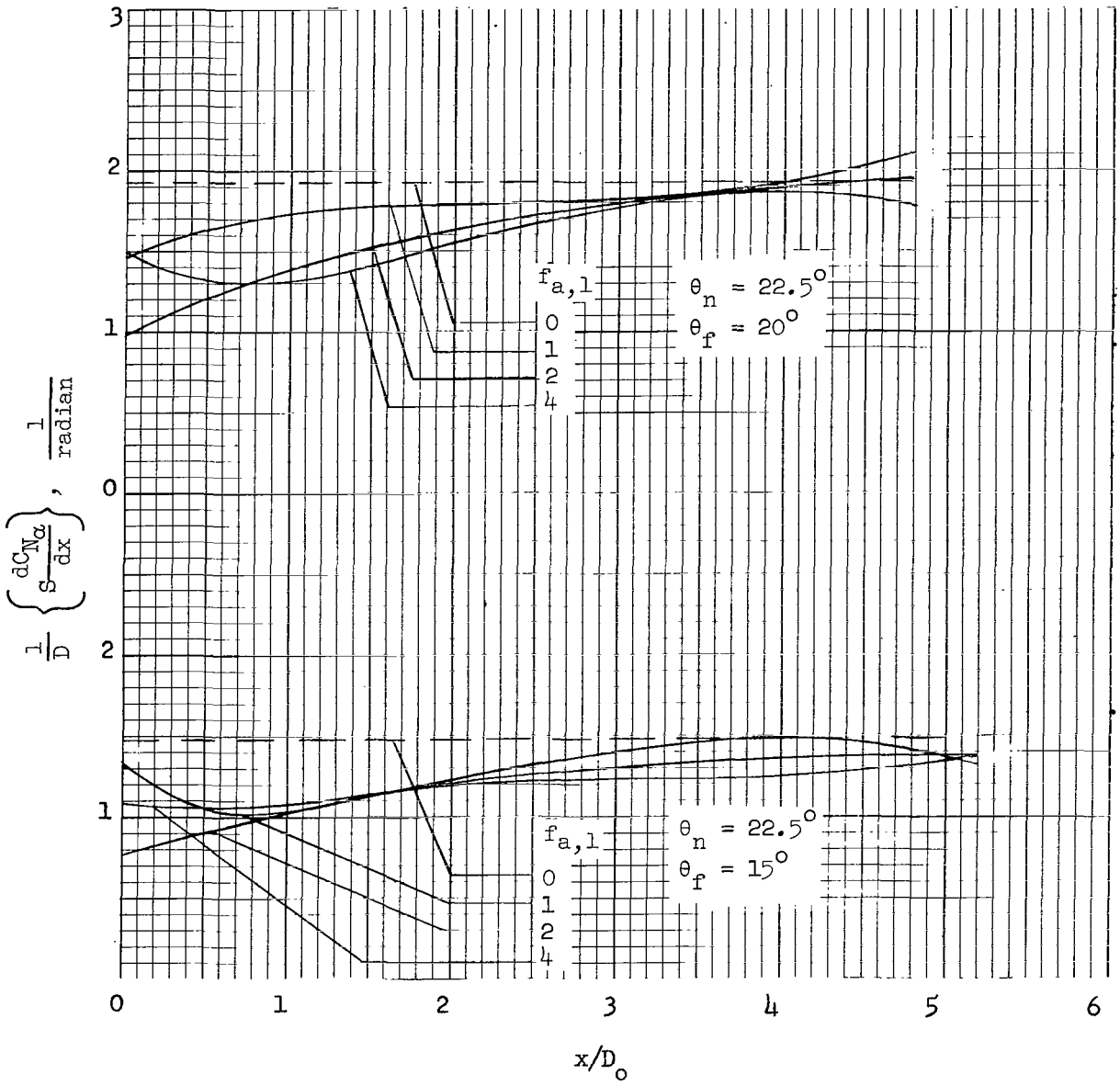


(h) M = 2.81.

Figure 7.- Continued.

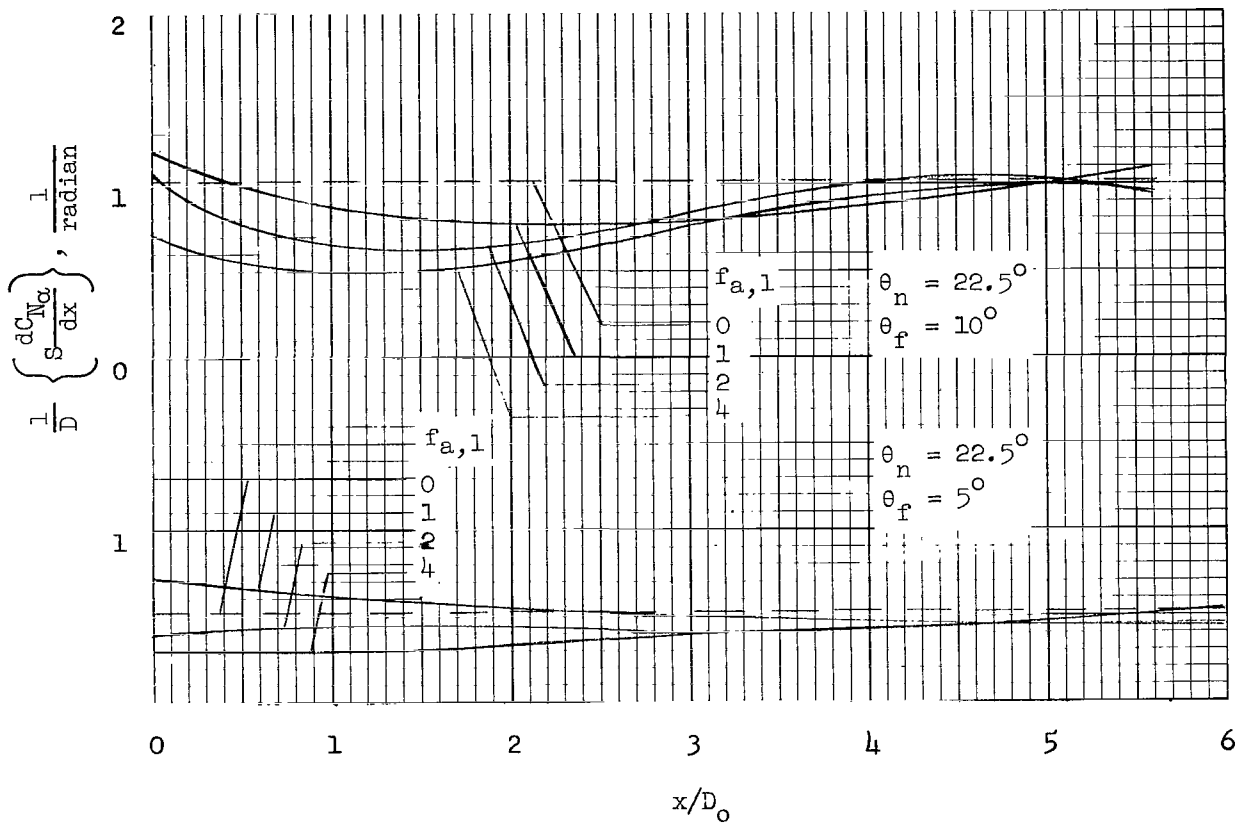


(i) M = 4.04.

Figure 7.- Continued.

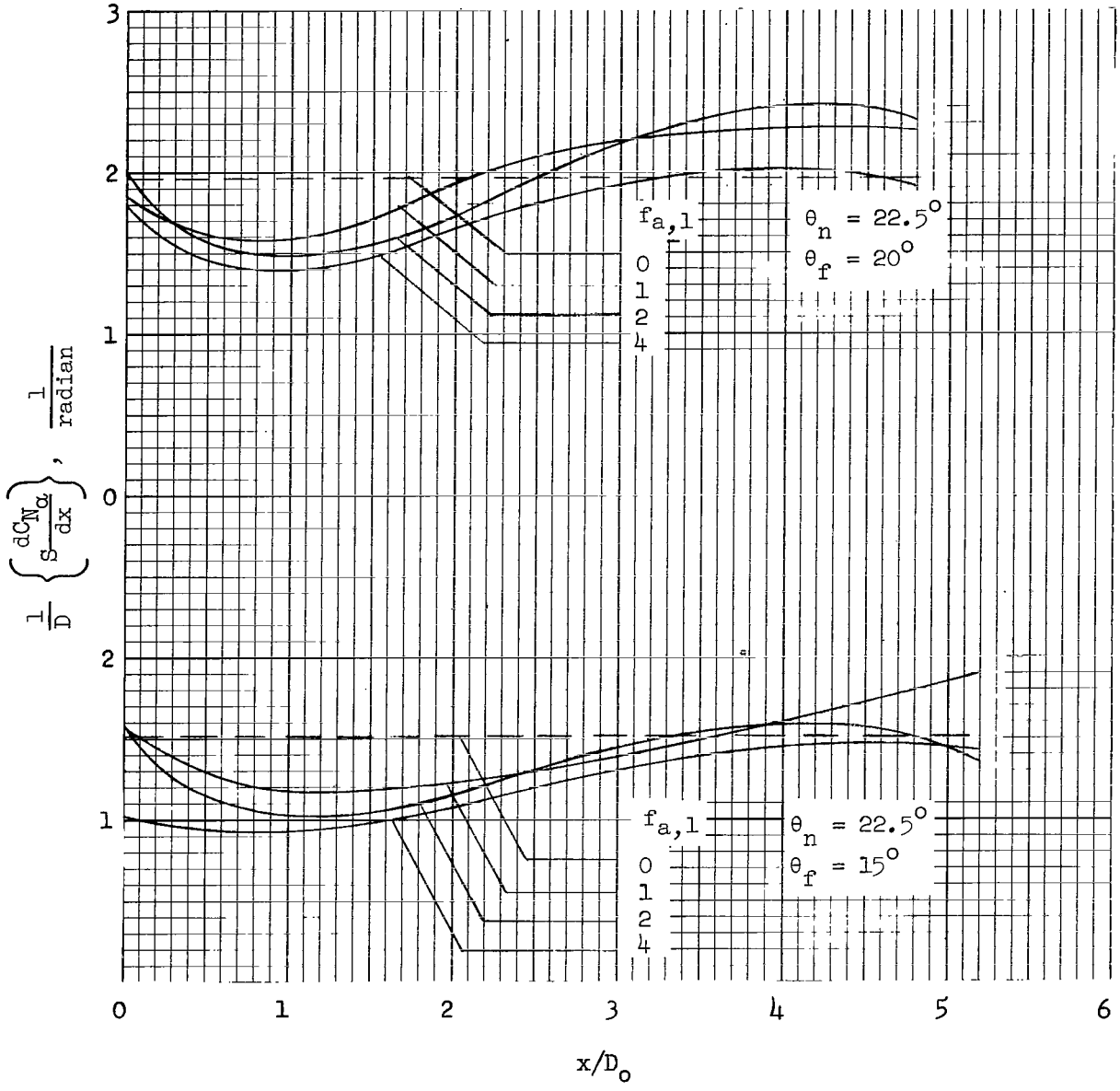


(j) M = 4.04.

Figure 7.- Concluded.

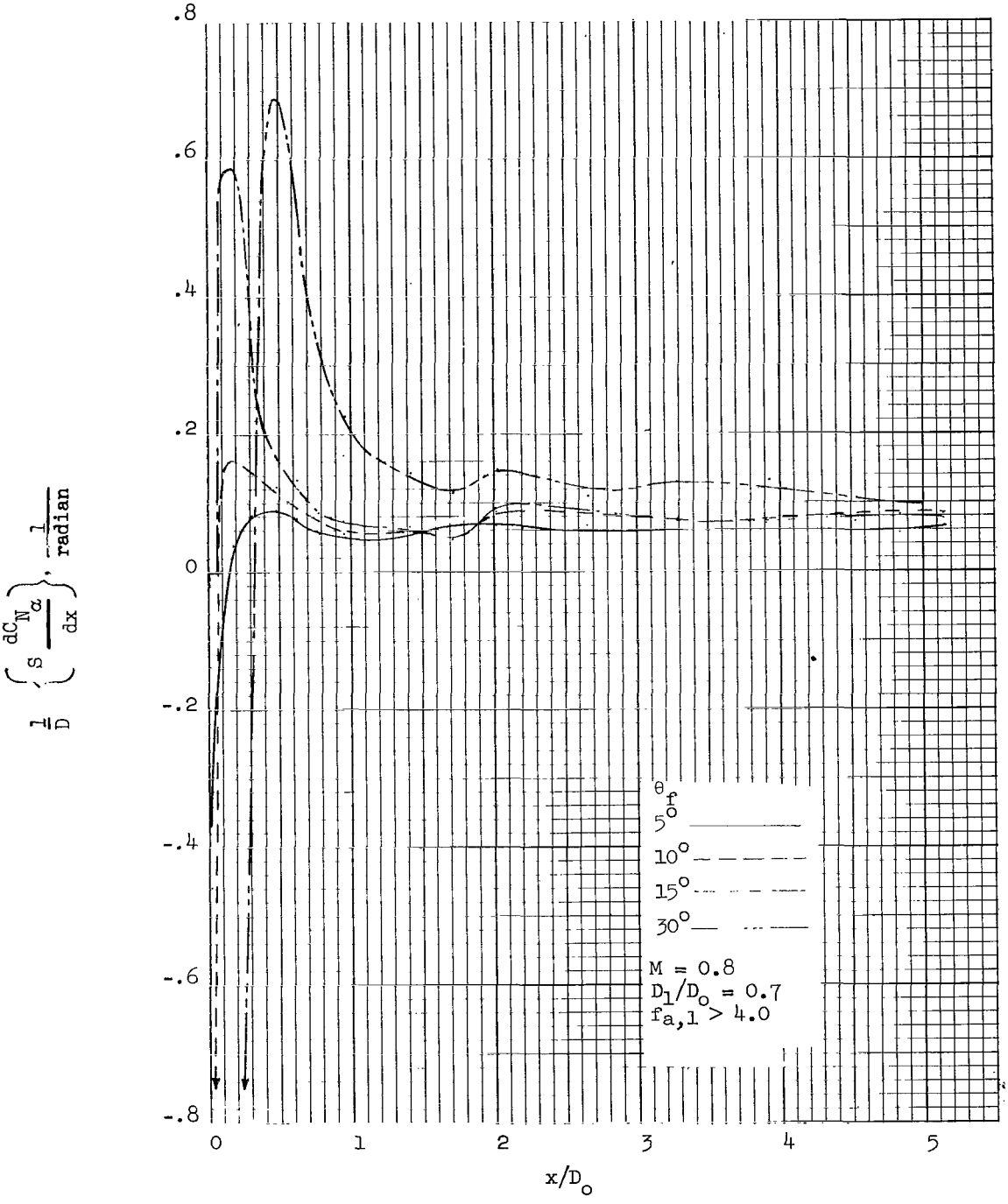


(a) M = 0.8.

Figure 8.- Loading functions for cylinders following frustums.

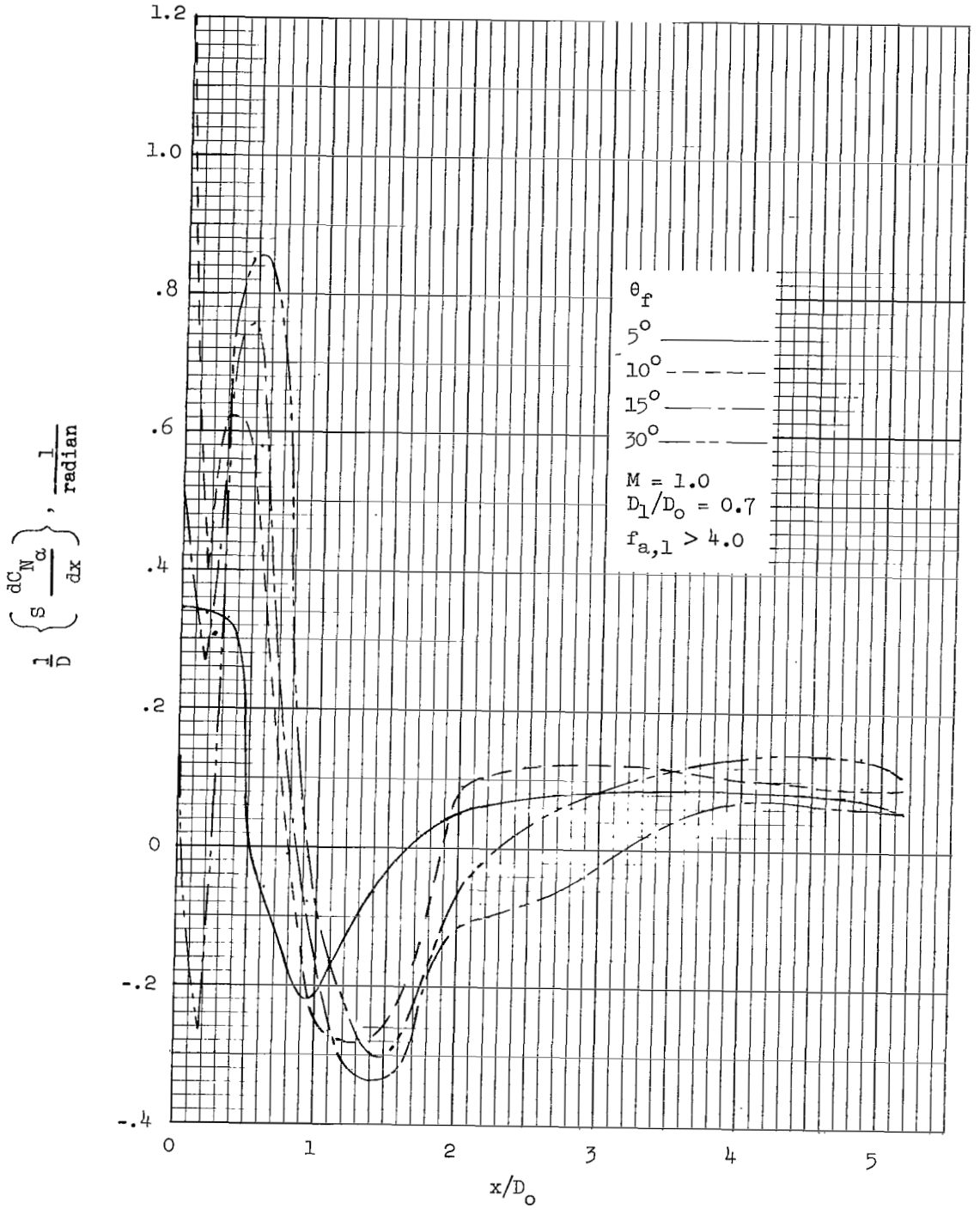


(b) M = 1.0.

Figure 8.- Continued.

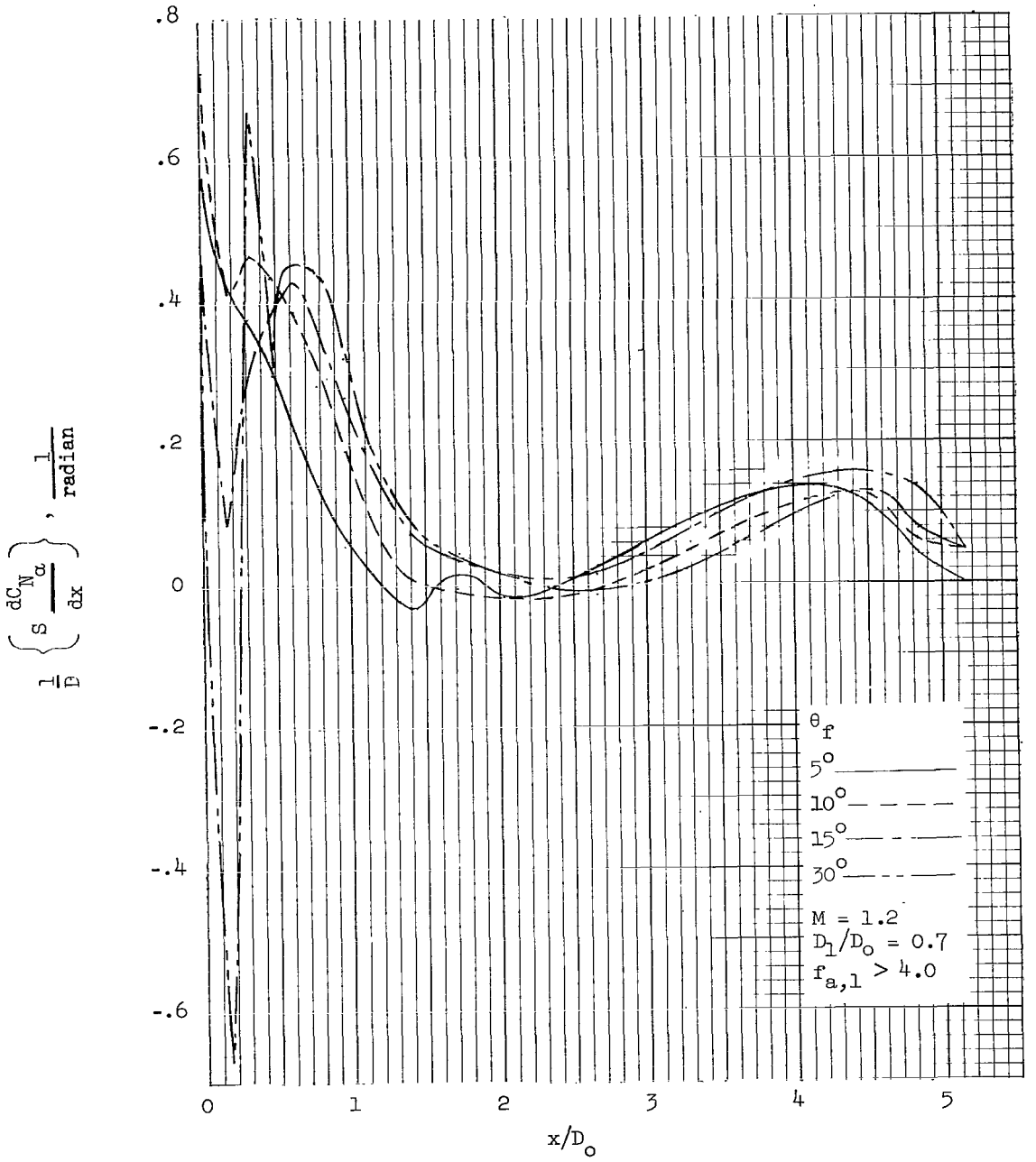


(c) M = 1.2.

Figure 8.- Continued.

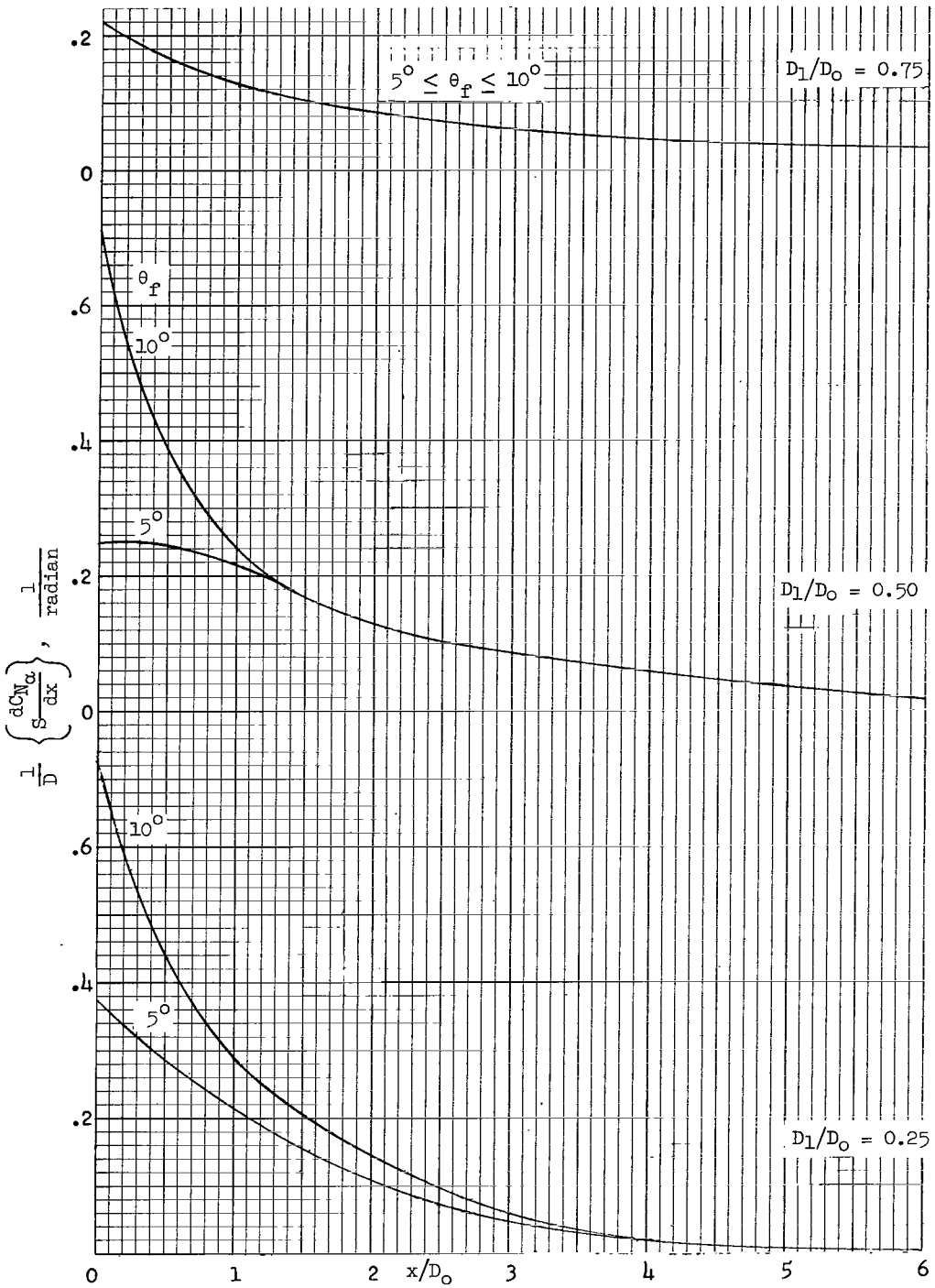


(d) M = 1.5.

Figure 8.- Continued.

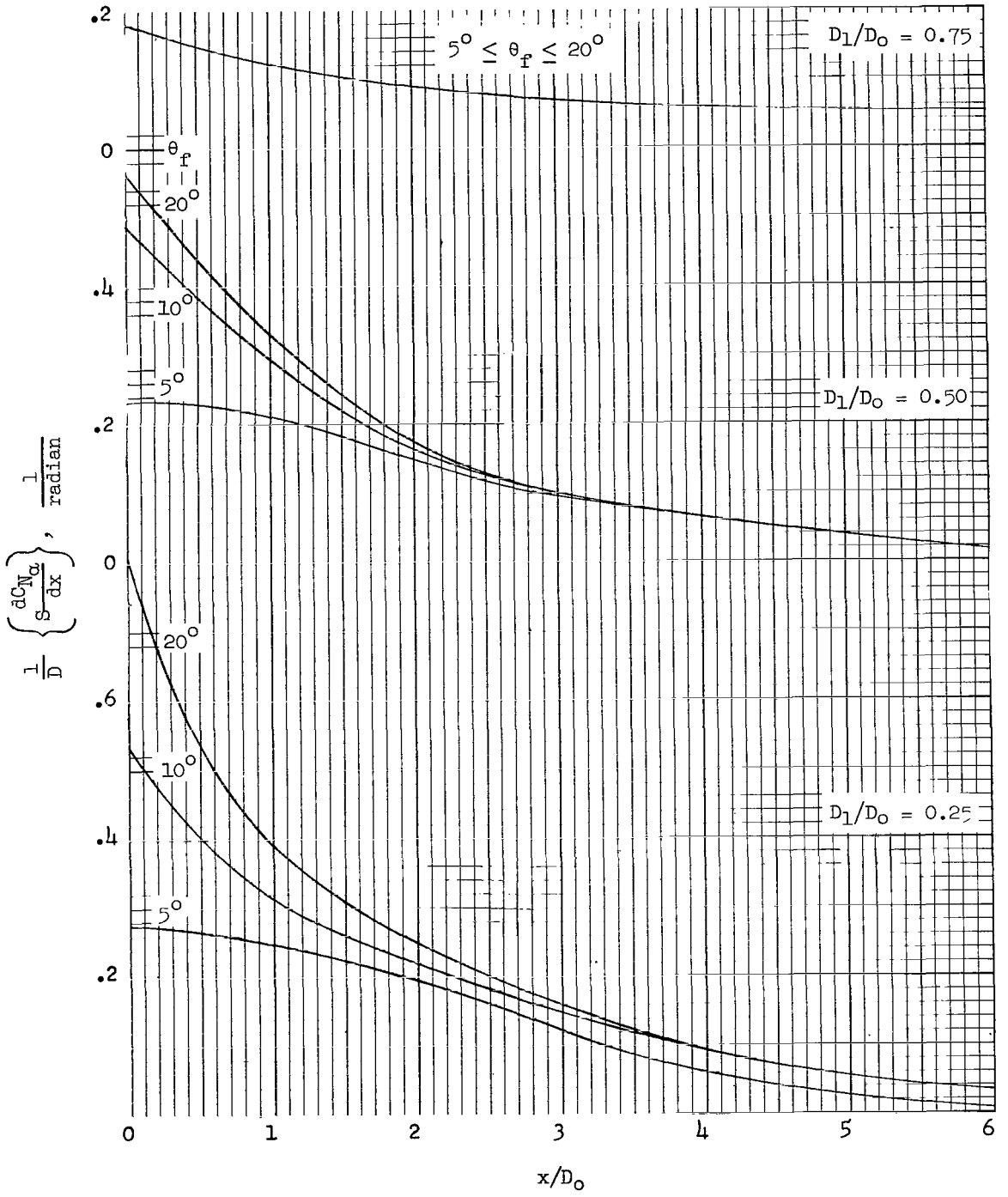


(e) M = 2.5.

Figure 8.- Continued.

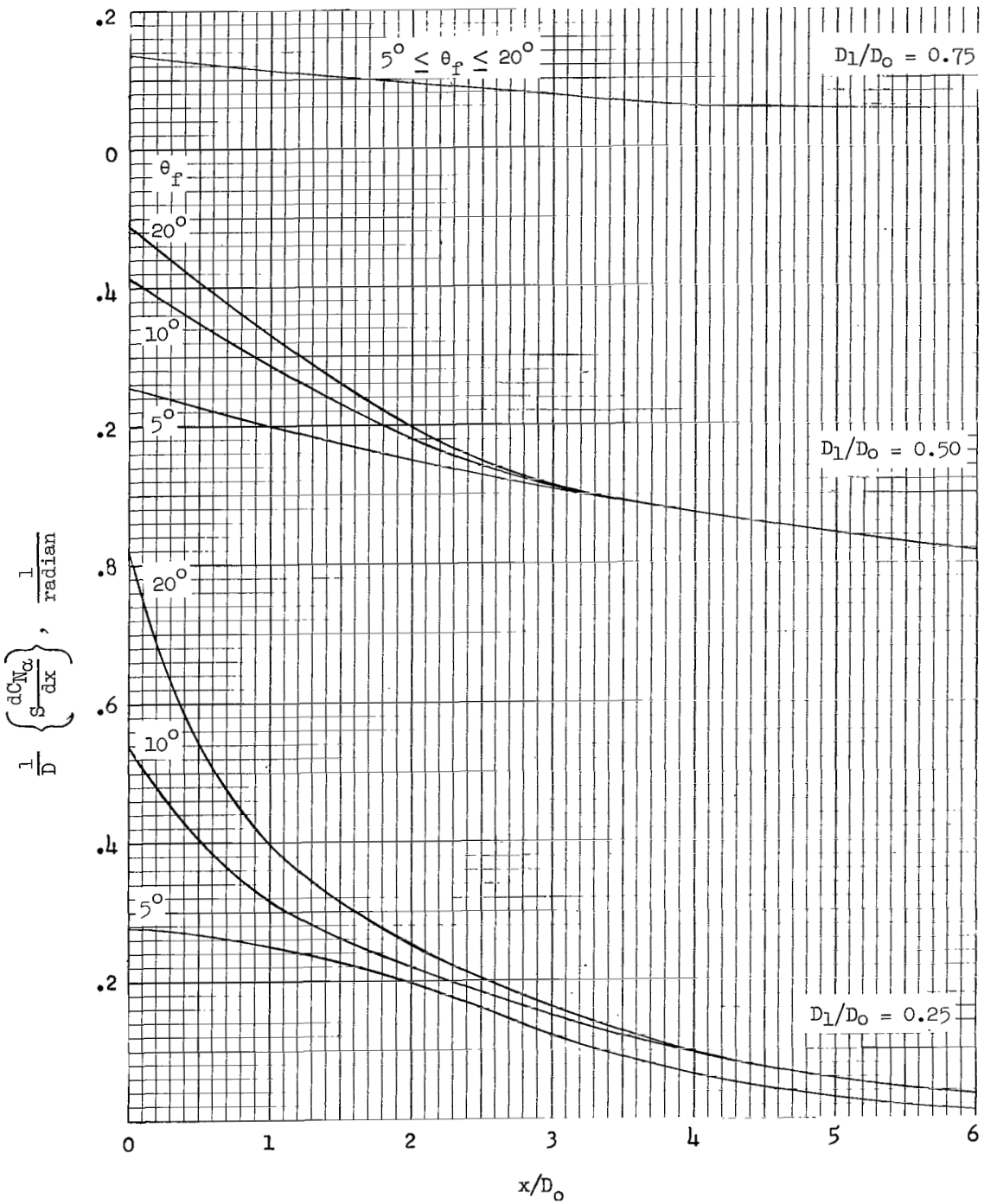


(f) M = 3.5.

Figure 8.- Continued.

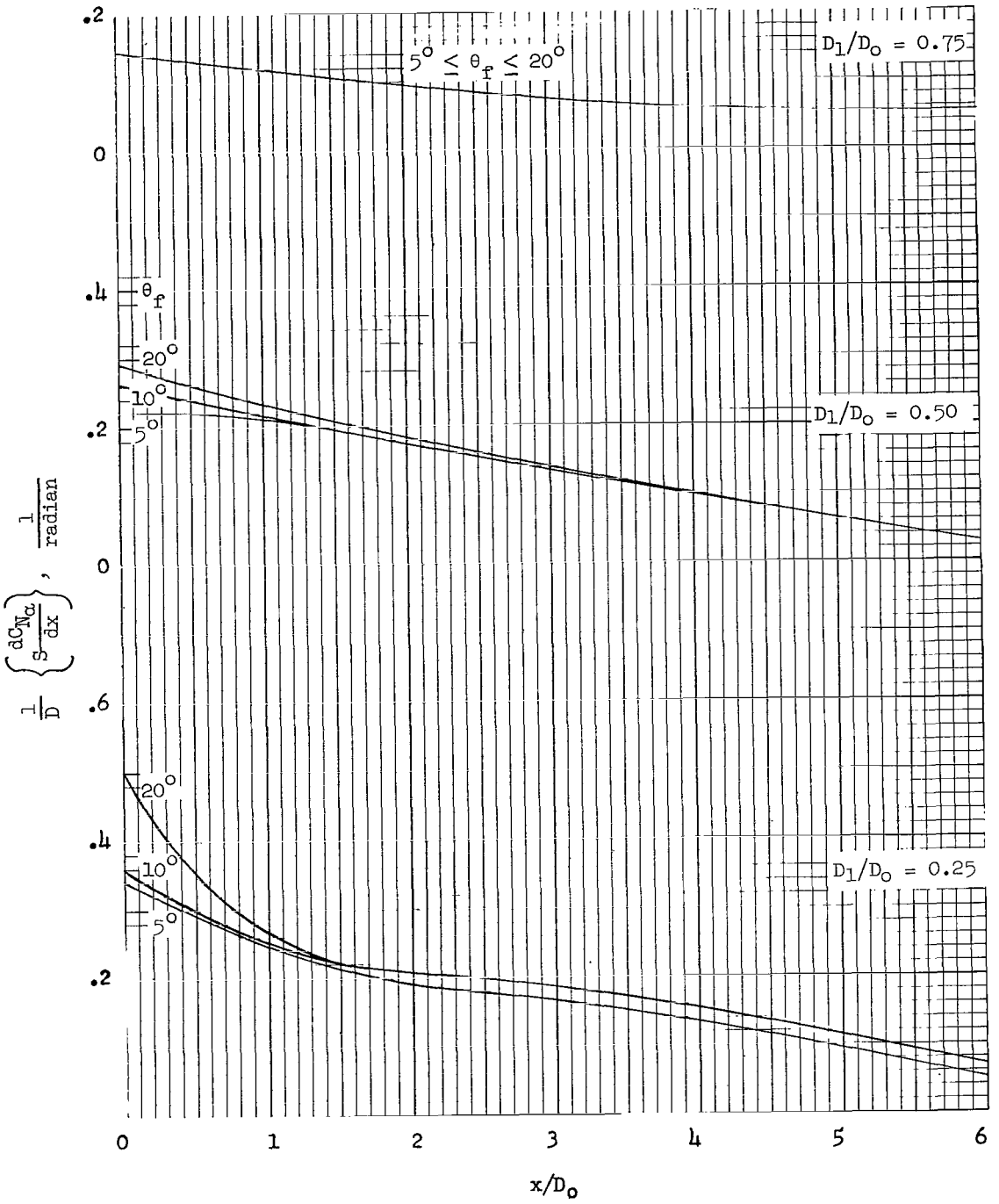


(g) M = 5.0.

Figure 8.- Concluded.

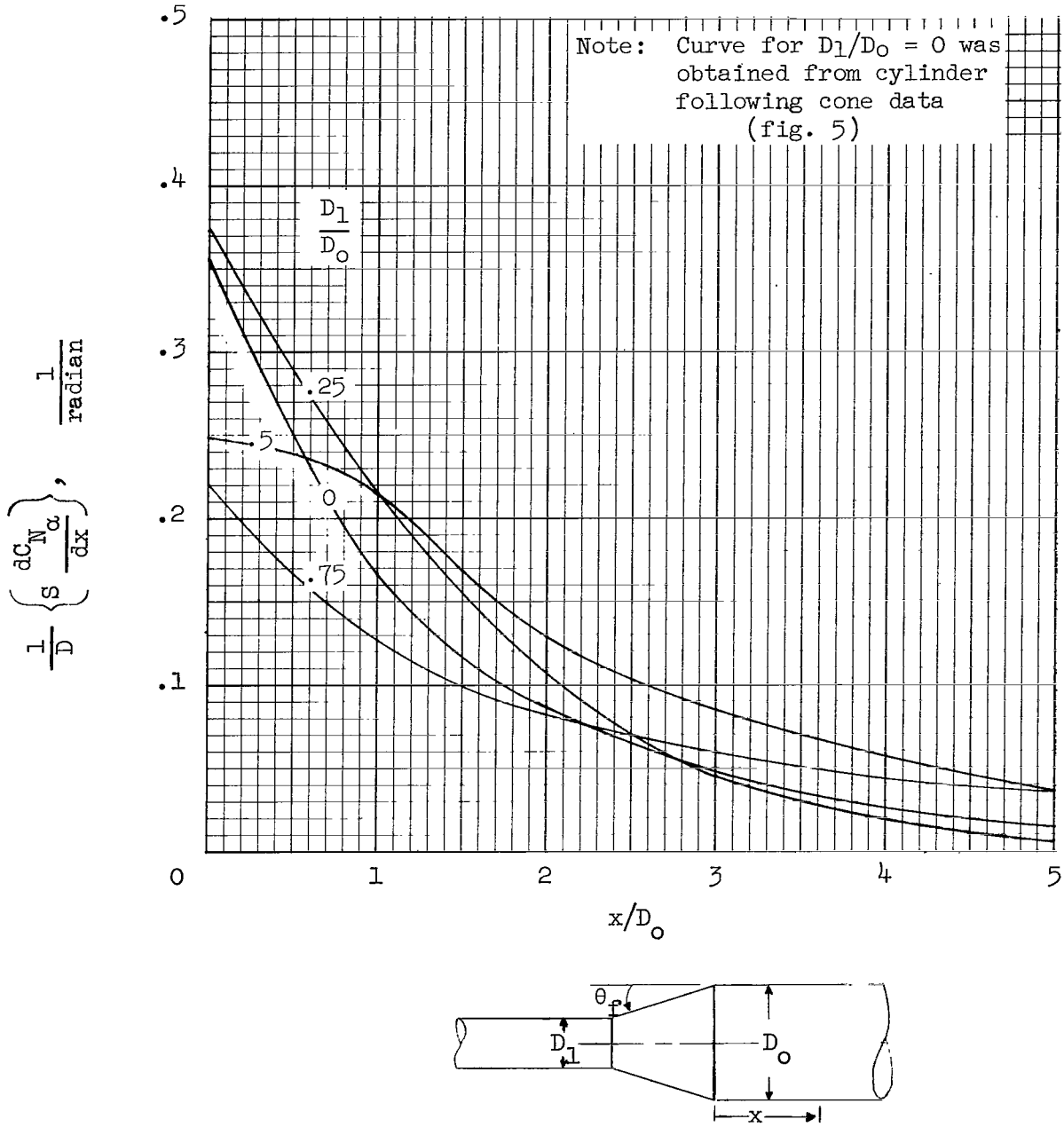


(a) M = 1.5; $\theta_f = 5^\circ$.

Figure 9.- Loading functions for cylinders following frustums. (Cross plots from fig. 8.)

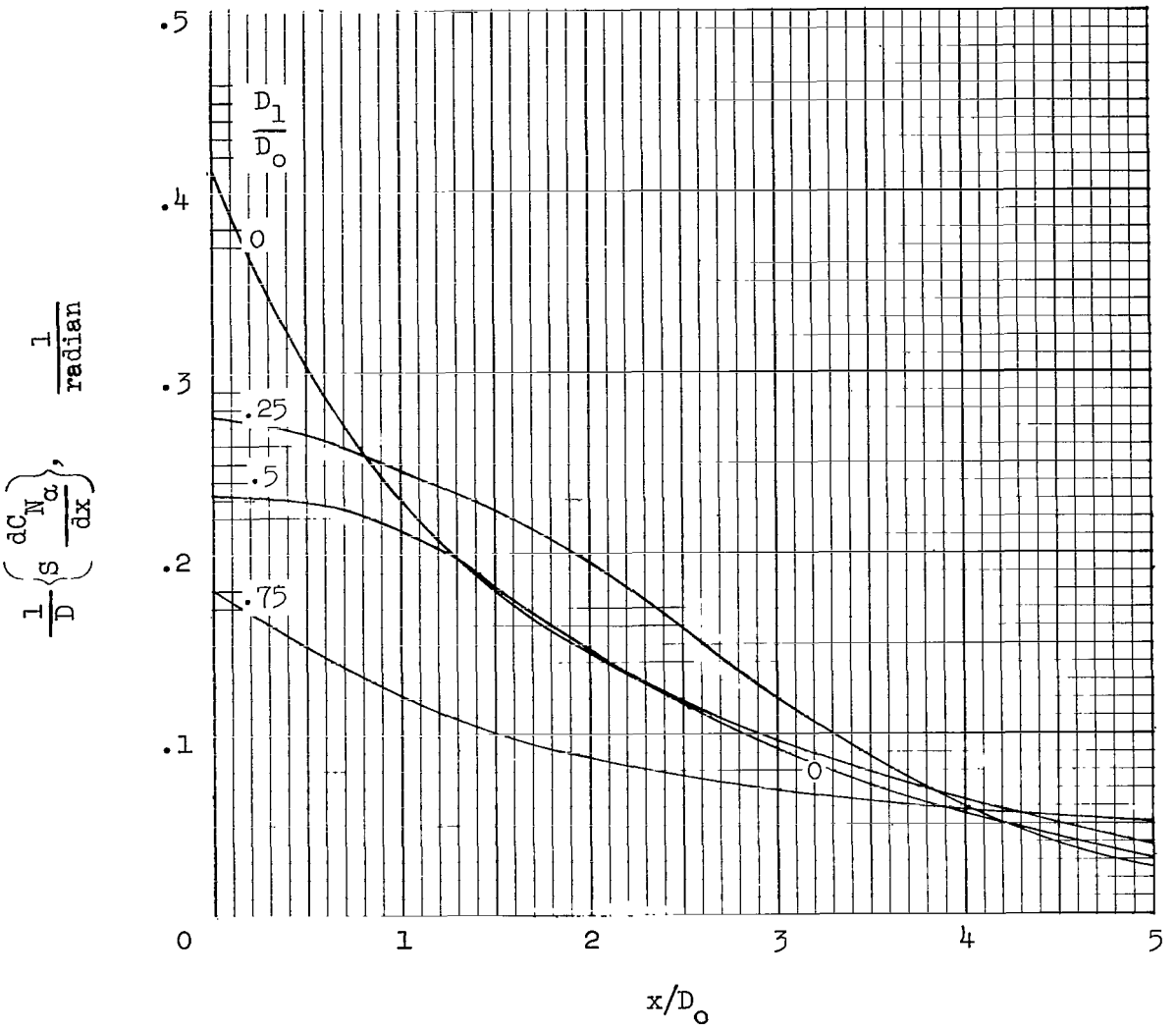


(b) $M = 2.5$; $\theta_f = 5^\circ$.

Figure 9.- Continued.

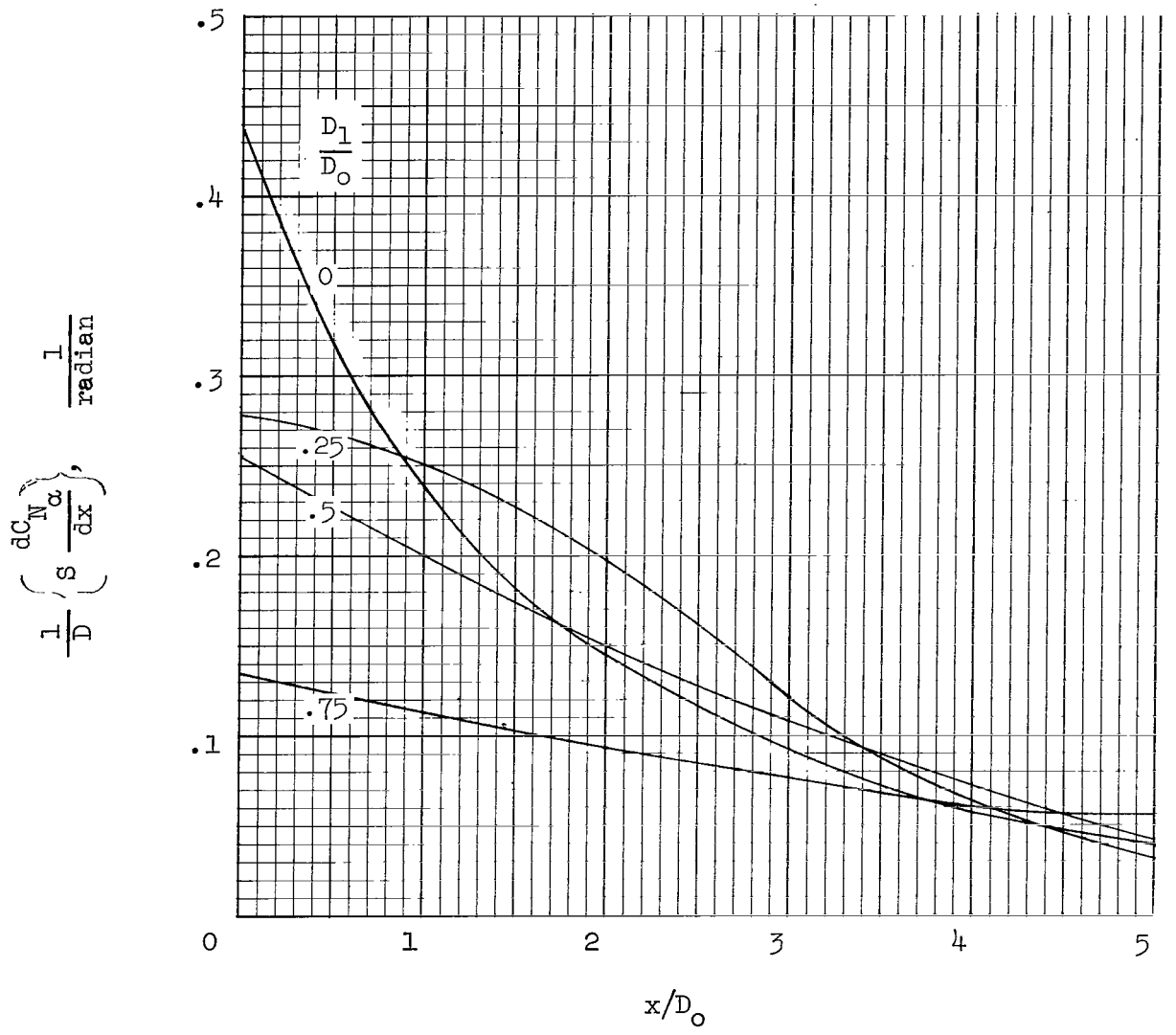


(c) $M = 3.5$; $\theta_f = 5^\circ$.

Figure 9.- Continued.

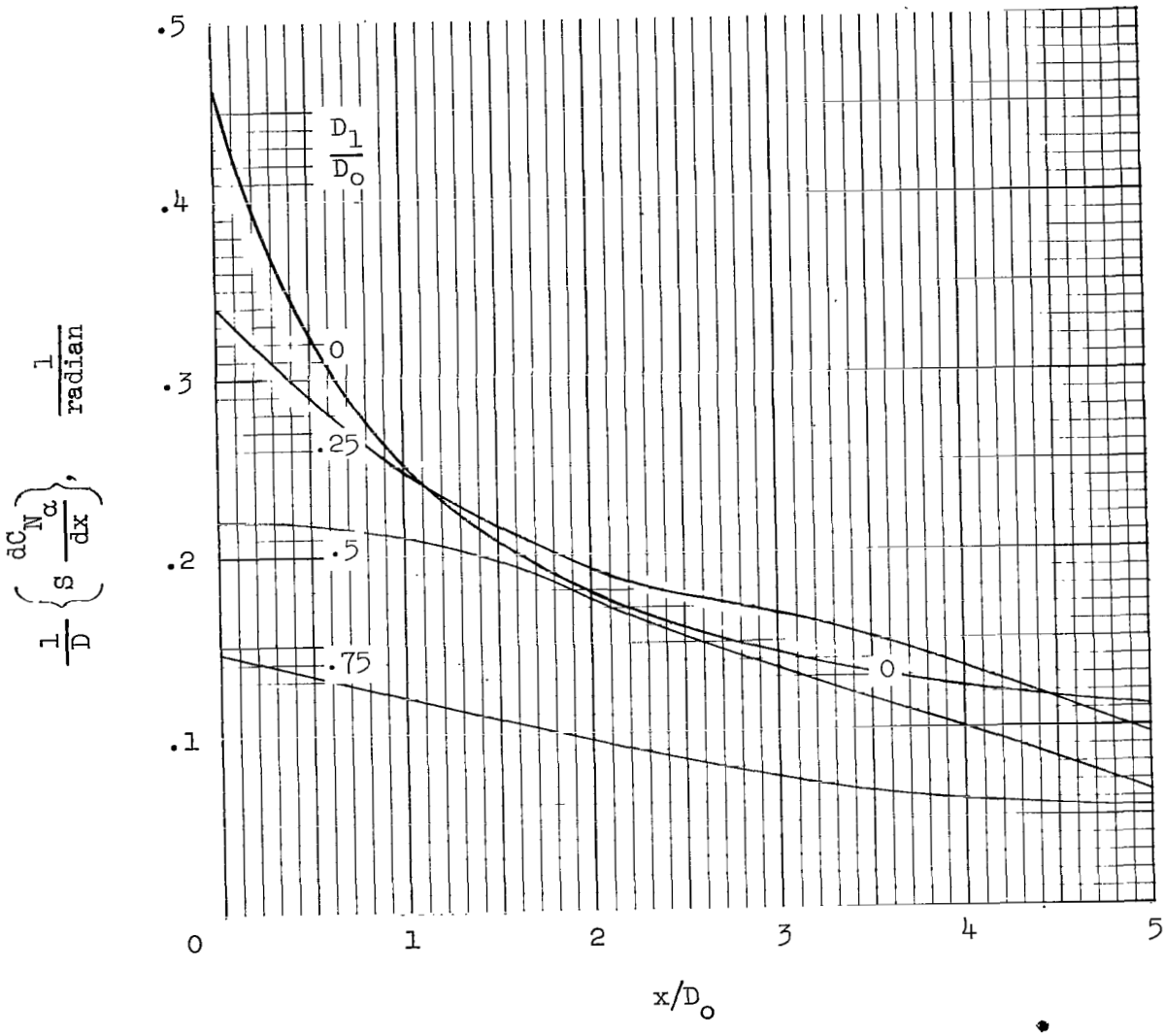


(d) $M = 5.0$; $\theta_f = 5^\circ$.

Figure 9.- Continued.

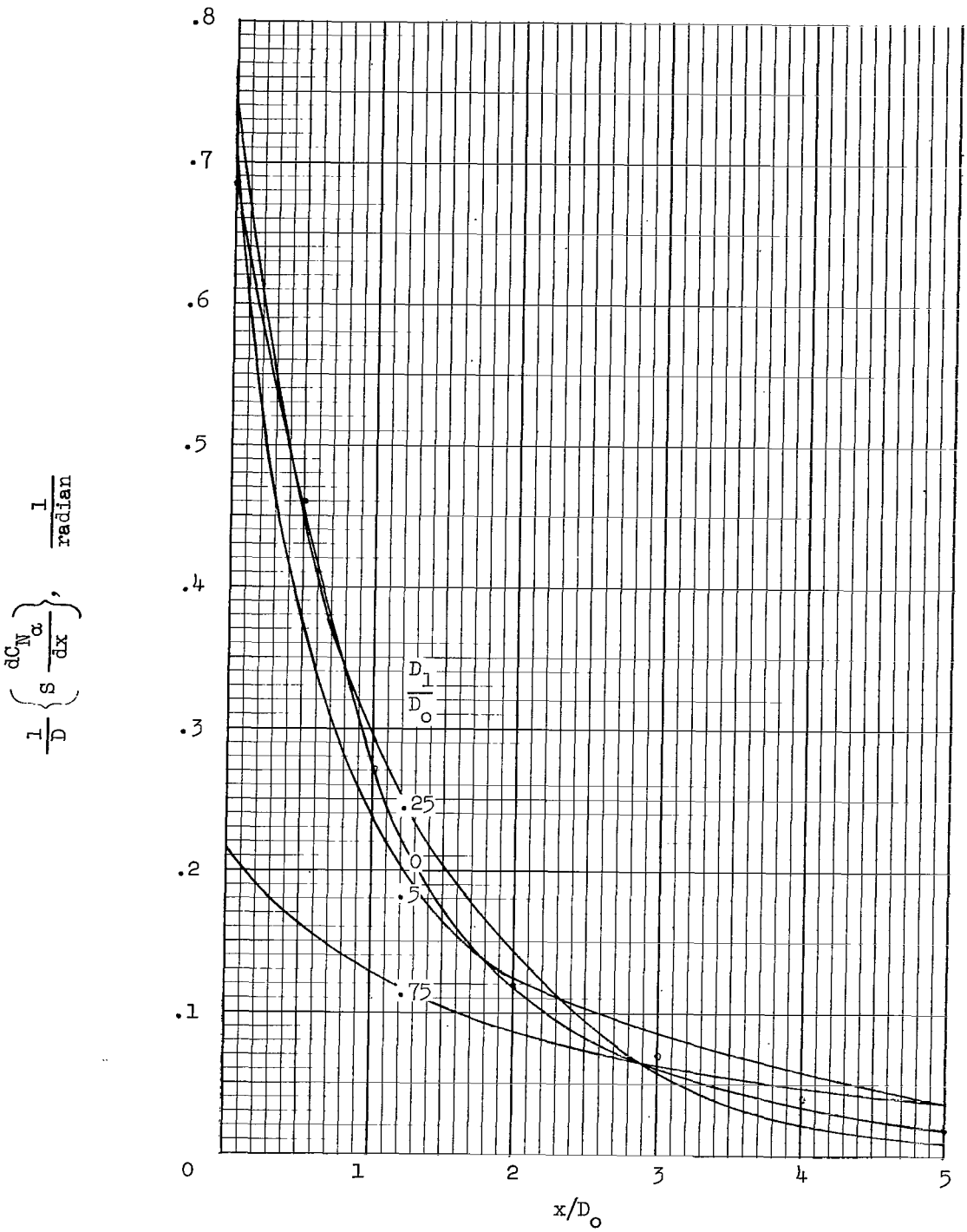


(e) $M = 1.5$; $\theta_f = 10^{\circ}$.

Figure 9.- Continued.

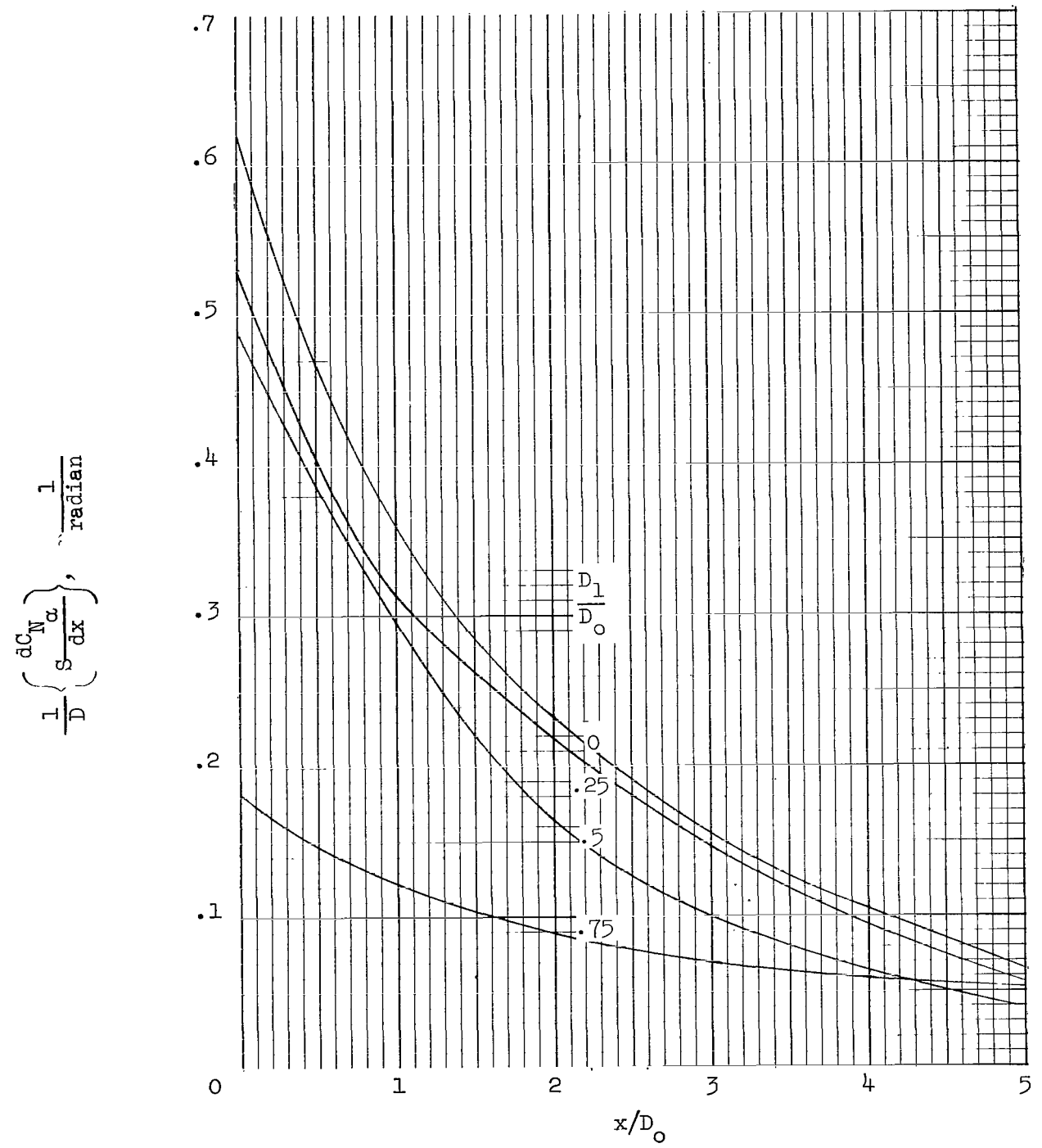


(f) $M = 2.5$; $\theta_f = 10^\circ$.

Figure 9.- Continued.

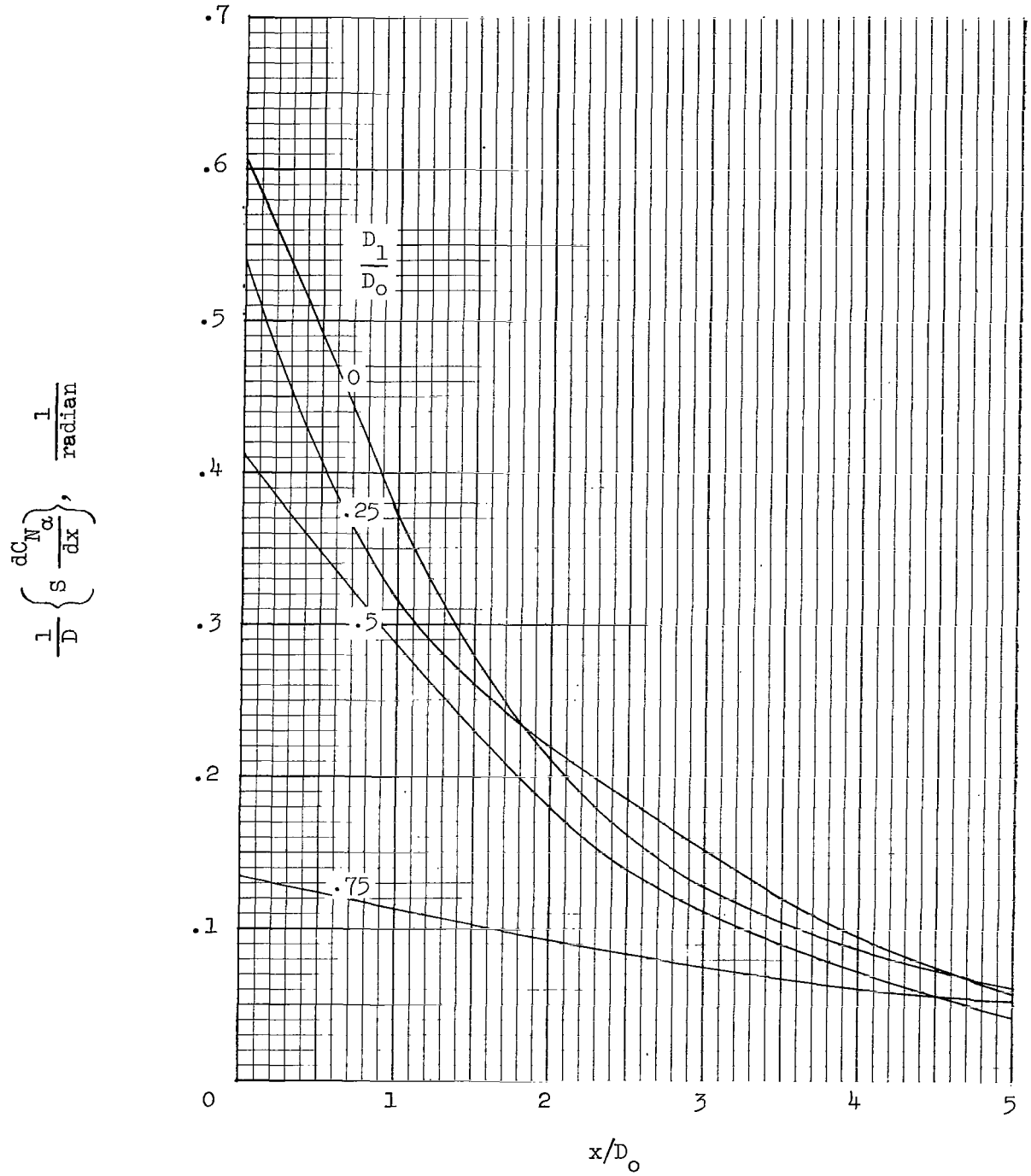


(g) $M = 3.5$; $\theta_f = 10^\circ$.

Figure 9.- Continued.

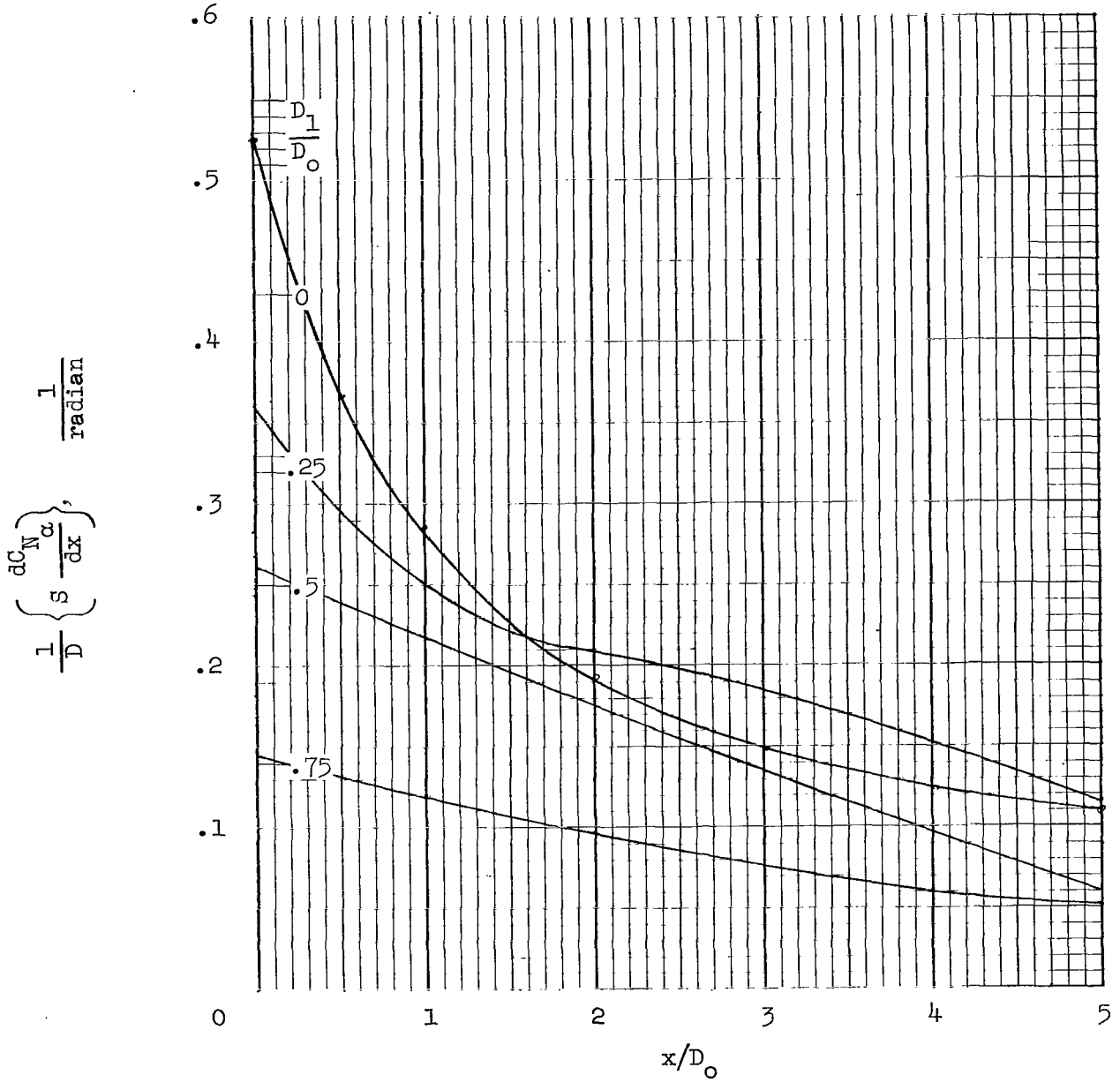


(h) $M = 5.0$; $\theta_f = 10^\circ$.

Figure 9.- Continued.

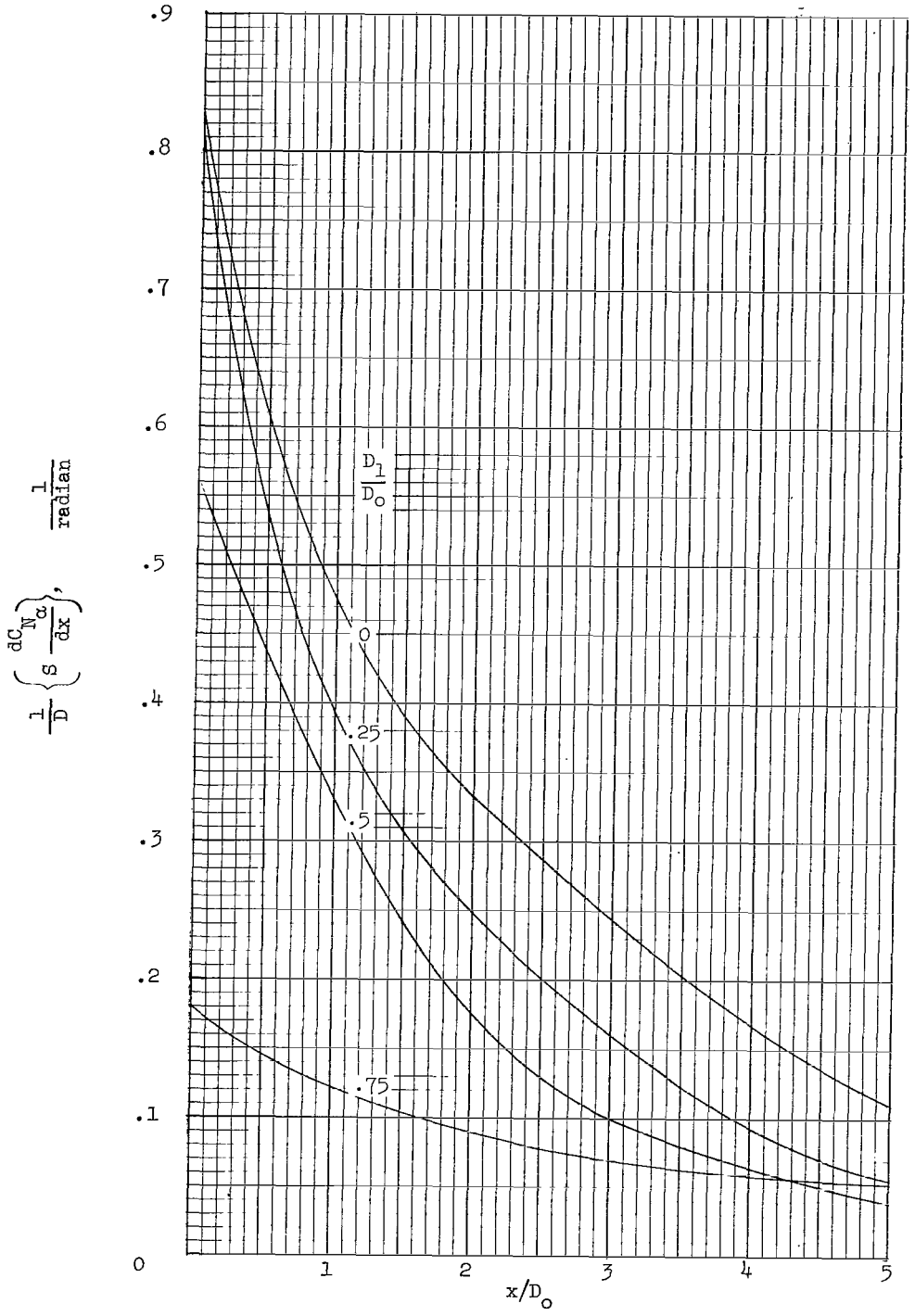


(i) $M = 2.5$; $\theta_f = 20^{\circ}$.

Figure 9.- Continued.

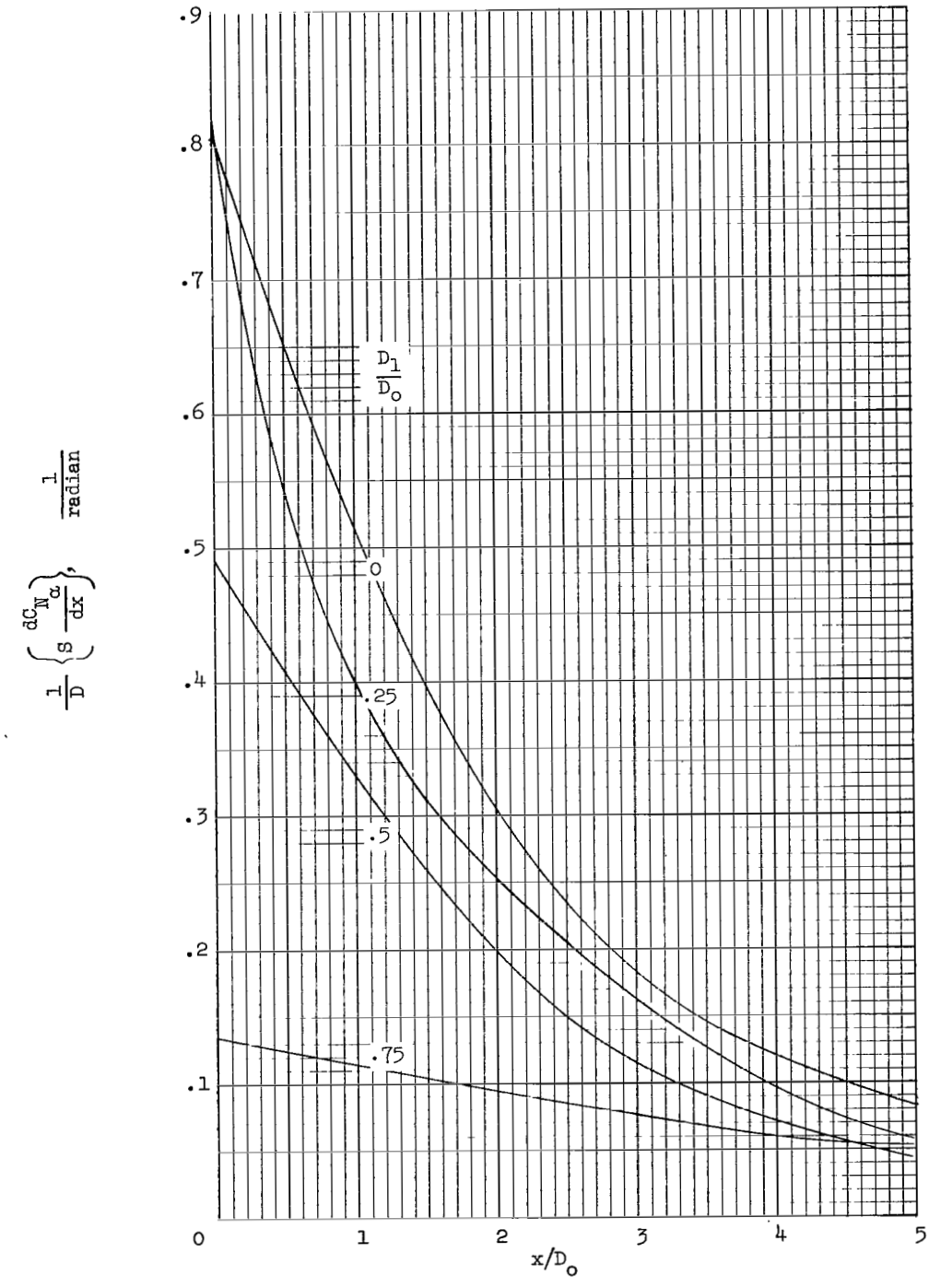


(j) M = 3.5; $\theta_f = 20^\circ$.

Figure 9.- Continued.

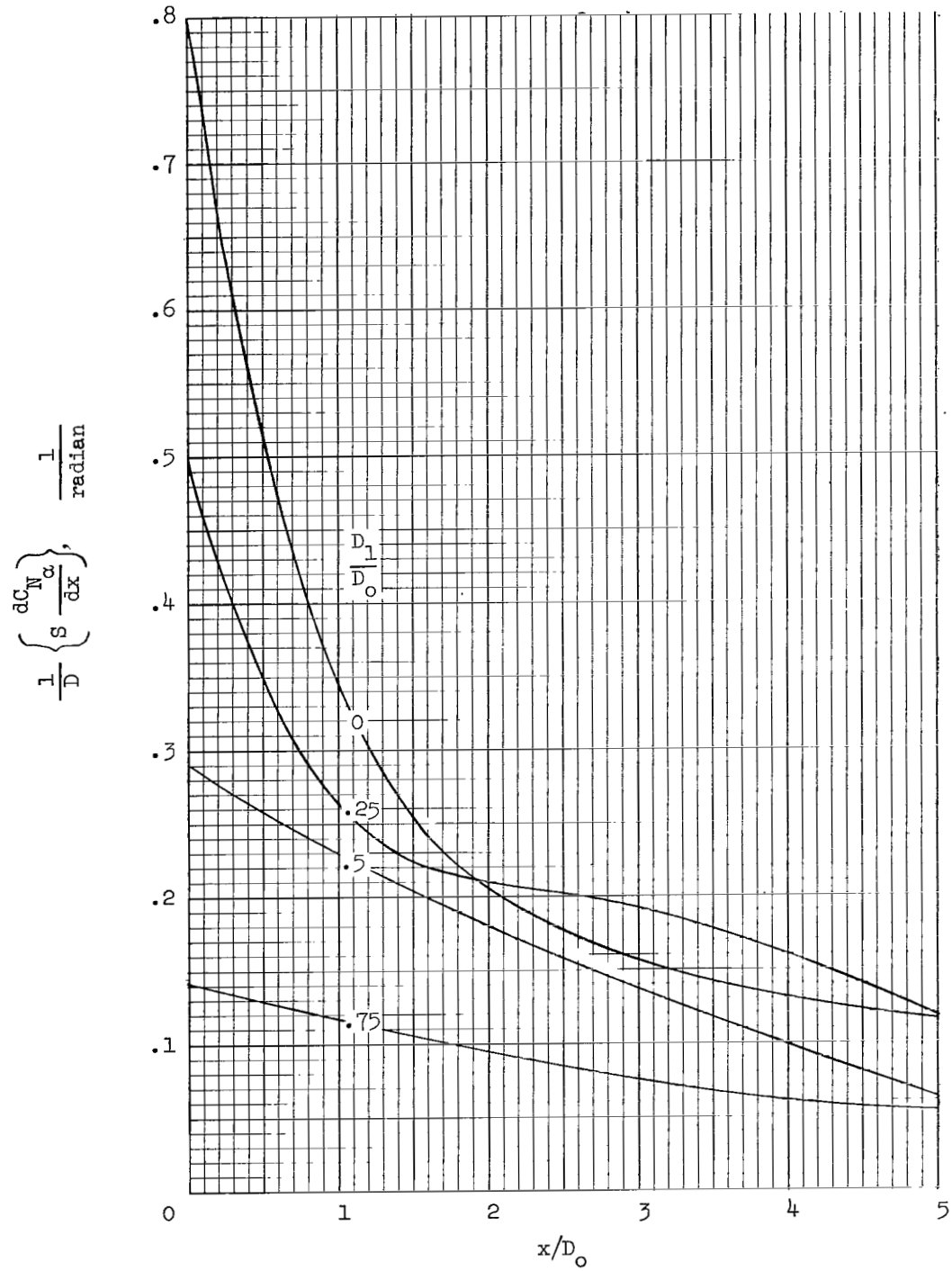


(k) $M = 5.0$; $\theta_f = 20^\circ$.

Figure 9.- Concluded.

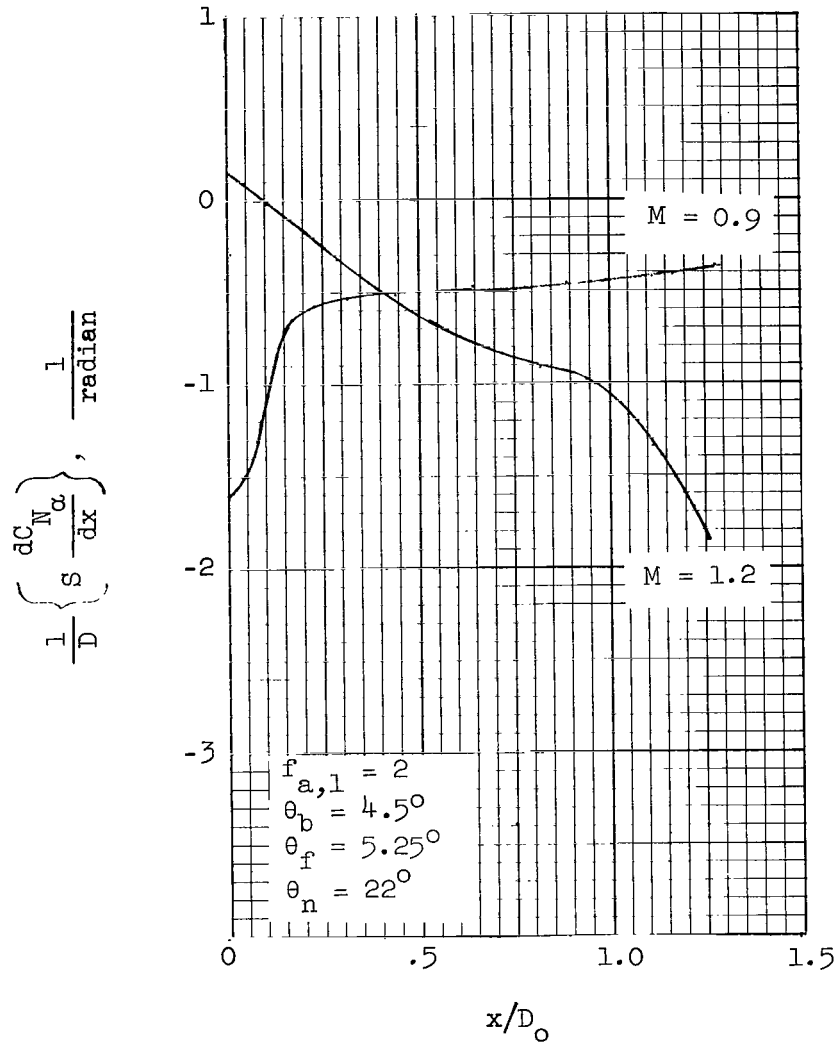


(a) Boattail following a short cone-cylinder and preceding a frustum.

Figure 10.- Loading functions for boattails.

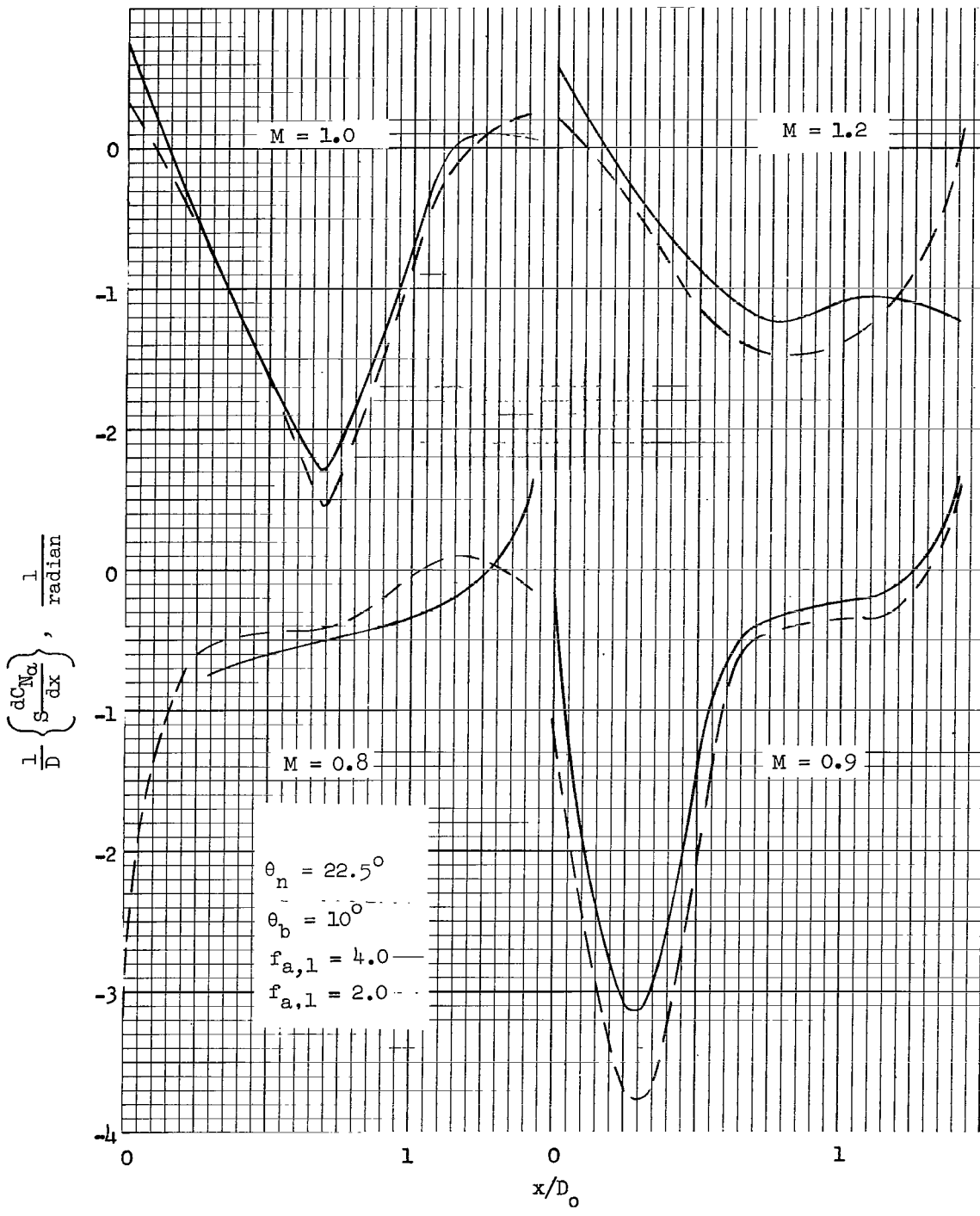


(b) Boattail following a short cone-cylinder and preceding a cylinder.

Figure 10.- Concluded.

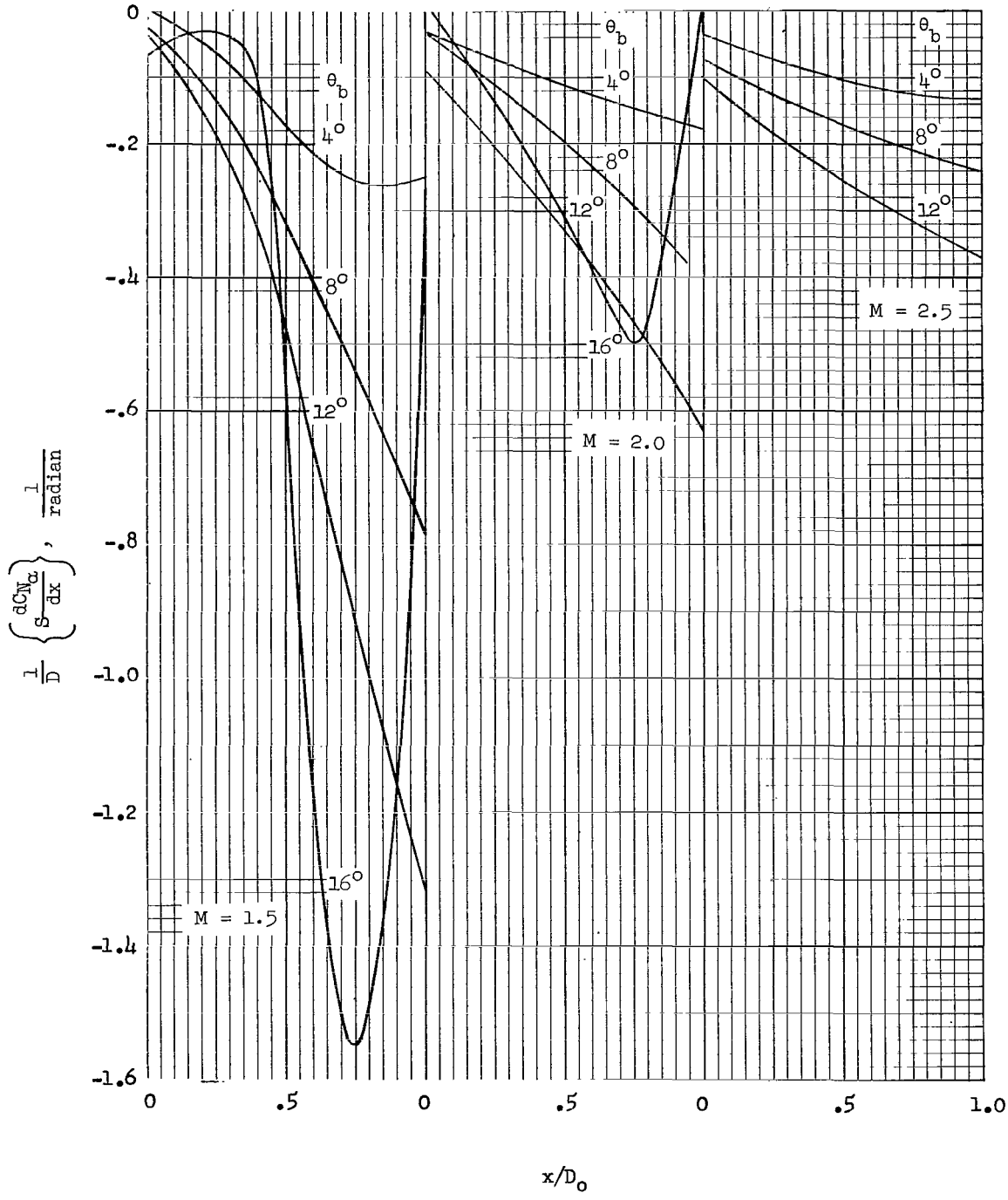


(a) M = 1.5, 2.0, and 2.5.

Figure 11.- Loading functions for boattails following long cylinders.

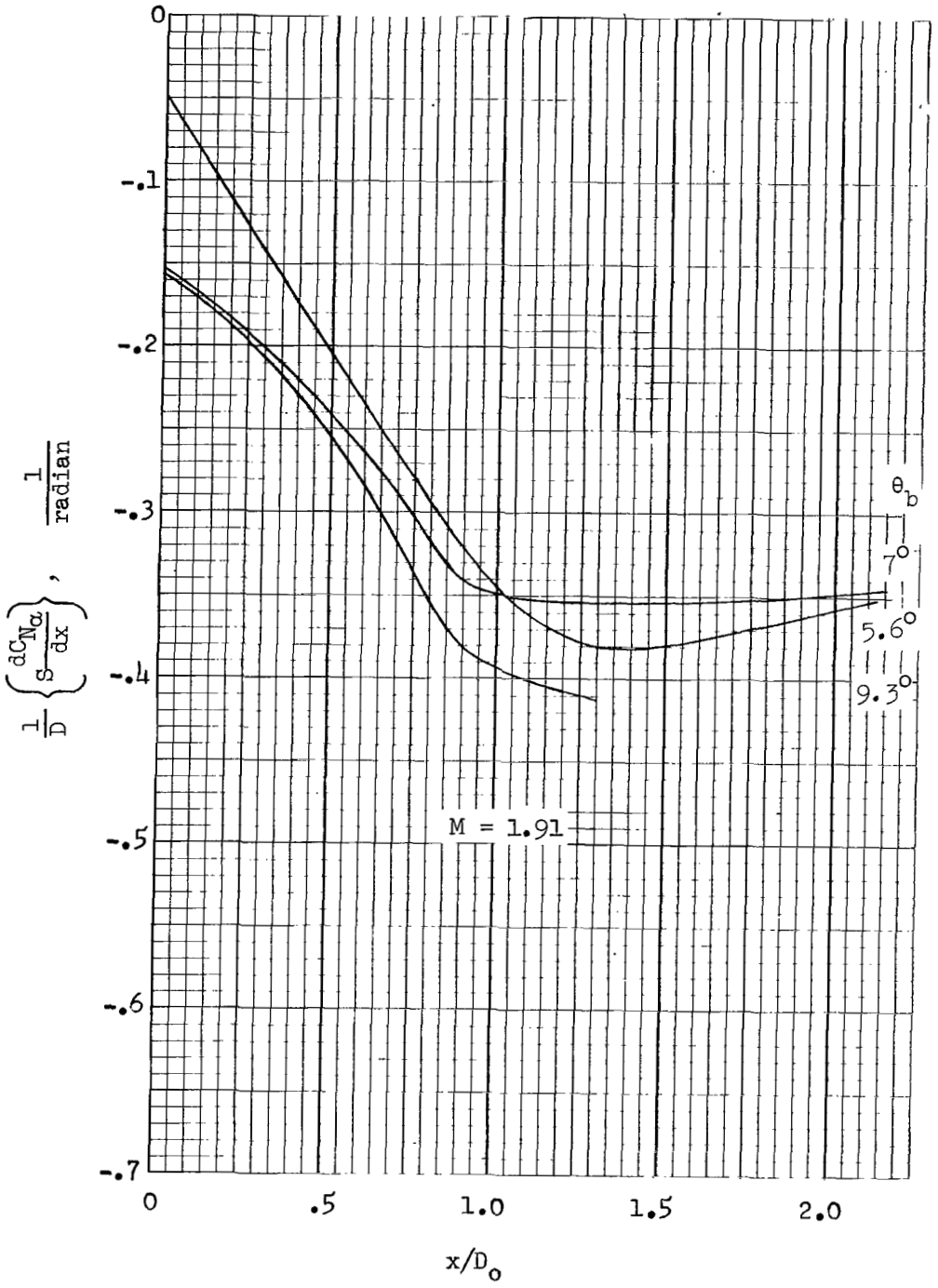


(b) M = 1.91.

Figure 11.- Continued.

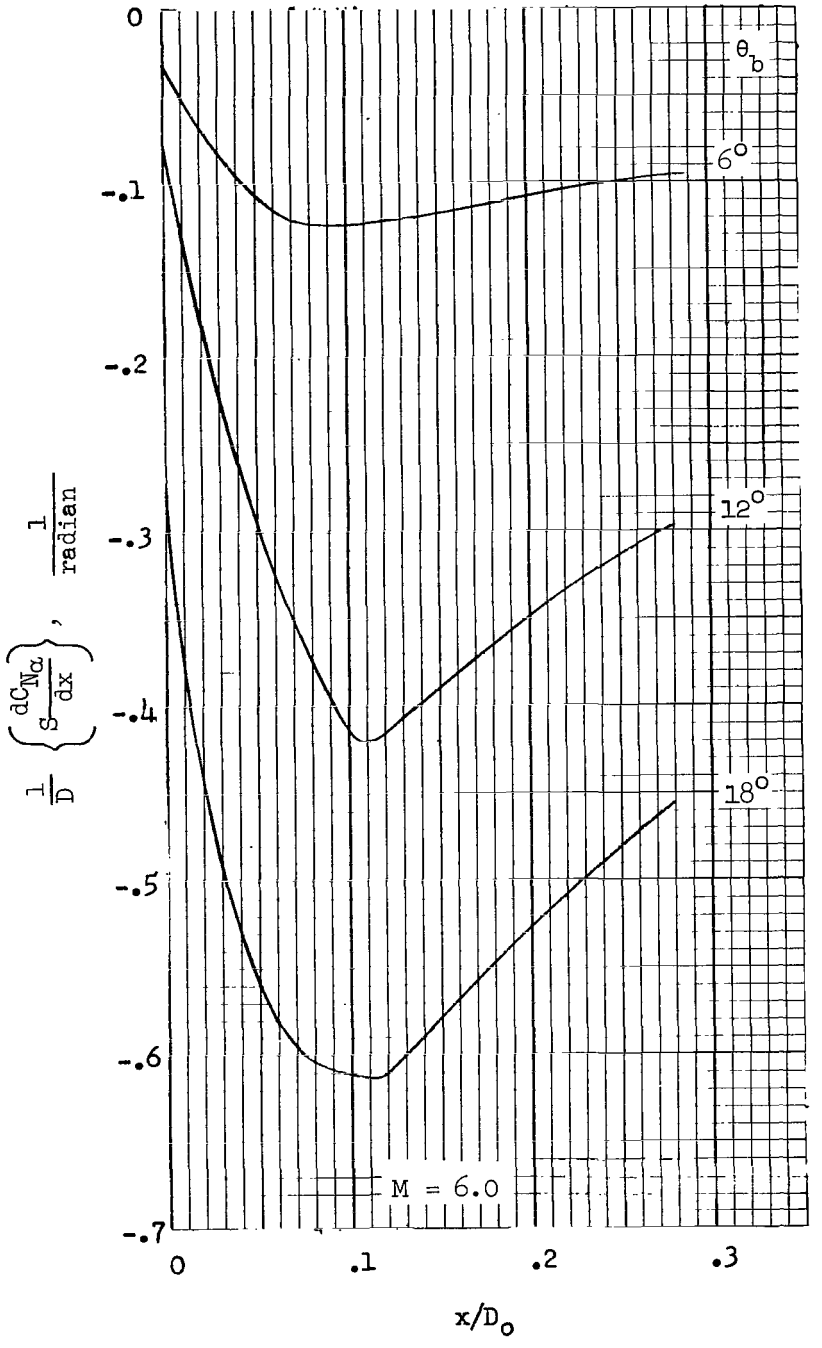


(c) M = 6.0.

Figure 11.- Concluded.

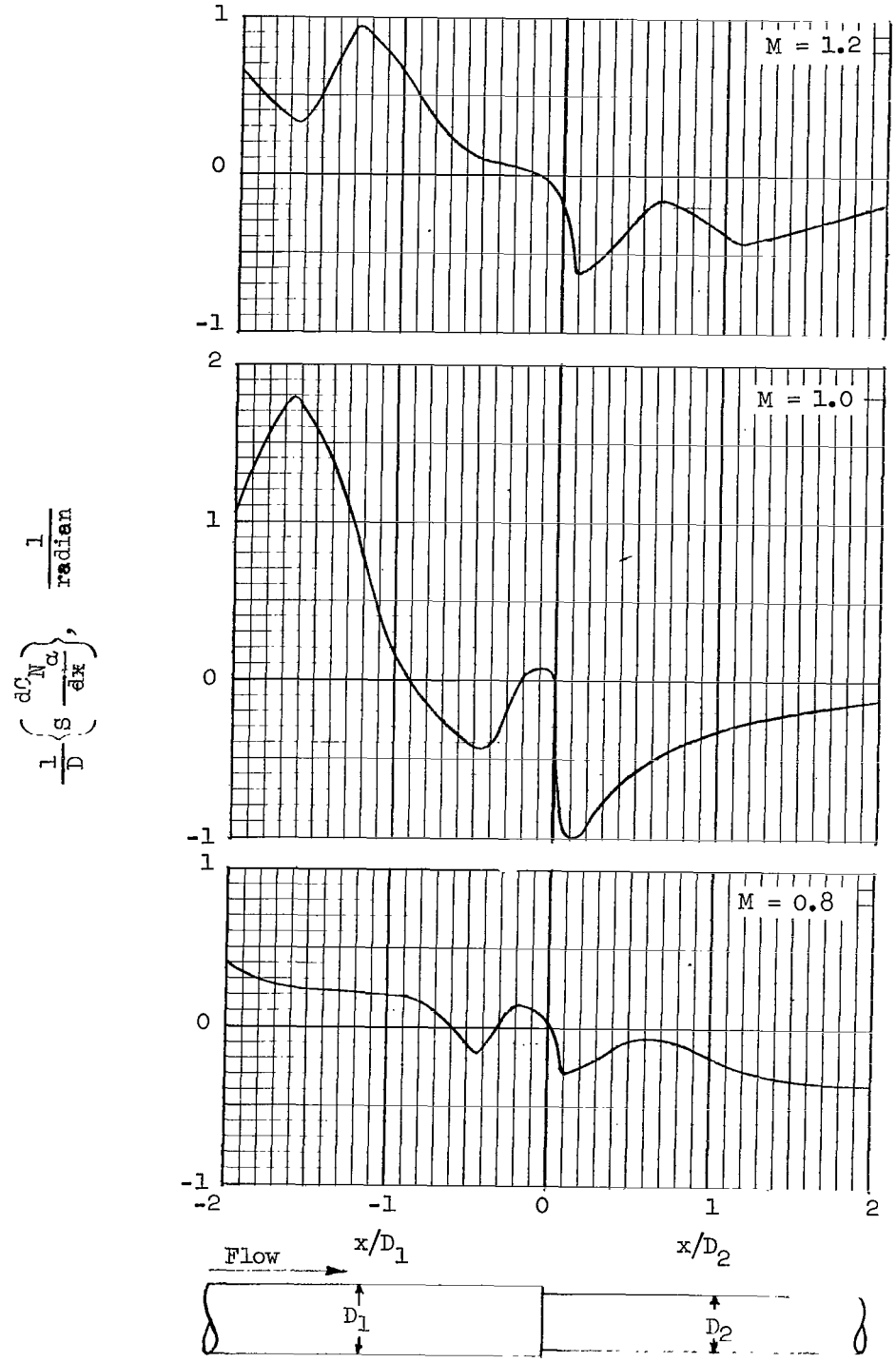


(a) M = 0.8 to 1.2.

Figure 12.- Loading functions in the vicinity of a rearward-facing step with $D_1/D_2 = 1.083$.

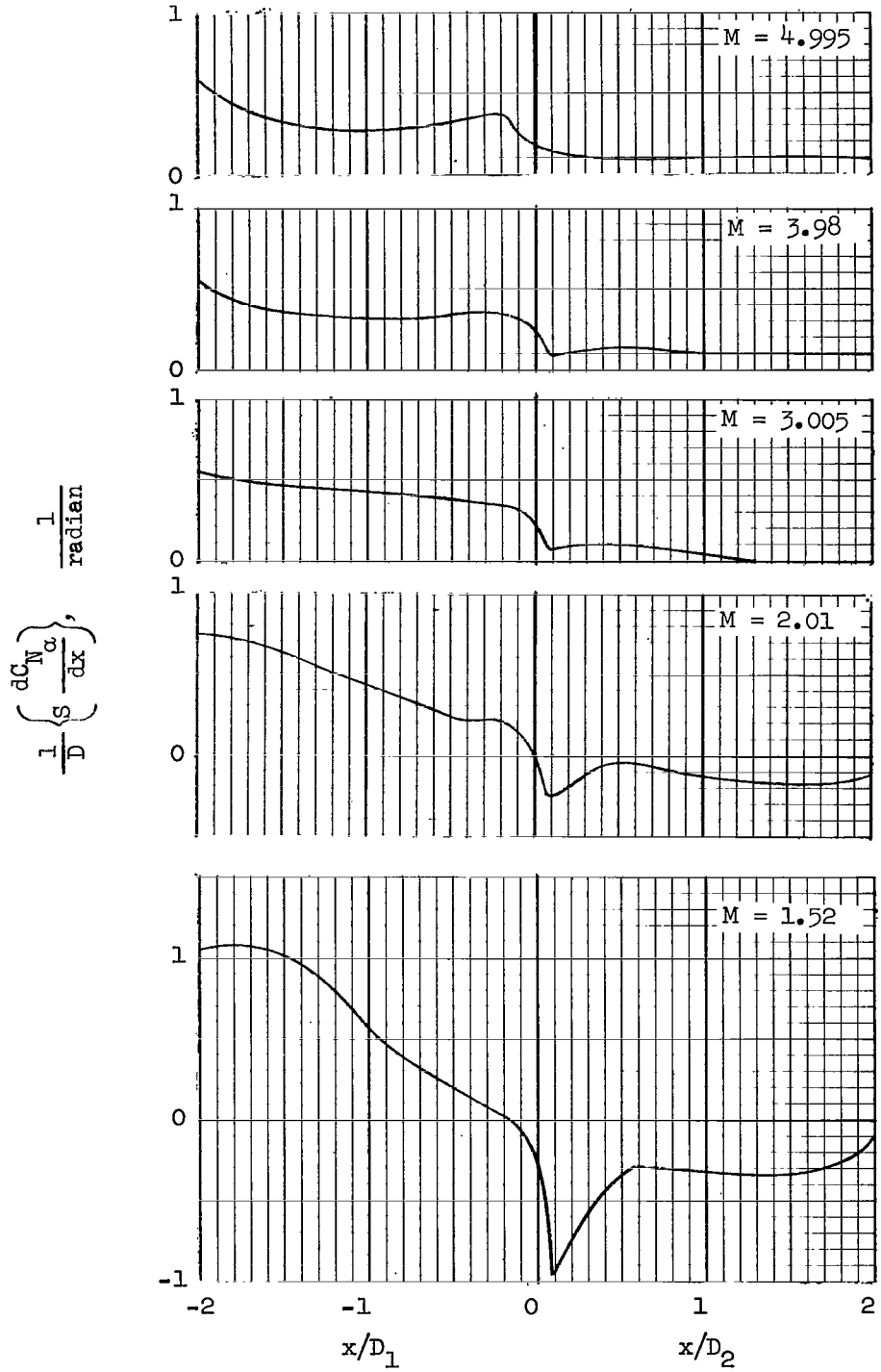


(b) M = 1.52 to 4.995.

Figure 12.- Concluded.

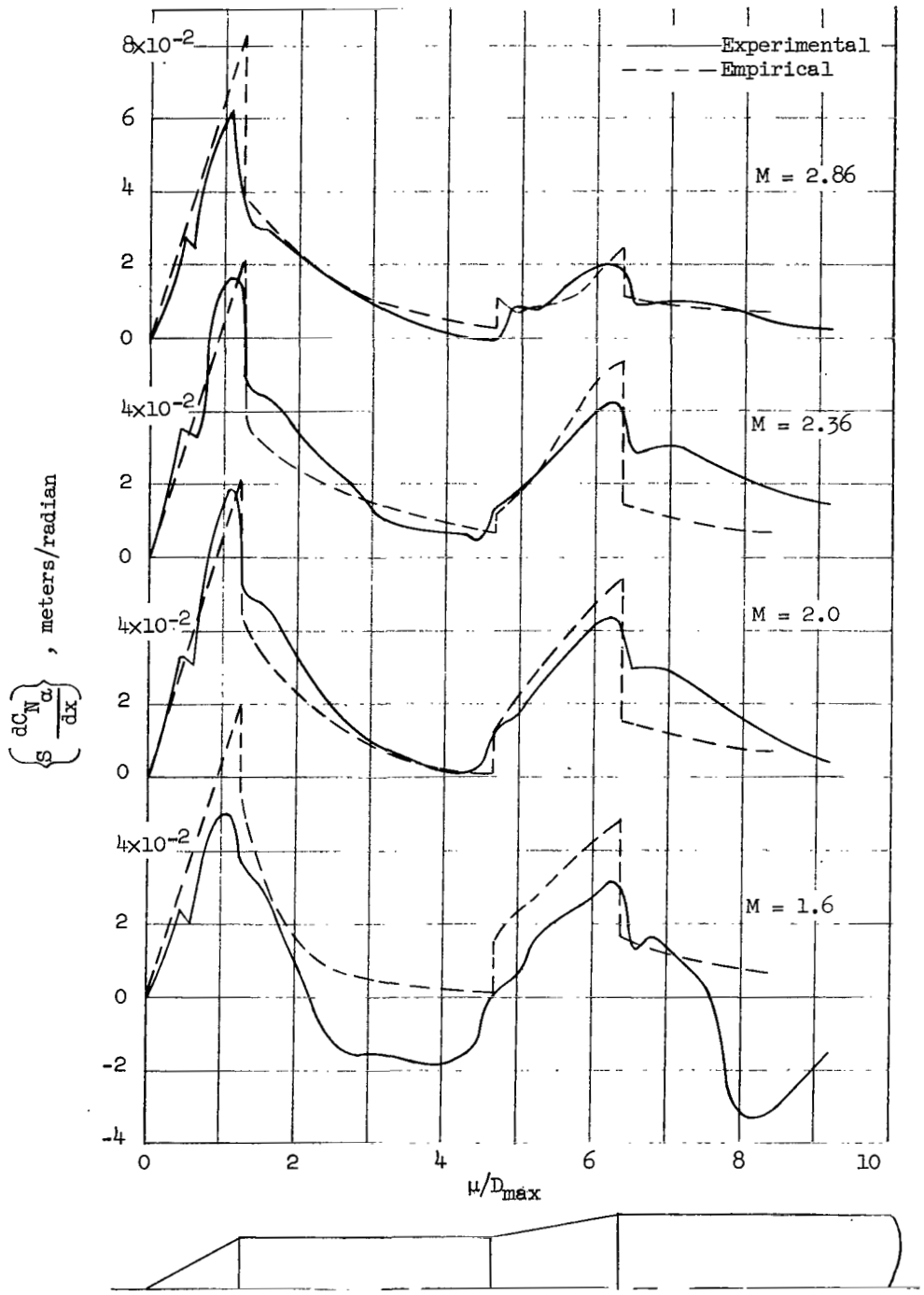


(a) $\theta_n = 15^\circ$; $f_{a,1} = 4.67$; $\theta_f = 5^\circ$.

Figure 13.- Comparison of distributed normal-force-coefficient slope from experimental and empirical data.

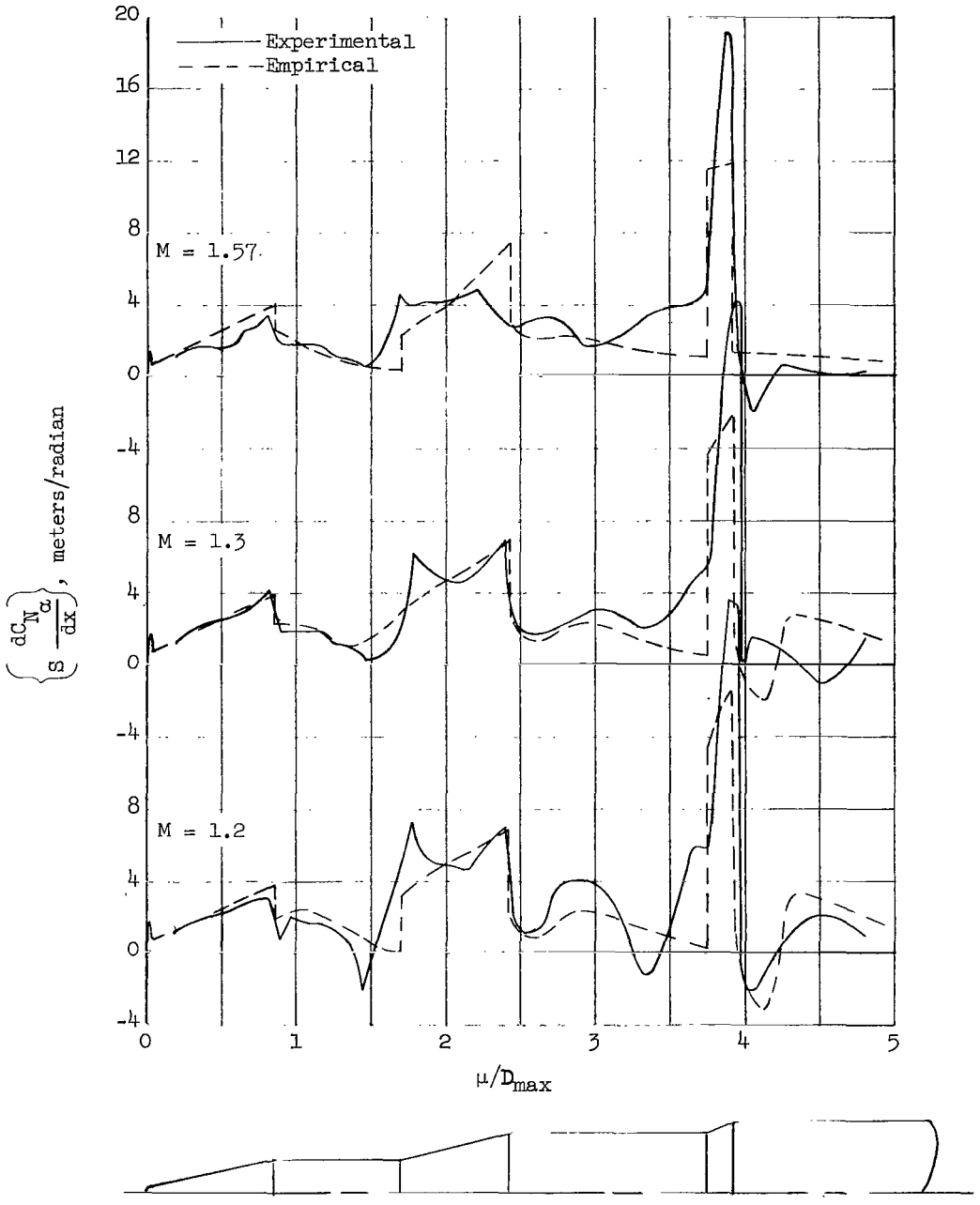


(b) $\theta_n = 13^\circ$; $f_{a,1} = 1.836$; $\theta_{f,1} = 15^\circ$; $f_{a,2} = 1.55$; $\theta_{f,2} = 24.5^\circ$.

Figure 13.- Continued.

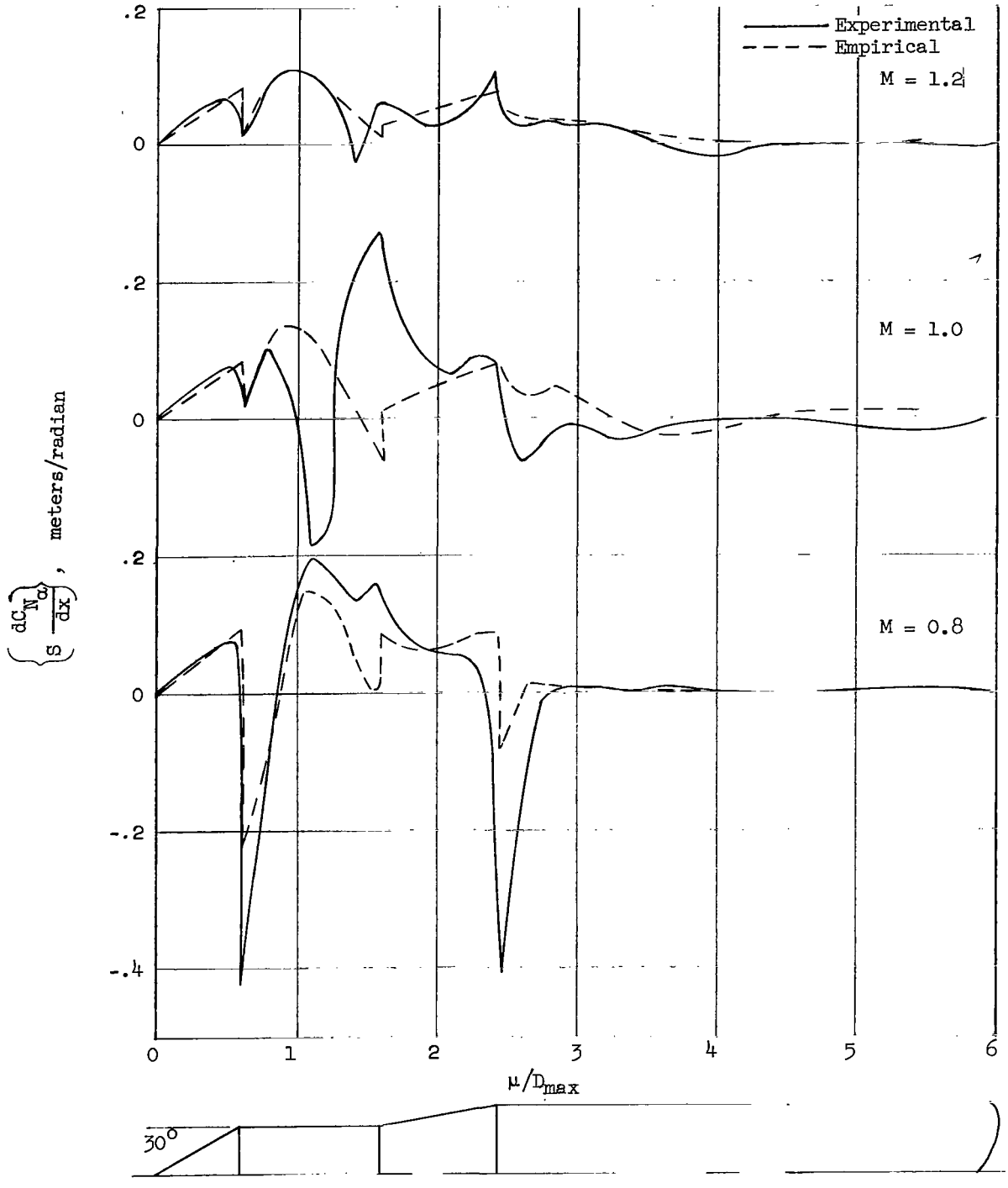


(c) $\theta_n = 30^\circ$; $f_{a,1} = 1.423$; $\theta_f = 10^\circ$.

Figure 13.- Concluded.



NASA-Langley, 1966 L-4669

*"The aeronautical and space activities of the United States shall be conducted so as to contribute . . . to the expansion of human knowledge of phenomena in the atmosphere and space. The Administration shall provide for the widest practicable and appropriate dissemination of information concerning its activities and the results thereof."*

—NATIONAL AERONAUTICS AND SPACE ACT OF 1958

# NASA SCIENTIFIC AND TECHNICAL PUBLICATIONS

TECHNICAL REPORTS: Scientific and technical information considered important, complete, and a lasting contribution to existing knowledge.

TECHNICAL NOTES: Information less broad in scope but nevertheless of importance as a contribution to existing knowledge.

TECHNICAL MEMORANDUMS: Information receiving limited distribution because of preliminary data, security classification, or other reasons.

CONTRACTOR REPORTS: Technical information generated in connection with a NASA contract or grant and released under NASA auspices.

TECHNICAL TRANSLATIONS: Information published in a foreign language considered to merit NASA distribution in English.

TECHNICAL REPRINTS: Information derived from NASA activities and initially published in the form of journal articles.

SPECIAL PUBLICATIONS: Information derived from or of value to NASA activities but not necessarily reporting the results of individual NASA-programmed scientific efforts. Publications include conference proceedings, monographs, data compilations, handbooks, sourcebooks, and special bibliographies.

***Details on the availability of these publications may be obtained from:***

**SCIENTIFIC AND TECHNICAL INFORMATION DIVISION**

**NATIONAL AERONAUTICS AND SPACE ADMINISTRATION**

**Washington, D.C. 20546**